NASA Contractor Report 195473

High Temperature Kinetic Study of the Reactions $H + O_2 = OH + O$ and $O + H_2 = OH + H$ in H_2/O_2 System by Shock Tube - Laser Absorption Spectroscopy

Si-Ok Ryu, Soon Muk Hwang, and Kenneth J. DeWitt
University of Toledo
Toledo, Ohio

May 1995

National Aeronautics and
Space Administration

N95-27695

Unclas

G3/25   0049831

(NASA-CR-195473)   HIGH TEMPERATURE
KINETIC STUDY OF THE REACTIONS H +
O2 = OH + O AND O + H2 = OH + H IN
H2/O2 SYSTEM BY SHOCK TUBE-LASER
ABSORPTION SPECTROSCOPY Final
Contractor Report (Toledo Univ.)
123 p

High Temperature Kinetic Study of the Reactions $H + O_2 = OH + O$ and $O + H_2 = OH + H$ in H_2/O_2 System by Shock Tube - Laser Absorption Spectroscopy

Si - Ok Ryu, Soon Muk Hwang and Kenneth J. De Witt
Department of Chemical Engineering
The University of Toledo
Toledo, OH 43606

Acknowledgments

Abstract

The reactions (1) $H + O_2 = OH + O$ and (2) $O + H_2 = OH + H$ are the most important elementary reactions in gas phase combustion. They are the main chain-branching reaction in the oxidation of H_2 and hydrocarbon fuels.

In this study, rate coefficients of the reactions (1) and (2) have been measured over a wide range of composition, pressure, density and temperature behind the reflected shock waves. The experiments were performed using the shock tube- laser absorption spectroscopic technique to monitor OH radicals formed in the shock-heated $H_2/O_2/Ar$ mixtures. The OH radicals were detected using the $P_1(5)$ line of (0,0) band of the $A^2\Sigma^+ \leftarrow X^2\Pi$ transition of OH at 310.023 nm (air). The data were analyzed with the aid of computer modeling. In the experiments great care was exercised to obtain high time resolution, linearity and signal-to-noise.

The results are well represented by the Arrhenius expressions. The rate coefficient expression for reaction (1) obtained in this study is $k_1 = (7.13 \pm 0.31) \times 10^{13} \exp(-6957 \pm 30 \text{ K/T}) \text{ cm}^3\text{mol}^{-1}\text{s}^{-1}$ (1050 K $\leq$ T $\leq$ 2500 K) and a consensus expression for k_1 from a critical review of the most recent evaluations of k_1 (including our own) is $k_1 = 7.82 \times 10^{13} \exp(-7105 \text{ K/T})$ $\text{cm}^3\text{mol}^{-1}\text{s}^{-1}$ (960 K $\leq$ T $\leq$ 5300 K). The rate coefficient expression for k_2 is given by $k_2 = (1.88 \pm 0.07) \times 10^{14} \exp(-6897 \pm 53 \text{ K/T}) \text{ cm}^3\text{mol}^{-1}\text{s}^{-1}$ (1424 K $\leq$ T $\leq$ 2427 K). For k_1, the temperature dependent A-factor and the correlation between the values of k_1 and the inverse reactant densities were not found. In

the temperature range of this study, non-Arrhenius expression of k_2 which shows the upward curvature was not supported.

Table of Contents

List of Tables

List of Figures

Chapter I. H + O$_2$ = OH + O Reaction

Introduction

The reaction between hydrogen atoms and oxygen molecules

$$H + O_2 = OH + O \qquad \Delta_r H^{\circ}_{298} = 70.2 \text{ kJ/mol} \qquad (1)$$

is the most important elementary reaction in gas phase combustion systems. It is the main chain branching reaction in the oxidation of H$_2$ and hydrocarbon fuels. About 80 % of the O$_2$ is removed from the main reaction zone of typical stoichiometric hydrocarbon-air flames at atmospheric pressure by this step [1]. Because of the large reaction endothermicity, this reaction is likely to have a high activation energy, hence, this reaction is rate controlling even at high temperatures. Therefore, the induction delay and the flame speed are sensitive to the rate coefficient of this reaction. At high temperature and low pressure, reaction (1) produces O-atom and OH radical as the further chain branching and propagating carriers, respectively, according to the following reactions,

$$O + H_2 = OH + H \qquad \Delta_r H^{\circ}_{298} = 7.8 \text{ kJ/mol} \qquad (2)$$

$$OH + H_2 = H_2O + H \qquad \Delta_r H^{\circ}_{298} = -62.8 \text{ kJ/mol} \qquad (3)$$
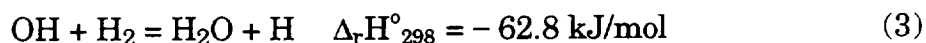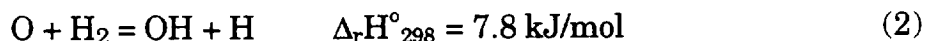
thus maintaining the chain branching process. Reaction (1) also determines the first and the second explosion limits of the H_2/O_2 system which are primarily dependent upon the chain branching reaction.

As reaction (1) plays a central role in the oxidation of H_2 and hydrocarbon fuels at high temperature, it has been the subject of numerous investigations and reviews. Baulch et al. [2] reviewed the rate coefficient data up to 1972 and recommended $k_1 = 2.2 \times 10^{14} \exp(-8450 \text{ K/T}) \text{ cm}^3\text{mol}^{-1}\text{s}^{-1}$ over the temperature range 700 - 2500 K. Based on the molecularity and the activation energy of the reverse of reaction (1), they claimed that the activation energy would not be less than the endothermicity. In 1973 Schott [3] measured the exponential growth of chemiluminescence from CO + O = $CO_2^* + h\nu$ during the branched-chain ignition of $H_2/CO/O_2/Ar$ mixtures behind reflected shock waves and reported a rate coefficient expression with a temperature dependent A-factor, $k_1 = 1.22 \times 10^{17} \text{ T}^{-0.907} \exp(-8369 \text{ K/T})$ $\text{cm}^3\text{mol}^{-1}\text{s}^{-1}$ in the temperature interval of 1250 to 2500 K. The reviews by Warnatz [1], Cohen and Westberg [4], and Cohen [5] essentially adopted Schott's results as their recommended rate coefficient expression. Thus Schott's rate coefficient expression was recognized as the most reliable one and was widely used in the modeling of hydrogen and hydrocarbon combustion systems. However, Schott's rate coefficient data were questioned by Frank and Just [6]. They shock-heated $H_2/O_2/N_2O/Ar$ mixtures and initiated the reactions with O-atoms produced by thermal decomposition of N_2O. The O- and H-atoms formed were monitored using Atomic Resonance Absorption Spectroscopy (ARAS). Reaction rate coefficient expressions of k_1 and k_3 were

obtained by simulating O- and H-atom concentration profiles with a reaction mechanism of 10 elementary reactions. From their experimental results it was concluded that Schott's expression of k_1 gave too low a value by a factor of more than 1.8 at temperature of 2000 K. Their results, however, agreed well with the recommended values of Baulch et al. [2]. A negative temperature dependence of the A-factor of k_1 was not found. Prompted by this experiment, the title reaction was reinvestigated by many authors using laser absorption spectroscopic or ARAS methods or both under various experimental conditions. Pirraglia et al. [7] reported k_1 values obtained under pseudo-first-order conditions by the flash photolysis-shock tube technique that used the ARAS method to monitor H-atom concentrations in the temperature range from 962 to 1705 K. The Arrhenius rate coefficient expression reported was k_1 = 1.68 × 10^{14} exp(− 8119 K/T) $cm^3mol^{-1}s^{-1}$ which was essentially the low temperature extension of Frank and Just's results. Masten et al. [8] measured k_1 values in the rich $H_2/O_2/Ar$ system using laser absorption spectroscopy behind incident and reflected shock waves. OH radicals formed were monitored by utilizing the $R_1(5)$ line in OH $A^2\Sigma^+ \leftarrow X^2\Pi$ transitions. The rate coefficient expression of k_1 = 9.33 × 10^{13} exp(−7448 K/T) $cm^3mol^{-1}s^{-1}$ over the temperature range 1450 - 3370 K was reported. Yuan et al. [9] performed experiments using the same technique of Masten et al. but substituting the $P_1(5)$ line for the $R_1(5)$ line as a monitoring wavelength of OH radicals and presented a k_1 expression with a temperature dependent A-factor similar to that of Schott, k_1 = 1.59 × 10^{17} $T^{-0.927}$ exp(−8493 K/T) $cm^3mol^{-1}s^{-1}$ in the temperature interval of 1050 - 2700 K. However the mixture compositions chosen were mostly stoichiometric or lean, from which the OH profiles generated were not sufficiently sensitive to derive k_1 values with confidence.

Shin and Michael [10] studied reaction (1) using the laser photolysis-shock tube technique over the temperature range of 1103 - 2055 K. H-atoms were produced by photolyzing NH_3 or H_2O with an excimer laser and H-atom decay due to the reaction with a large amount of O_2 molecules present (pseudo-first-order condition) was monitored by ARAS. The rate coefficient expression reported was $k_1 = 6.93 \times 10^{13}$ exp(- 6917 K/T) $cm^3mol^{-1}s^{-1}$. Du and Hessler [11] also investigated reaction (1) together with the H_2 decomposition reaction at very high temperatures (2050 K $\leq$ T $\leq$ 5300 K) by using a laser flash absorption - shock tube technique to monitor the OH radicals formed behind incident shock waves. They combined their results with the analytical expressions of Shin and Michael, Masten et al. and Pirraglia et al. and presented a rate coefficient expression of $k_1 = 9.76 \times 10^{13}$ exp(- 7474 K/T) $cm^3mol^{-1}s^{-1}$ over the wide temperature range of 960 - 5300 K. Recently Yu et al. [12] reexamined both data of Masten et al. and Yuan et al. by a rigorous optimization using two different model responses, the characteristic times(t_{25}, t_{50}, t_{75}) and the time difference($t_{75} - t_{25}$), and reported the source of the previous disagreement between their results to be the vibrational relaxation of O_2. They extracted a new rate coefficient expression, $k_1 = 8.30 \times 10^{13}$ exp(- 7253 K/T) $cm^3mol^{-1}s^{-1}$ over the temperature range of 1336 - 3370 K. Yang et al. [13] also reinvestigated their previous work [14, 15] for k_1 using a single beam laser absorption study of OH radical and then combined their data with that of Shin and Michael to obtain a new expression over the temperature range of 1100 - 3550 K, $k_1 = 7.60 \times 10^{13}$ exp(- 7065 K/T) $cm^3mol^{-1}s^{-1}$.

Even though numerous experimental studies have been done by many investigators, there still remains significant discrepancies in k_1 at high and low

temperatures, for example, factors of 2.5 and 1.5 discrepancies at 2500 K and 1050 K, respectively. Recently Schott [16] compared the previously published k_1 values with reactant densities at 2000 K and pointed out that there seemed to be a correlation between the derived k_1 values and the inverse of reactant densities. The intermediate hydroperoxyl radical (HO_2^*) formed by reaction (1) can be stabilized to HO_2 by transferring excessive energy to collision partners at low temperature and high pressure (density). In this case, k_1 would be density dependent. It is well known that HO_2 is thermodynamically unstable at temperatures above ~1300 K. If HO_2 radicals formed at high temperatures decompose immediately to the reactants (H + O_2), not the products (OH + O), then it may be possible to obtain lower k_1 values.

Generally, reaction rate coefficients can be expressed in two different ways: two-parameter Arrhenius type, $k = A \exp(- \theta/T)$; and three-parameter non-Arrhenius type, $k = A T^n \exp(- \theta/T)$. In the second expression, the A-factor is a function of temperature. The experimentally determined temperature dependence of the A-factor, n, was either 0 or in the range from $- 0.927$ to 2.0 [3, 8, 9, 14]. Also, in theoretical studies, Miller [17, 18] calculated k_1 and k_{-1} using quasiclassical trajectory (QCT) and quasiclassical trajectory - quantum mechanical threshold (QCT-QMT) methods based on the potential energy surface of Melius and Blint [19]. The calculation resulted in negative Arrhenius curvature and it was explained by the nonstatistical "recrossing effects" at high temperatures. However, according to the recent theoretical calculation of Varandas et al. [20] for k_1 using quasiclassical trajectory-internal energy quantum mechanical threshold (QCT-IEQMT) and an improved version of QCT-IEQMT methods which employed their fourth version of a double many

body expansion (DMBE IV) potential energy surface, the temperature dependence of the A-factor, n, was found to be zero in the temperature range of 1000 - 3000 K. Hence, the curvature of the Arrhenius expression of k_1 is not firmly established.

In this study, a series of experiments over a wide range of composition, pressure, density, and temperature were performed behind reflected shock waves to address these problems mentioned above, i.e., (1) the values of k_1; (2) the inverse density dependence of k_1; and (3) the temperature dependence of the A-factor. The reaction progress was followed by state-selective cw laser absorption spectroscopic measurements of OH radicals produced in shock heated $H_2/O_2/Ar$ mixtures. The data were analyzed with the aid of computer modeling. In the experiment great care was taken to guarantee high signal-to-noise ratio, linearity, and time resolution.

Experimental Section

The experimental setup including optical, mechanical and electronic components is shown in Figure I.1.

A. Shock Tube System

Experiments were performed in a rolled square stainless steel pressure driven shock tube with internal cross section of 63.5mm × 63.5mm. The length
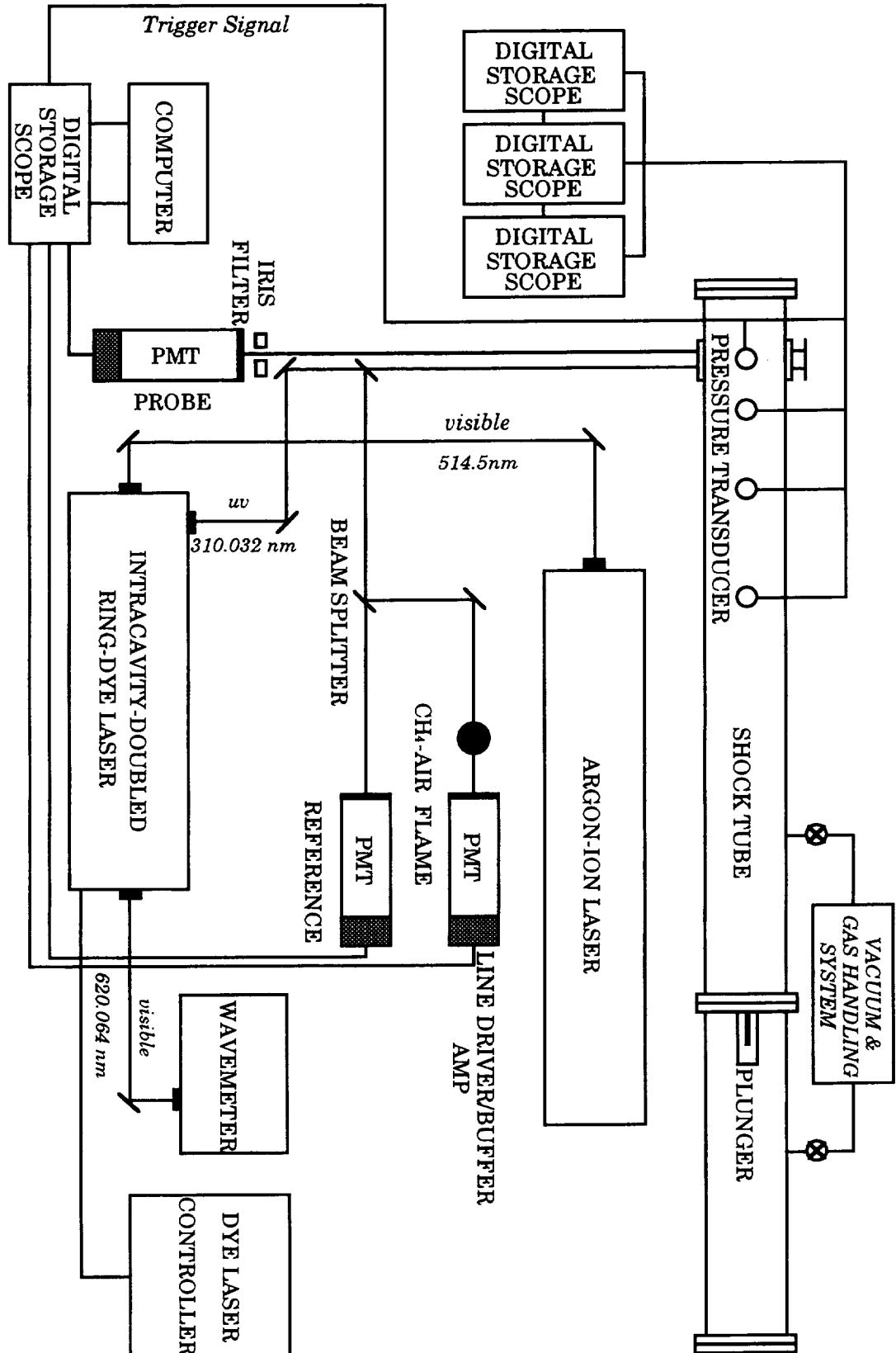
Figure I.1 Schematic diagram of the experimental setup.

of the driven section was 5.5 m and the driver section was 2.2 m. The driver section was separated from the driven section by an unscored dead-soft-temper aluminum diaphragm (Alufoil Products Co.) and pumped with a Welch Duo-Seal vacuum pump. A Varian zeolite-sieve was used to trap the oil backstreaming from the roughing pump. Pressure in the driver section was always maintained above 500 micron to further reduce effects of back streaming. The diaphragm was burst with a cross-shaped plunger. Mixtures of He and Ar served as the driver gas.

The driven section was routinely pumped between experiments to 3×10^{-6} Torr by a Varian SD-700 roughing pump and a Varian Turbo-V60 pump equipped with a Varian SD-90 fore pump. The combined leak and outgassing rate was about 5×10^{-6} Torr/min. Driven section pressure was always maintained above 500 micron when pumped by the SD-90 fore pump in order to reduce backstreaming. The same type of sieve was used to trap the residual back flow of contaminants from the roughing pump to the shock tube.

The gas handling system was constructed with high vacuum Varian valves (Model No. L6591-301) and seals. The vacuum pressure of the driven section and the gas handling system was measured by three Varian 0531 thermocouple gauges coupled to Varian 801 vacuum readouts and a Varian 525 cold cathode gauge with a Varian 860A vacuum readout. Both the reactant pressures in the mixing tanks and the initial test gas pressures in the shock tube were measured by a Druck Model DPI-260 250 Torr pressure transducer (accuracy of 0.01 Torr) and DPI-260 5000 Torr pressure transducer (accuracy of 1 Torr, Druck, Inc.).

Two 25.4 mm diameter S1-UVA quartz windows were flush mounted on opposite sides of the shock tube's inner walls. Their centers were located 1.27 cm from the reflective surface of the end plate. The shock velocities were measured by four 113A21 PCB Piezotronics pressure transducers mounted flush to the inner wall of the shock tube and powered by a PCB 482A05 Piezotronics power supply. The distances between the pressure transducers were 45.72 cm, 30.48 cm, and 22.86 cm, respectively, downstream from the diaphragm. The last pressure transducer was positioned 1.27 cm from the end plate, center of the observation windows.

Pressure transducer signals were fed into three two channel Nicolet digital oscilloscopes each set to 0.5 μs per point time resolution. Incident shock velocities measured between pressure transducer signals were fitted to a second order polynomial as a function of distance from the first pressure transducer. The shock velocity for the calculation of shock parameters at the reflected shock front was obtained by extrapolation of the fitted polynomial to the end plate. In this way the attenuation of shock velocity was automatically measured. Shock parameters were computed by standard methods [21] assuming full vibrational relaxation and no chemical reaction at the shock front and using NASA thermochemical data [22]. Later, the computed shock parameters were corrected for effects due to the interaction between the reflected shock front and the boundary layer built.

B. Laser System

The concentration of OH radicals during the course of reaction was

monitored using the $P_1(5)$ line of (0,0) band of the $A^2\Sigma^+ \leftarrow X^2\Pi$ transition at 310.032 nm (air). A Coherent CR-699-21 ring-dye laser running with Kiton Red 620 dye (Exciton Chemical Co.) was pumped by a Coherent Innova 200 argon ion laser. The dye solution, Kiton Red 620 dye dissolved in methanol and ethylene glycol, was circulated by a Coherent 5920 Dye Circulator at pressures between 35 psi and 42 psi. The temperature of the dye solution was maintained at 5 °C by a Neslab CFT-25 Refrigerated Recirculator in order to achieve maximum conversion efficiency. The concentration of the dye solution was controlled so that 90% of the argon ion laser beam power was absorbed in the dye jet. The argon ion laser is operated in single line (514.5 nm) and light regulation (7.5 ± 0.038 W) modes. The ring-dye laser was actively stabilized by adjusting the dye laser cavity length. An error signal generated by filtering out the amplitude information of a mode locked laser beam in a reference cavity was amplified and used to drive a high frequency piezoelectric mounted folding mirror and a scanning brewster plate to adjust the cavity length. Single frequency operation out of the CR-699-21 ring-dye laser was achieved by using a three-plate birefringent filter and an intracavity assembly (a thin etalon and a piezoelectric driven thick etalon).

UV output (~310 nm) was generated via intracavity doubling of the fundamental beam using a Coherent Model 7500 frequency doubler ($LiIO_3$ crystal). The wavelength of the primary beam was monitored by a Burleigh WA-10 Wavemeter with a readout precision of ± 0.001 nm. The resulting single mode UV beam had a line width of 2 MHz and a typical output power of 5 mW. The center wavelength of the OH absorption line was determined by passing part of the UV beam (see Detection System) through a burner

stabilized CH_4/Air flame. Laser wavelength was varied using the electronic controller until maximum absorption within the flame was reached. At that time the 699-21 ring-dye laser was placed in a "Locked" mode. Frequency lock was then actively controlled by the laser electronics with no measurable deviation for the time between wavelength locking and shock arrival, i.e., approximately 30 seconds. The lasers, optical components, as well as the detection system described below were mounted on a pneumatically stabilized Newport MST series optical table.

C. Detection System

For signal detection a double beam scheme was employed. The UV beam was split into two beams using a UV beam splitter (Esco Products, Inc.). The first beam was directed through the shock tube at the center of the windows. If the expected absorbance for an experiment was small, the beam was reflected back through the shock tube at the same streamwise distance but vertically displaced from the incoming beam and onto the detector, i.e., double pass. For experiments with large expected absorbance, the beam was returned to the detector after being steered around the shock tube, i.e., single pass. An iris was set in front of the detector both to limit emission from the hot gases within the shock tube and to help establish the "Time Zero" measurement from the schlieren caused by shock passage. The second beam was split again and one part was directed to a reference detector and the other directed to a third detector through a CH_4/air flame. All three detectors were THORN EMI Model 9924QB Photomultiplier tubes (PMT) powered by THORN EMI Model PM28B power supplies. A customized five dynode configuration

was used for each PMT to guarantee optimum linearity for the light intensity of the UV laser beams. A high speed buffer/amplifier (National Semiconductor LH0033CG) isolated the anode from the coaxial signal cable. An overall electronic time constant of 0.2 μs was determined electronically for the entire PMT/electronic/cable system. Background light reduction was achieved by mounting a narrow band interference filter (Pomfret Research Optics, Inc., Model No. 20-3100-1, λ_o 310 nm and $\Delta\lambda$ at FWHM 0.1 nm) in front of each PMT. Also, during the course of experiments the room lights were extinguished. The reference signal, the probe signal, the difference (probe DC − reference AC), and the signal from the last pressure transducer were recorded by a four-channel Nicolet 4094C digital oscilloscope with Nicolet 4570 plug-in units and a Nicolet XF-44 disk recorder. The pressure signal served as the trigger source for the oscilloscope. Reaction progress was followed using the difference signal. The signal-to-noise ratio was typically 120-250. A laboratory PC (Dell 486P /33) running Asystant GPIB Program was used to control the Nicolet 4094C oscilloscope through an IOtech IEEE488 (Driver488, version 2.5) interface.

Absolute pressure in the shock tube was measured using the voltage signal of the 113A21 PCB Piezotronics pressure transducer, coincidently mounted with the windows, and then converted to an absolute pressure using a calibration curve supplied with the transducer by the manufacturer (the calibration was validated against a dead weight gauge at the NASA Lewis Research Center Calibration Laboratory before use). The initial test gas pressure was added to this pressure. All shocks were initiated within one minute of filling the driver section with test gas. This actual pressure was used in the temperature correction for the boundary layer effect.

D. Test Gas Mixtures

The test gas mixtures were prepared manometrically and allowed to stand for 48 hours before use. The maximum uncertainty of the final reactant concentrations was about 0.5% or less for each component. The purities of the gases stated were also confirmed by in-house gas chromatographic analysis using the flame ionization detector. They were: H_2, 99.9995% (Linde Research Grade, THC as $CH_4 < 0.3$ ppm), O_2, 99.6% (Linde zero grade, THC as $CH_4 < 0.3$ ppm), Ar, 99.996% (Linde zero grade, THC as $CH_4 < 0.3$ ppm). H_2, O_2, and Ar were used without further purification.

Results

A. Experimental Conditions and Results

Typical transmitted light intensity profiles at different experimental conditions are shown in Figures I.2 (a) - (d). After an initiation - induction period, forming small amounts of chain carriers H, O, and OH, the light absorption rises rapidly due to essentially exponential growth of OH caused by the chain branching and chain propagating reactions. Depending upon experimental conditions the OH concentration reaches a maximum and decays down later or reaches a partial equilibrium.

In order to obtain the full information content of the absorption profiles
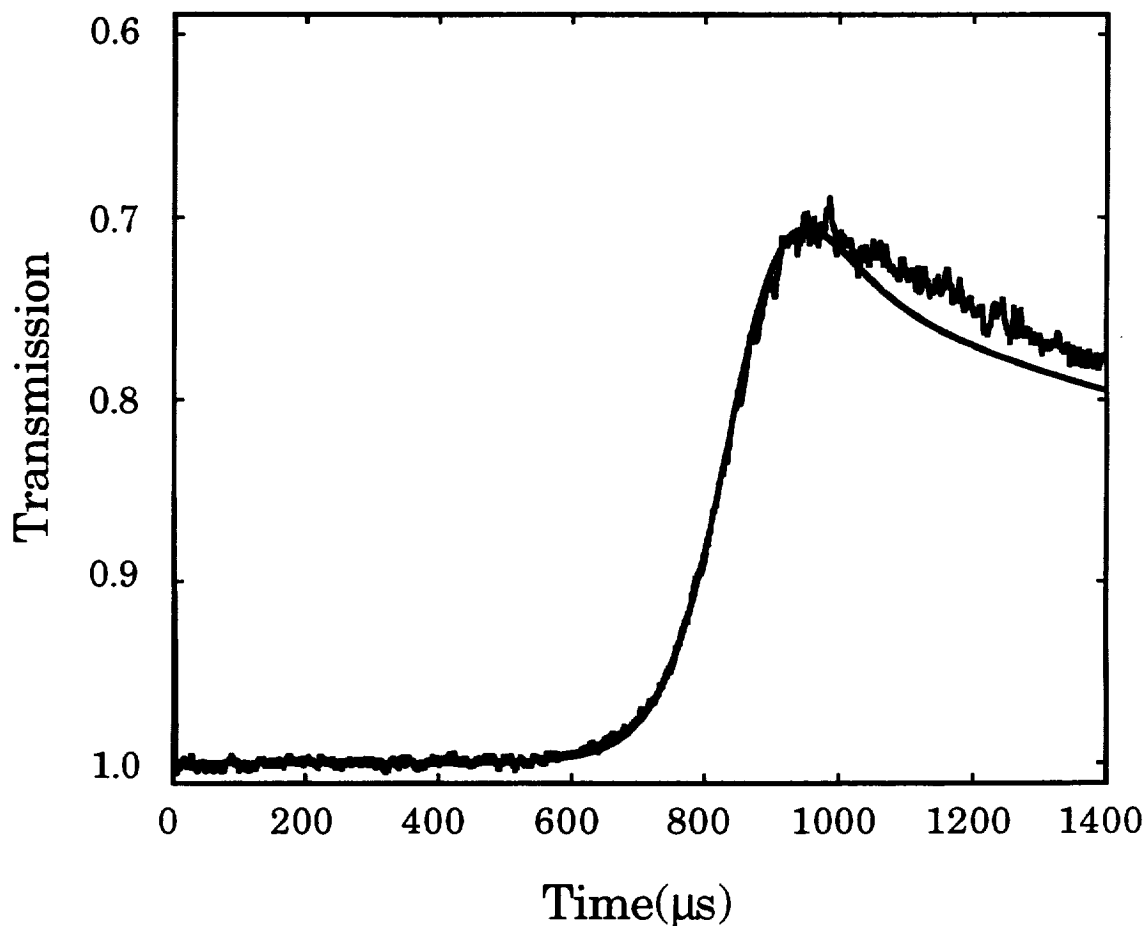
Figure I.2(a) A typical experimental record of OH absorption at low temperature. $X_{H_2} = 0.02$, $X_{O_2} = 0.005$, $X_{Ar} = 0.975$, $T_5 = 1234$ K and $P_5 = 0.945$ atm. NS_{max} and A_{max} were chosen as simulation parameters. The schlieren signal corresponds to passage of the reflected shock front. The smooth line indicates the computed OH absorption profile using the Table I.3 reaction mechanism and the OH absorption coefficient obtained from self-calibration at maximum absorption (A_{max}). The mismatch of the computed profiles after the peak do not affect determination of k_1. See text for details.
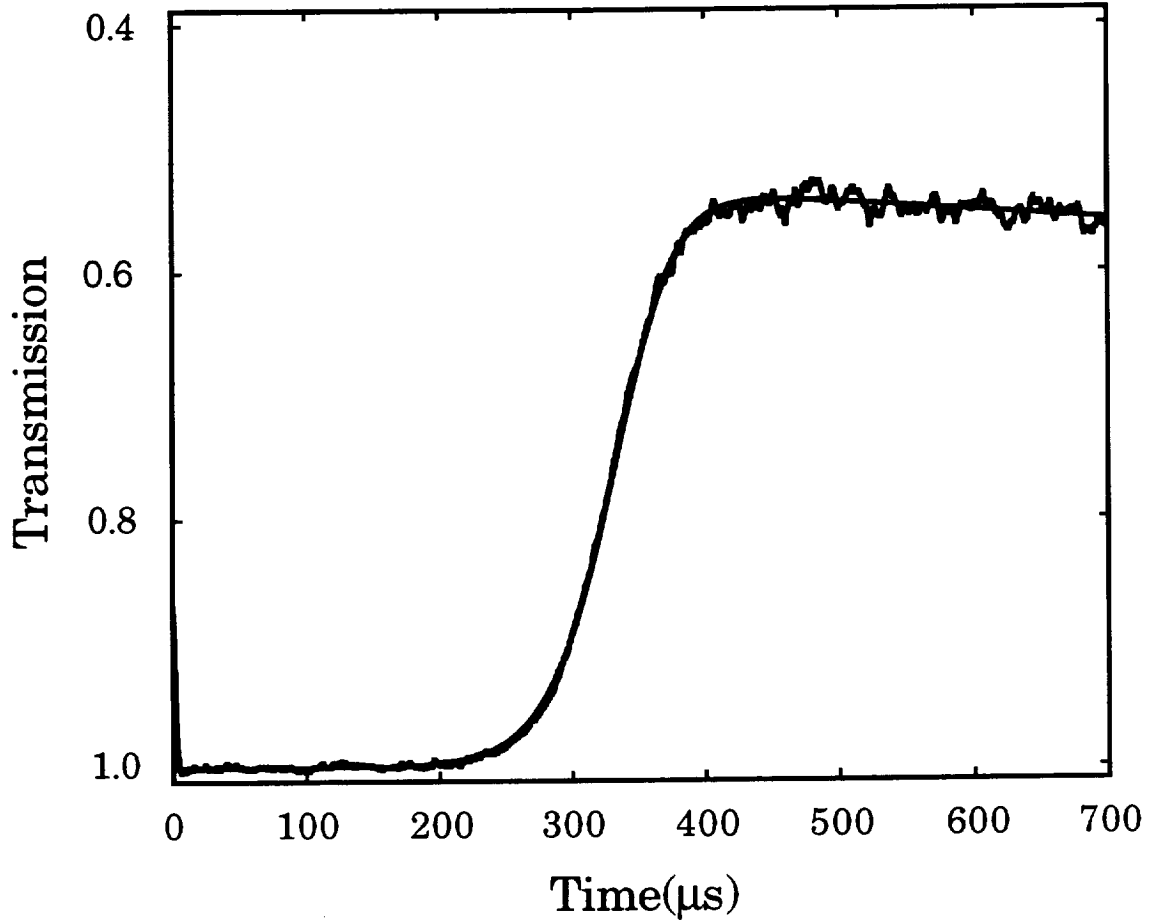
Figure I.2(b)   A typical experimental record of OH absorption at low-middle temperature. $X_{H_2} = 0.02$, $X_{O_2} = 0.005$, $X_{Ar} = 0.975$, $T_5 = 1556$ K and $P_5 = 0.751$ atm. NS_{max} and A_{max} were chosen as simulation parameters. The schlieren signal corresponds to passage of the reflected shock front. The smooth line indicates the computed OH absorption profile using the Table I.3 reaction mechanism and the OH absorption coefficient obtained from self-calibration at maximum absorption (A_{max}).
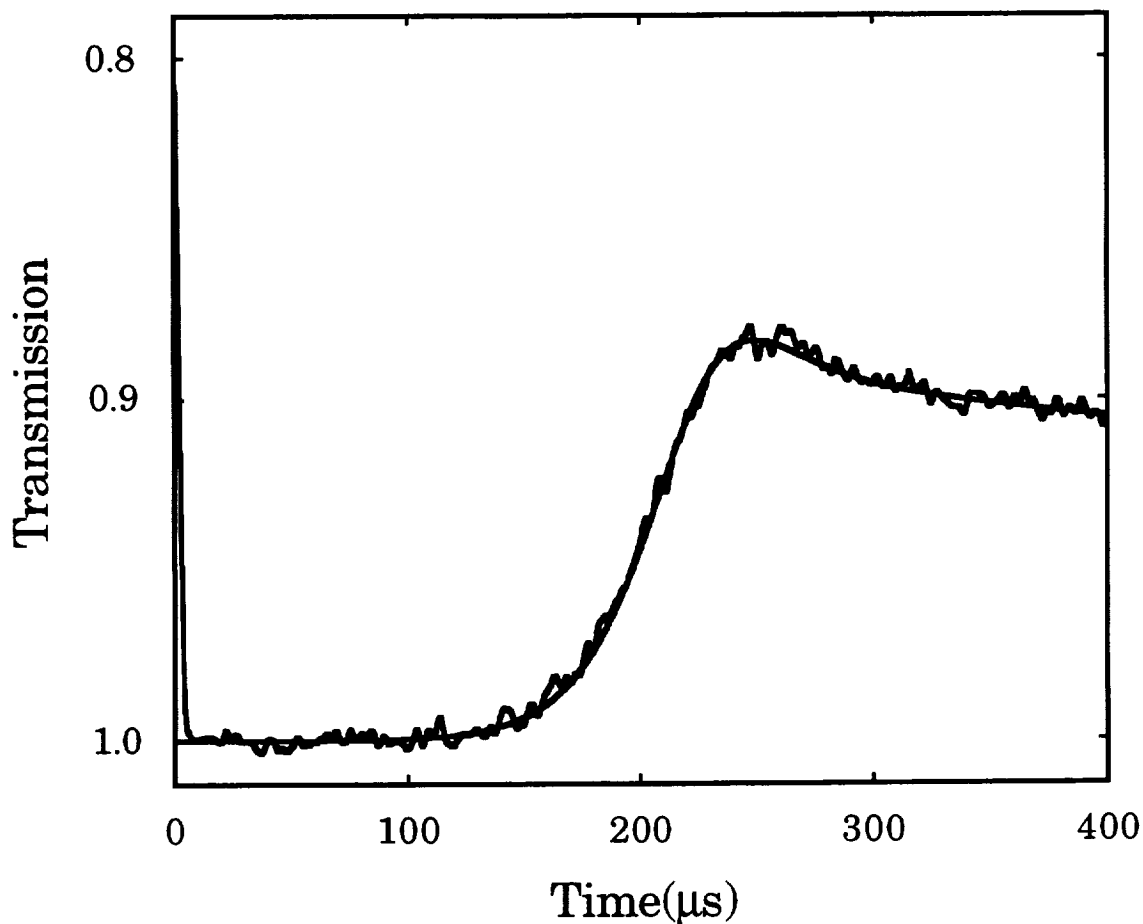
Figure I.2(c) A typical experimental record of OH absorption at high-middle temperature. $X_{H_2} = 0.01$, $X_{O_2} = 0.001$, $X_{Ar} = 0.989$, $T_5 = 1700$ K and $P_5 = 3.203$ atm. NS_{max} and A_{max} were chosen as simulation parameters. The schlieren signal corresponds to passage of the reflected shock front. The smooth line indicates the computed OH absorption profile using the Table I.3 reaction mechanism and the OH absorption coefficient obtained from self-calibration at maximum absorption (A_{max}).
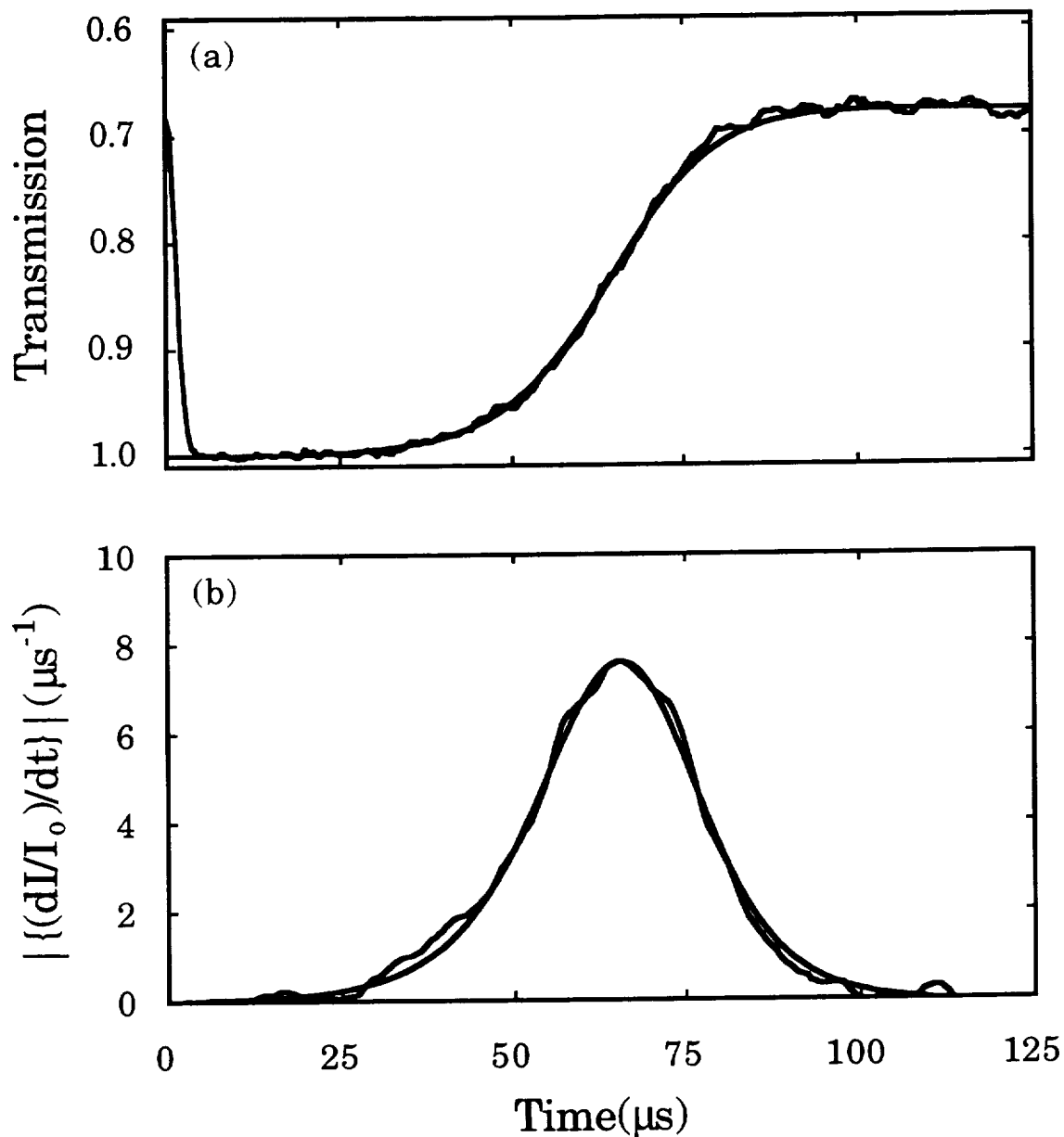
Figure I.2(d) Typical experimental and normalized slope records of OH absorption at high temperature. The upper panel shows an experimental profile of OH absorption at the condition of $X_{H_2} = 0.02$, $X_{O_2} = 0.002$, $X_{Ar} = 0.978$, $T_5 = 2163$ K and $P_5 = 1.994$ atm. The lower panel shows the normalized slope for the absorption profile in the upper panel. Smooth line represents the computed profiles using the Table I.3 reaction mechanism and the OH absorption coefficient obtained from self-calibration at maximum absorption (A_{max}).

while keeping the number of data points within reasonable bounds, five parameters were measured to characterize each experimental record [23], namely, $A_{max} = (1 - I/I_o)_{max}$; $NS_{max} = |\{d(I/I_o)/dt)_{max}\}|$ (s^{-1}); three characteristic times, t_{25}, t_{50}, t_{75}, at which the absorbed light intensity has reached 25%, 50%, 75% of A_{max}, respectively. The value of NS_{max} was obtained from each experimental profile in the following manner: the maximum slope $((dI/dt)_{max})$ was evaluated with the "Derivative" Standard Package Program for the Nicolet 4094 digital oscilloscope (lower panel of Figure I.2 (d)) and normalized with I_o; then the absolute value was taken.

The upper bound for the experimental temperature range was set by the appearance of OH absorption in a series of shocks in a 2.0% O_2 / 98.0% Ar mixture. This mixture was chosen for its sensitivity to possible hydrocarbon contamination. At temperatures exceeding 2700K, a small but noticeable absorption was observed at long times. It is speculated that contaminants (possibly residual pump oil) swept off the shock tube walls or impurities in the test gas may be responsible. The lower temperature bound was set to 1050 K by the limit of the available observation time and the loss of signal due to the diminishing amounts of OH generated at low temperatures. Eight rich mixtures of equivalence ratio(ϕ) of 2, 5, and 10 were used. Reflected shock temperatures ranged from 1050 to 2500 K and pressures ranged from 0.7 to 4.0 atm. Mixture compositions were selected such that maximum absorption was less than 0.55 for all mixtures.

The temperature behind the reflected shock wave was corrected for the boundary layer effect with the measured absolute pressure (P_5) using the

adiabatic equation of state method described by Michael and Sutherland [24]. The corrected temperatures were always higher than the ideal shock temperatures by an average of 1.4%. A dependence of the temperature (T_5) and the initial pressure (P_1) upon the corrected temperature was not observed.

Experimental conditions and results of k_1 are shown in Table I.1.

B. Computer Simulation

Computer simulations were performed using the detailed reaction mechanism of Yuan et al. [9], with the following modifications. The rate coefficient expression for the $OH + H_2$ reaction was taken from Ref. 25; and the $H + OH + M$ reaction was added with the rate coefficient expression and third body efficiencies from Masten et al. [8]. The reaction mechanism and rate coefficient expressions are given in Table I.2. Reverse reaction rate coefficients were automatically calculated from the principle of detailed balancing. NASA thermodynamic data [22] for the species were used in the calculation of shock parameters and equilibrium constants. The LSODE integrator [26] was utilized to solve a set of stiff differential equations describing chemical kinetics under assumed constant density conditions, calculated for the reflected shock waves [21].

The center line absorption coefficient of OH used to generate the OH absorption profile by computer simulation was computed according to the formula in the literature [9, 27, 28, 29, 30], namely:

Table I.1 Experimental Conditions and Results of $k_1{}^a$

T_5	P_5	A_{max}	NS_{max}	t_{25}	t_{50}	t_{75}	$k_1{}^b/10^{12}$
X_{H_2}=0.04, X_{O_2}=0.01, X_{Ar}=0.95 (ϕ=2)							
1052	2.289	0.334	5246	597	618	650	0.092
1074	0.964	0.303	2210	974	1005	1050	0.104
1086	0.940	0.294	1953	922	985	1053	0.112
1102	0.960	0.344	2495	802	836	861	0.124
1115	2.248	0.492	9088	371	393	411	0.130
X_{H_2}=0.02, X_{O_2}=0.005, X_{Ar}=0.975 (ϕ=2)							
1155	0.957	0.215	999	1188	1274	1343	0.172
1164	0.892	0.220	1012	1204	1283	1349	0.179
1170	0.950	0.232	1134	1111	1183	1245	0.186
1174	0.945	0.237	1098	1080	1153	1218	0.181
1228	0.734	0.227	1057	1079	1153	1217	0.242
1234	0.945	0.294	1806	768	819	863	0.257
1246	0.877	0.307	1814	753	803	848	0.271
1248	0.756	0.257	1386	886	943	989	0.281
1264	0.773	0.271	1562	856	911	961	0.293
1274	0.781	0.302	1774	761	814	860	0.312
1285	0.794	0.294	1859	738	794	843	0.325
1313	0.936	0.326	2331	572	616	653	0.338
1323	0.800	0.310	2280	649	696	737	0.386
1352	0.766	0.351	2761	581	620	658	0.433
1357	0.771	0.356	2550	572	612	651	0.420

Table I.1 Experimental Conditions and Results of $k_1{}^a$ (continued)

T_5	P_5	A_{max}	NS_{max}	t_{25}	t_{50}	t_{75}	$k_1{}^b/10^{12}$
			X_{H_2}=0.02, X_{O_2}=0.005, X_{Ar}=0.975 (ϕ=2)				
1358	0.772	0.353	2784	590	633	670	0.439
1359	0.774	0.354	2543	571	611	643	0.419
1387	0.778	0.368	2862	500	537	576	0.474
1472	0.859	0.437	4375	355	384	412	0.601
1516	0.699	0.226	2109	426	453	498	0.707
1556	0.751	0.460	5044	302	329	354	0.820
1558	0.733	0.445	4844	316	343	369	0.837
1570	0.737	0.267	3259	287	316	347	0.933
1577	0.962	0.554	7836	240	261	280	0.853
1578	0.788	0.463	5205	283	308	333	0.829
1581	0.761	0.352	4200	257	279	303	0.870
1596	0.852	0.503	6488	248	269	290	0.894
1627	0.738	0.315	4169	227	250	275	1.05
1649	0.733	0.488	6273	248	272	296	1.07
1652	0.769	0.328	4289	214	242	262	1.06
1667	0.744	0.499	6887	232	253	276	1.15
1708	0.771	0.517	7298	208	228	248	1.20
1715	0.797	0.361	5761	198	220	241	1.32
1726	0.784	0.364	5283	196	214	235	1.24
1747	0.795	0.344	5641	186	204	223	1.41
1760	1.034	0.480	9796	132	150	163	1.39
1809	0.846	0.409	7655	146	161	177	1.55
1915	0.876	0.407	9445	118	129	141	2.08

Table I.1 Experimental Conditions and Results of $k_1{}^a$ (continued)

T_5	P_5	A_{max}	NS_{max}	t_{25}	t_{50}	t_{75}	$k_1{}^b/10^{12}$
$X_{H_2}=0.02$, $X_{O_2}=0.005$, $X_{Ar}=0.975$ ($\phi=2$)
1924	0.735	0.393	6855	130	146	164	1.88
1998	1.018	0.484	12376	90	99	111	2.03
2017	0.757	0.429	9198	114	128	143	2.40
2030	0.854	0.430	10030	101	113	125	2.27
2099	0.772	0.450	9978	97	108	121	2.48
2136	0.851	0.487	12045	81	92	101	2.78
$X_{H_2}=0.004$, $X_{O_2}=0.001$, $X_{Ar}=0.995$ ($\phi=2$)
1525	2.005	0.210	1206	628	703	770	0.734
1639	2.049	0.270	1821	485	550	607	1.00
1692	2.029	0.284	2115	391	432	490	1.17
1934	1.922	0.341	3430	266	293	335	2.07
2044	2.146	0.438	5582	173	199	222	2.52
2068	1.819	0.390	3841	200	236	264	2.32
2082	1.857	0.375	3836	196	224	254	2.35
2132	2.094	0.439	5835	161	185	205	2.83
2256	2.050	0.439	5956	141	163	184	3.10
2409	2.095	0.453	6978	107	127	145	3.67
$X_{H_2}=0.002$, $X_{O_2}=0.0005$, $X_{Ar}=0.9975$ ($\phi=2$)
1527	3.770	0.156	928	573	647	704	0.753

Table I.1 Experimental Conditions and Results of $k_1{}^a$ (continued)

T_5	P_5	A_{max}	NS_{max}	t_{25}	t_{50}	t_{75}	$k_1{}^b/10^{12}$
X_{H_2}=0.002, X_{O_2}=0.0005, X_{Ar}=0.9975 (ϕ=2)							
1593	3.704	0.143	961	481	534	592	0.912
1658	3.654	0.168	1164	433	476	515	1.09
1716	3.792	0.217	1580	352	397	445	1.24
1725	3.905	0.233	1783	319	360	406	1.27
1763	3.843	0.195	1595	312	356	390	1.41
1888	3.880	0.242	2194	239	270	302	1.77
1977	4.050	0.271	2862	176	203	229	2.09
1999	3.697	0.224	2102	208	237	264	2.08
2001	4.088	0.276	3270	179	203	229	2.35
2092	3.681	0.257	2938	166	193	217	2.66
2211	3.715	0.270	3433	137	158	178	3.14
X_{H_2}=0.05, X_{O_2}=0.005, X_{Ar}=0.945 (ϕ=5)							
1243	0.798	0.084	576	804	863	907	0.259
1246	0.795	0.086	630	781	822	866	0.272
1251	0.792	0.091	662	733	784	820	0.276
1252	0.800	0.084	595	760	807	848	0.267
1254	0.813	0.089	676	753	799	838	0.282
1301	0.754	0.101	818	597	643	680	0.337
1315	0.766	0.112	961	539	581	614	0.359
1330	0.784	0.108	1009	542	578	606	0.387
1333	0.793	0.108	1025	540	578	610	0.391

Table I.1 Experimental Conditions and Results of $k_1{}^a$ (continued)

T_5	P_5	A_{max}	NS_{max}	t_{25}	t_{50}	t_{75}	$k_1{}^b/10^{12}$
		X_{H_2}=0.05, X_{O_2}=0.005, X_{Ar}=0.945 (ϕ=5)					
1336	0.797	0.110	1061	532	574	602	0.368
1336	0.794	0.107	964	526	559	586	0.392
1337	0.796	0.114	1098	527	561	593	0.395
1516	0.768	0.168	2369	252	274	294	0.722
1538	0.794	0.152	2252	260	280	296	0.755
1543	0.744	0.164	2181	245	269	291	0.725
1546	0.799	0.152	2333	248	269	286	0.777
1549	0.794	0.178	2893	236	257	273	0.822
1565	0.810	0.198	3219	213	235	250	0.833
1620	0.759	0.196	3095	201	220	236	0.910
1637	0.760	0.171	3094	199	216	231	1.03
1675	0.749	0.160	2969	184	200	214	1.13
1684	0.758	0.199	3847	173	191	205	1.17
1706	0.739	0.160	2941	174	190	203	1.18
1743	0.749	0.231	4392	154	168	179	1.26
1754	0.702	0.230	4009	163	177	191	1.26
1805	0.756	0.264	5378	128	140	155	1.43
1897	0.761	0.293	7001	109	121	133	1.80
1939	0.728	0.260	6414	107	118	130	2.02
2014	0.721	0.265	6173	94	105	117	2.11
2015	0.746	0.290	7531	89	102	112	2.25
2038	0.849	0.311	9328	79	86	95	2.34
2041	0.732	0.298	7081	87	98	108	2.18

Table I.1 Experimental Conditions and Results of $k_1{}^a$ (continued)

T_5	P_5	A_{max}	NS_{max}	t_{25}	t_{50}	t_{75}	$k_1{}^b/10^{12}$
$X_{H_2}=0.05$, $X_{O_2}=0.005$, $X_{Ar}=0.945$ ($\phi=5$)							
2125	0.721	0.324	8794	75	88	95	2.69
2151	0.724	0.337	8907	79	84	100	2.69
2188	0.775	0.343	9794	65	74	83	2.78
2376	0.756	0.383	12817	50	58	66	3.69
2414	0.725	0.366	11792	49	57	65	3.84
$X_{H_2}=0.02$, $X_{O_2}=0.002$, $X_{Ar}=0.978$ ($\phi=5$)							
1509	1.629	0.098	1259	307	338	361	0.736
1522	1.754	0.107	1430	278	313	334	0.760
1531	1.673	0.108	1513	294	321	340	0.802
1578	1.682	0.126	1641	240	264	285	0.808
1667	1.725	0.154	2477	188	209	224	1.06
1746	1.744	0.170	3527	149	165	181	1.44
1819	1.757	0.195	4428	127	144	155	1.69
1850	1.759	0.184	3775	121	136	148	1.60
1884	1.893	0.223	5429	104	116	128	1.81
1948	1.834	0.215	5174	93	106	117	1.98
1989	1.579	0.201	4373	101	113	126	2.16
1997	1.838	0.229	5587	86	97	107	2.11
2026	1.786	0.244	6289	83	95	104	2.34
2029	1.613	0.219	5124	92	106	115	2.36
2049	1.578	0.197	4731	91	103	114	2.50

Table I.1 Experimental Conditions and Results of $k_1{}^a$ (continued)

T_5	P_5	A_{max}	NS_{max}	t_{25}	t_{50}	t_{75}	$k_1{}^b/10^{12}$
			X_{H_2}=0.02, X_{O_2}=0.002, X_{Ar}=0.978 (ϕ=5)				
2094	1.816	0.271	7590	70	81	90	2.65
2134	1.783	0.294	8239	67	78	87	2.80
2163	1.994	0.323	10388	56	64	72	2.95
2165	1.981	0.294	9250	59	67	75	2.91
2184	1.780	0.289	8400	60	71	80	3.02
2282	1.849	0.265	8422	51	59	67	3.41
2293	1.852	0.303	9469	50	58	65	3.38
2345	1.915	0.358	12328	49	52	60	3.70
2379	2.024	0.372	13641	40	47	54	3.81
2501	2.013	0.356	14388	34	40	46	4.46
			X_{H_2}=0.01, X_{O_2}=0.001, X_{Ar}=0.989 (ϕ=5)				
1521	3.263	0.090	1077	298	328	352	0.724
1533	3.303	0.075	976	291	323	345	0.760
1557	3.382	0.088	1281	255	280	298	0.850
1579	3.054	0.104	1359	258	286	308	0.888
1583	3.510	0.106	1455	220	246	270	0.818
1609	3.387	0.091	1203	216	241	261	0.833
1611	3.720	0.109	1672	202	224	239	0.881
1647	3.342	0.100	1597	211	231	247	1.05
1664	3.868	0.123	2241	165	185	201	1.07
1700	3.203	0.117	2004	180	201	217	1.25

Table I.1 Experimental Conditions and Results of $k_1{}^a$ (continued)

T_5	P_5	A_{max}	NS_{max}	t_{25}	t_{50}	t_{75}	$k_1{}^b/10^{12}$
$X_{H_2}=0.01$, $X_{O_2}=0.001$, $X_{Ar}=0.989$ ($\phi=5$)
1714	3.237	0.120	1957	176	197	214	1.19
1792	3.275	0.144	2958	147	165	178	1.59
1809	3.331	0.148	2891	139	153	168	1.53
1841	3.811	0.157	3219	108	122	136	1.46
1846	3.364	0.150	3032	123	138	153	1.61
1895	3.285	0.179	3492	114	130	143	1.72
1913	3.378	0.183	3716	104	118	131	1.76
1945	3.117	0.195	3843	110	126	140	1.91
1976	3.280	0.189	3928	99	111	122	1.97
2057	3.329	0.195	5030	82	93	103	2.55
2104	3.439	0.253	6653	71	82	93	2.65
2107	3.403	0.251	6045	73	84	95	2.49
2142	3.444	0.208	5561	65	77	86	2.78
2155	3.383	0.223	5730	65	77	87	2.75
2213	3.370	0.224	6294	56	67	76	3.13
2305	3.442	0.255	8044	50	59	66	3.65
2355	3.478	0.229	7196	45	53	60	3.73
2379	3.313	0.249	7732	47	56	64	3.91
2413	3.384	0.262	8553	41	49	57	4.10
$X_{H_2}=0.10$, $X_{O_2}=0.005$, $X_{Ar}=0.895$ ($\phi=10$)
1514	0.722	0.075	1131	269	288	307	0.746

Table I.1 Experimental Conditions and Results of $k_1{}^a$ (continued)

T_5	P_5	A_{max}	NS_{max}	t_{25}	t_{50}	t_{75}	$k_1{}^b/10^{12}$
			X_{H_2}=0.10, X_{O_2}=0.005, X_{Ar}=0.895 (ϕ=10)				
1569	0.804	0.096	1714	207	229	244	0.845
1575	0.809	0.093	1783	200	217	231	0.904
1579	0.718	0.091	1538	207	226	245	0.900
1616	0.796	0.086	1755	176	193	205	1.01
1698	0.812	0.115	2865	142	155	167	1.30
1715	0.827	0.117	2960	138	152	162	1.32
1782	0.978	0.136	3988	94	104	113	1.39
1801	0.784	0.132	3341	114	127	138	1.52
1869	0.851	0.169	4725	94	104	112	1.67
1883	0.850	0.148	4527	91	102	110	1.82
2042	0.836	0.143	4876	65	74	81	2.41
2081	0.861	0.157	5804	60	68	74	2.63
2407	0.897	0.206	9744	33	39	44	4.16
2481	0.902	0.211	9930	31	36	41	4.31
2494	0.856	0.215	9787	31	37	42	4.42

[a] Units are K for T_5, atmosphere for P_5, s^{-1} for NS_{max}, μs for t_{25}, t_{50}, and t_{75} and $cm^3mol^{-1}s^{-1}$ for k_1.

[b] $k_1(NS_{max})$

Table I.2 Reaction Mechanism for $k_1{}^a$

	Reaction	A	n	θ	Reference
1.	$H + O_2 = OH + O$	7.13E+13	0.0	6957	*This study*
2.	$O + H_2 = OH + H$	1.87E+14	0.0	6854	31
3.	$OH + H_2 = H_2O + H$	2.14E+08	1.52	1736	25
4.	$O + H_2O = OH + OH$	4.51E+04	2.70	7323	32
5.	$O + O + M = O_2 + M$	1.00E+17	–1.0	0	33
	$Ar=1.0, H_2=2.9, O_2=1.2, H_2O=18.5$				
6.	$H + H + M = H_2 + M$	6.40E+17	–1.0	0	33
	$Ar=1.0, H_2=4.0, H_2O=12.0, H=26.0$				
7.	$H + O + M = OH + M$	6.20E+16	–0.6	0	8
	$Ar=1.0, H_2O=5.0$				
8.	$H + OH + M = H_2O + M$	8.40E+21	–2.0	0	33
	$Ar=1.0, H_2=2.5, H_2O=16.25$				
9.	$H + O_2 + M = HO_2 + M$	7.00E+17	–0.8	0	33
	$Ar=1.0, H_2=3.33, O_2=1.33, H_2O=21.3$				
10.	$HO_2 + H = OH + OH$	2.20E+14	0.0	710	34
11.	$HO_2 + H = H_2 + O_2$	2.50E+13	0.0	350	1
12.	$HO_2 + H = H_2O + O$	5.00E+12	0.0	710	34
13.	$HO_2 + O = O_2 + OH$	2.00E+13	0.0	0	1
14.	$HO_2 + OH = H_2O + O_2$	2.00E+13	0.0	0	1
15.	$HO_2 + HO_2 = H_2O_2 + O_2$	1.06E+11	0.0	–855	35
16.	$H_2O_2 + M = OH + OH + M$	1.20E+17	0.0	22900	33
	$Ar=0.67, O_2=0.78, H_2O=6.0$				
17.	$H_2O_2 + H = HO_2 + H_2$	1.70E+12	0.0	1900	1
18.	$H_2O_2 + H = H_2O + OH$	1.00E+13	0.0	1805	1
19.	$H_2O_2 + O = HO_2 + OH$	2.80E+13	0.0	3225	35
20.	$H_2O_2 + OH = H_2O + HO_2$	7.00E+12	0.0	720	1

^{a} Rate coefficients are in the form $k = A\,T^n \exp(-\theta / T)$.
Units are cm^3, K, mol, and s.

$$\varepsilon_{\omega_0} = S \times g(\omega_0)$$

$$= \frac{\pi e^2}{m_e c^2} \frac{n''}{n} f_{lu} \left(1 - e^{-h\omega_0/k_B T}\right) g(\omega_0), \tag{4}$$

where ε_{ω_0} is the spectral line absorption coefficient at $\omega_0(s^{-1})$, S is the integrated absorption, $g(\omega_0)$ is the value of the shape function (Voigt profile) at ω_0, e and m_e are the electronic charge and mass, respectively, c is the speed of light, n and n" are the total and ground state number densities of OH, respectively, k_B and h are the Boltzmann and Planck constants, respectively, and f_{lu} is the line absorption oscillator strength. The oscillator strength, f_{lu}, was calculated from the following expression [36, 37, 38] :

$$f_{lu} = \frac{f_{v'v''} S_{J'J''} T_{J'J''}}{2J'' + 1}, \tag{5}$$

where $f_{v'v''}$ is the $v' \leftarrow v''$ band oscillator strength, $S_{J'J''}$ is the $J' \leftarrow J''$ rotational line intensity factor (Hönl-London factor), and $T_{J'J''}$ is the correction factor for vibration-rotation interaction. For the $P_1(5)$ line of the (0,0) band of OH $A^2\Sigma^+$ $\leftarrow X^2\Pi$ transition employed in this study, $f_{v'v''} = 1.1 \times 10^{-3}$ [39], $S_{J'J''} = 6.13$ [40], and $T_{J'J''} = 0.978$ [41] were used. The fraction of molecules in the ground state (n"/n) was computed from the Boltzmann equation with the local thermal equilibrium (LTE) assumption,

$$\frac{n''}{n} = \frac{(2J'' + 1) \exp\left[-(E_v + E_J)/k_B T\right]}{Q} \tag{6}$$

where E_v and E_J are the vibrational and rotational energies, respectively, and

Q is the total internal partition function $(Q_{v,J} \times Q_{el})$. The rovibrational partition function, $Q_{v,J}$ was calculated using higher approximations for the rotational and vibrational energy levels [42], i.e., including terms for the anharmonicity of the potential energy curve, the influence of centrifugal force, and the fact that a molecule is a vibrating rotator. The reference energy level was defined as the $v=0$ state. In the rotational and vibrational energy calculation, the vibrational frequency (ω_e), the anharmonicity correction $(\omega_e x_e)$, the rotational-energy constant (B_e) at the equilibrium nuclear distance and the term for vibrating rotator (α) were taken from the literature [43]. For the electronic partition function, $Q_{el} = 4$ was assigned because of the Lambda-doubling of the ground Π state of OH due to the coupling of spin-orbit and spin-internuclear axis rotation [43].

In generating OH absorption profiles, because the information for the collision broadening for the $P_1(5)$ line is not known, the Voigt profile $(g(\omega_o))$ was not calculated. Instead, a self-calibration scheme was employed, i.e., the value of the shape function $(g(\omega_o))$, hence, $\varepsilon(OH)$, was systematically varied until satisfactory matches to the experimental observables were obtained. The absorption coefficients obtained in this way are shown in Figure I.3.

The local logarithmic response sensitivities defined below [44] were computed for the four experimental conditions presented before (Figures I.2 (a) - (d)). :

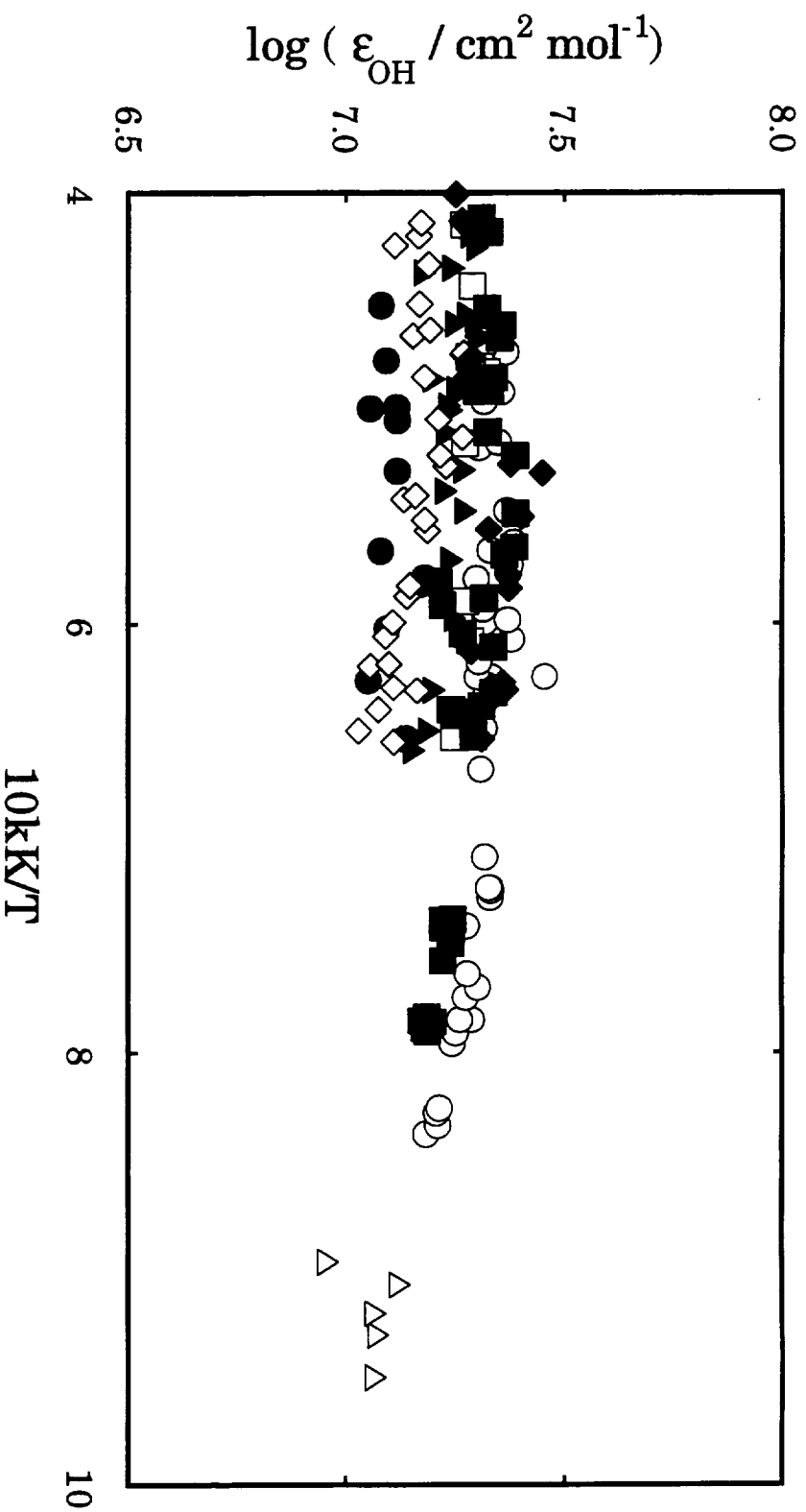$$S_{ij} = ln(R'_j / R_j) / ln(P'_i / P_i), \tag{7}$$

Figure I.3 Molar absorption coefficients (base e) of OH at 310.032 nm (air). Absorption coefficients show temperature and pressure dependence. Symbols are ▲ for X_{H_2} = 0.04, X_{O_2} = 0.01, X_{Ar} = 0.95, P = 0.95 ~ 2.3 atm, ○ for X_{H_2} = 0.02, X_{O_2} = 0.005, X_{Ar} = 0.975, P_{av} = 0.8 atm, □ for X_{H_2} = 0.004, X_{O_2} = 0.001, X_{Ar} = 0.995, P_{av} = 2.0 atm, ● for X_{H_2} = 0.002, X_{O_2} = 0.0005, X_{Ar} = 0.9975, P_{av} = 4.0 atm, ■ for X_{H_2} = 0.05, X_{O_2} = 0.005, X_{Ar} = 0.945, P_{av} = 0.8 atm, ▲ for X_{H_2} = 0.02, X_{O_2} = 0.002, X_{Ar} = 0.978, P_{av} = 1.8 atm, ◆ for X_{H_2} = 0.01, X_{O_2} = 0.001, X_{Ar} = 0.989, P_{av} = 3.4 atm, ▷ for X_{H_2} = 0.1, X_{O_2} = 0.005, X_{Ar} = 0.895, P_{av} = 0.8 atm.

where $P_i=\{k_i\}$ and $\varepsilon(OH)$, and $R_j = A_{max}$, NS_{max} and t_{50}. Figures I.4 (a) - (d) show the sensitivities for A_{max}, NS_{max} and t_{50} by raising $\{k_i\}$ and $\varepsilon(OH)$ by 30%. At 1234 K (Figure I.4 (a)), reactions (1), (2), (3) and $\varepsilon(OH)$ are sensitive to NS_{max} while reactions (1) and (2) are sensitive to t_{50}. When the rate coefficients of reactions (1) and (2) were increased, the values of A_{max} were also increased because of more OH production, whereas the increase of k_3 caused the decrease of A_{max} due to the consumption of OH by reaction (3), OH + H_2 = H_2O + H. The sensitivity of A_{max} on $\varepsilon(OH)$ is not shown here for obvious reasons. At 1556 K (Figure I.4 (b)), the sensitivities for NS_{max} and t_{50} are basically the same as at 1234 K, while only reaction (1) shows a little sensitivity for A_{max}. At Figure I.4 (c) condition (1700 K, 3.2 atm), the sensitivities of NS_{max} and t_{50} on reaction (2) disappear and reaction (11) becomes important. Again reactions (1) and (3) are sensitive to A_{max} as in the case of 1234 K. At 2163 K (Figure I.4 (d)), nothing shows sensitivity on A_{max}. NS_{max} is sensitive to reaction (1) and $\varepsilon(OH)$ while t_{50} is sensitive to the reactions (1), (3) and (11). Overall, NS_{max} is sensitive to reaction (1) and $\varepsilon(OH)$ while t_{50} is sensitive only to reaction (1). Therefore, k_1 could be determined by matching only characteristic times (t_{25}, t_{50} and t_{75}) without any interference from absorption characteristics. However, the effect of possible contaminants present must be considered. The influence of contaminants was investigated for test gas mixtures presumed to contain C_3H_8 or H-atom at the level of 0.05 to 0.5 ppm and 5 to 50 ppb, respectively. A reaction mechanism reported by Frenklach and Bornside [45] capable of simulating reaction paths for CH_4 and CH_4/C_3H_8 mixture oxidation was used. Absolute sensitivities of t_{50} defined as $(Y'-Y_0)/Y_0$, are given in Figures I.5 (a)-(d). At low to middle temperatures (Figures I.5 (a)-(c)), as $X_{C_3H_8}$ increases t_{50} decreases
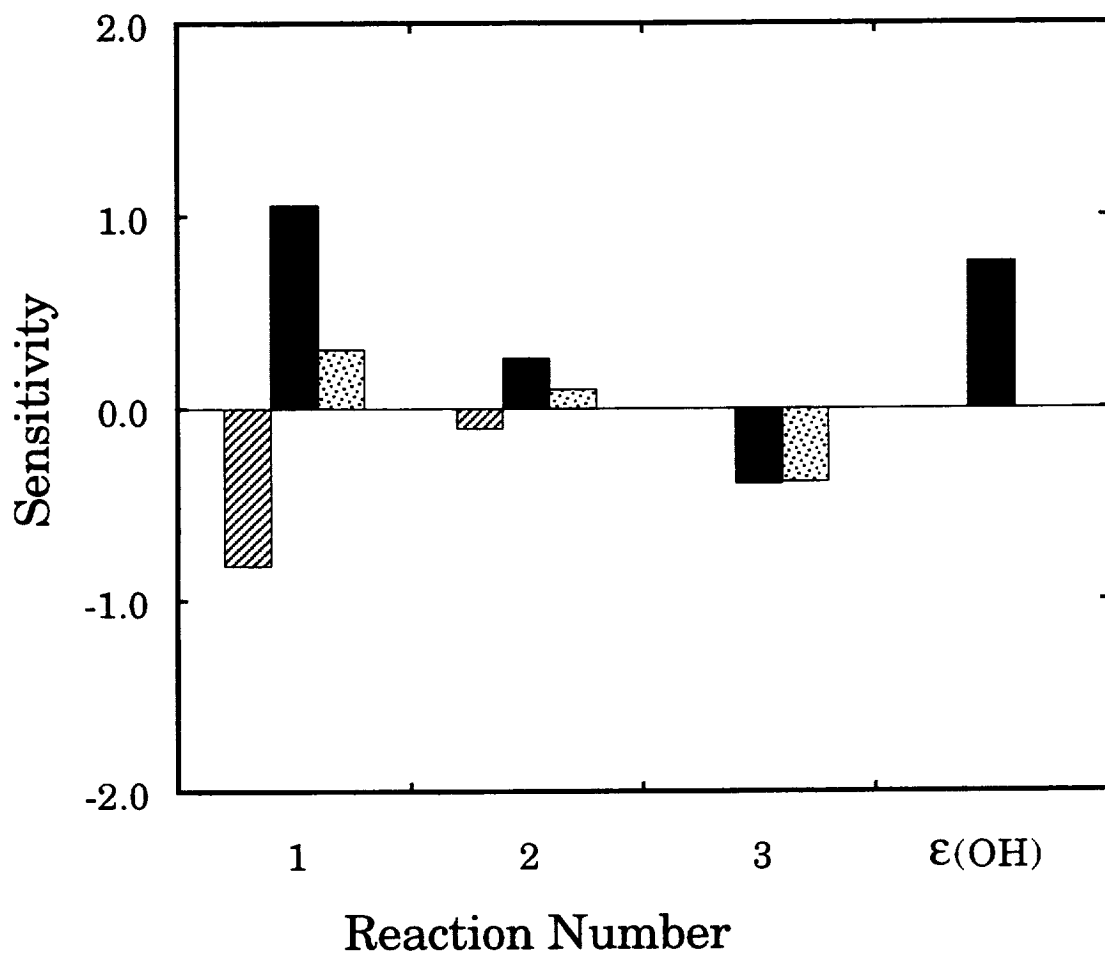
Figure I.4(a) Sensitivity spectrum for the experimental condition of X_{H_2} = 0.02, X_{O_2} = 0.005, X_{Ar} = 0.975, T_5 = 1234 K and P_5 = 0.945 atm. Ordinate is logarithmic sensitivity defined in the text. Reaction numbers are listed in Table I.3. Sensitivity was computed setting rate coefficients to 1.3 × Table I.3 values and the absorption coefficient obtained in Figure I.3. ■ NS_{max} sensitivity, ▣ A_{max} sensitivity and ▨ t_{50} sensitivity. All noticeable changes are included.
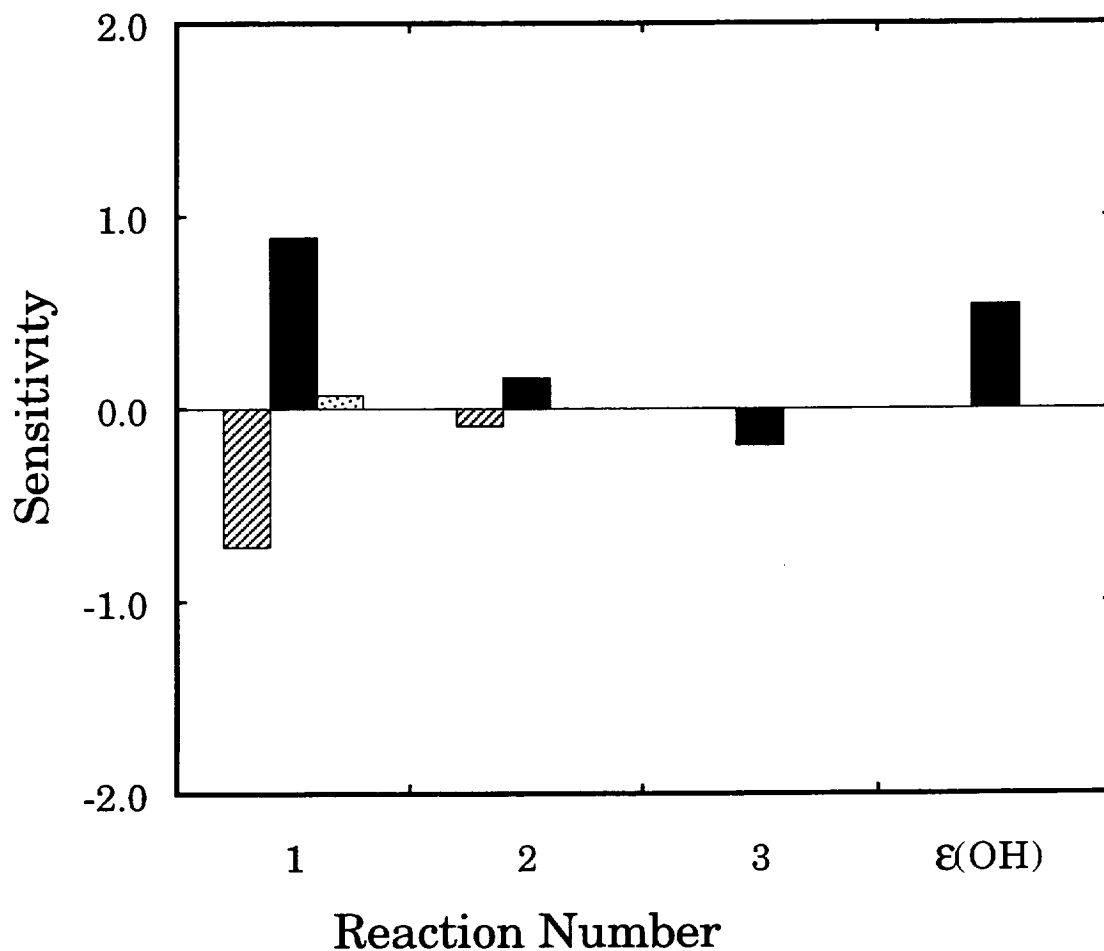
Figure I.4(b) Sensitivity spectrum for the experimental condition of X_{H_2} = 0.02, X_{O_2} = 0.005, X_{Ar} = 0.975, T_5 = 1556 K and P_5 = 0.751 atm. Ordinate is logarithmic sensitivity defined in the text. Reaction numbers are listed in Table I.3. Sensitivity was computed setting rate coefficients to 1.3 × Table I.3 values and the absorption coefficient obtained in Figure I.3. ■ NS_{max} sensitivity, ▣ A_{max} sensitivity and ▨ t_{50} sensitivity. All noticeable changes are included.
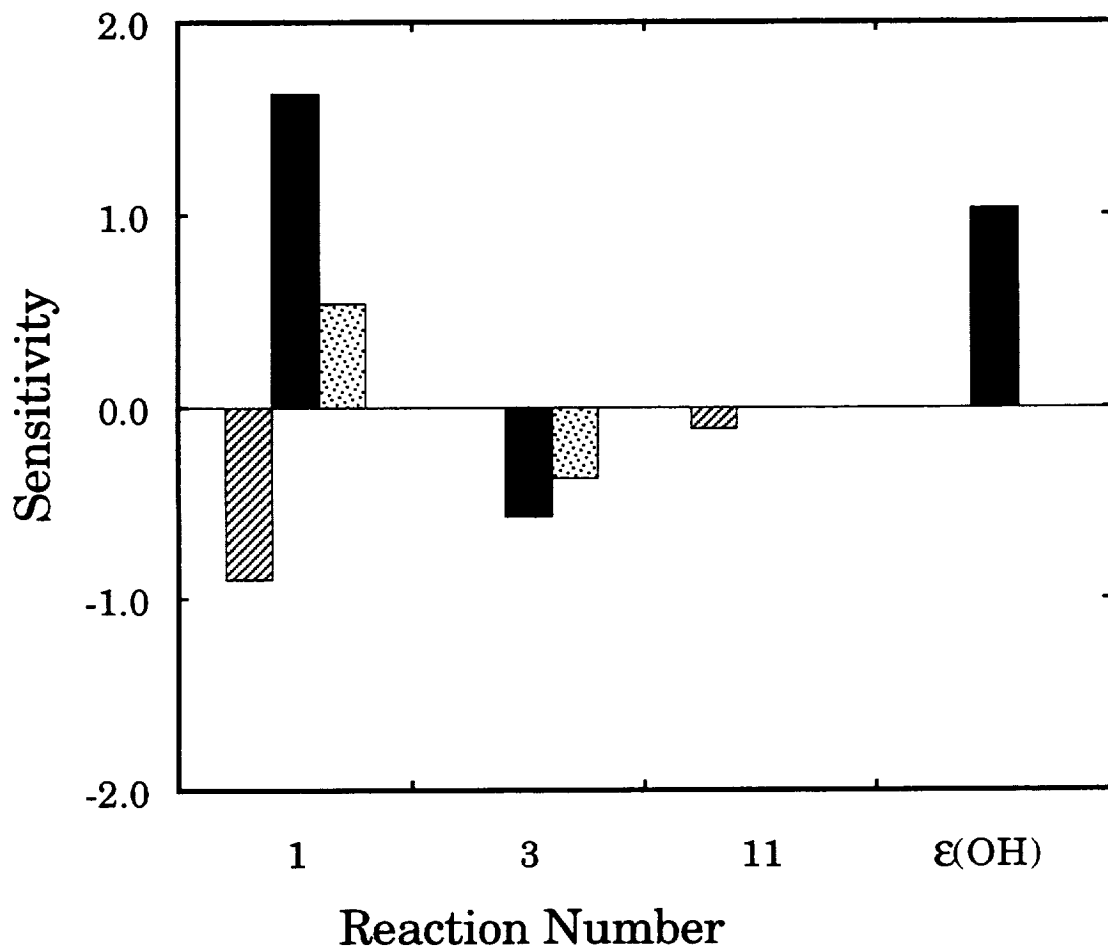
Figure I.4(c) Sensitivity spectrum for the experimental condition of $X_{H_2} =$ 0.01, $X_{O_2} = 0.001$, $X_{Ar} = 0.989$, $T_5 = 1700$ K and $P_5 = 3.203$ atm. Ordinate is logarithmic sensitivity defined in the text. Reaction numbers are listed in Table I.3. Sensitivity was computed setting rate coefficients to 1.3 × Table I.3 values and the absorption coefficient obtained in Figure I.3. ■ NS_{max} sensitivity, ⊡ A_{max} sensitivity and ▨ t_{50} sensitivity. All noticeable changes are included.

Figure I.4(d) Sensitivity spectrum for the experimental condition of X_{H_2} = 0.02, X_{O_2} = 0.002, X_{Ar} = 0.978, T_5 = 2163 K and P_5 = 1.994 atm. Ordinate is logarithmic sensitivity defined in the text. Reaction numbers are listed in Table I.3. Sensitivity was computed setting rate coefficients to 1.3 × Table I.3 values and the absorption coefficient obtained in Figure I.3. ■ NS_{max} sensitivity, ▨ A_{max} sensitivity and ▨ t_{50} sensitivity. All noticeable changes are included.
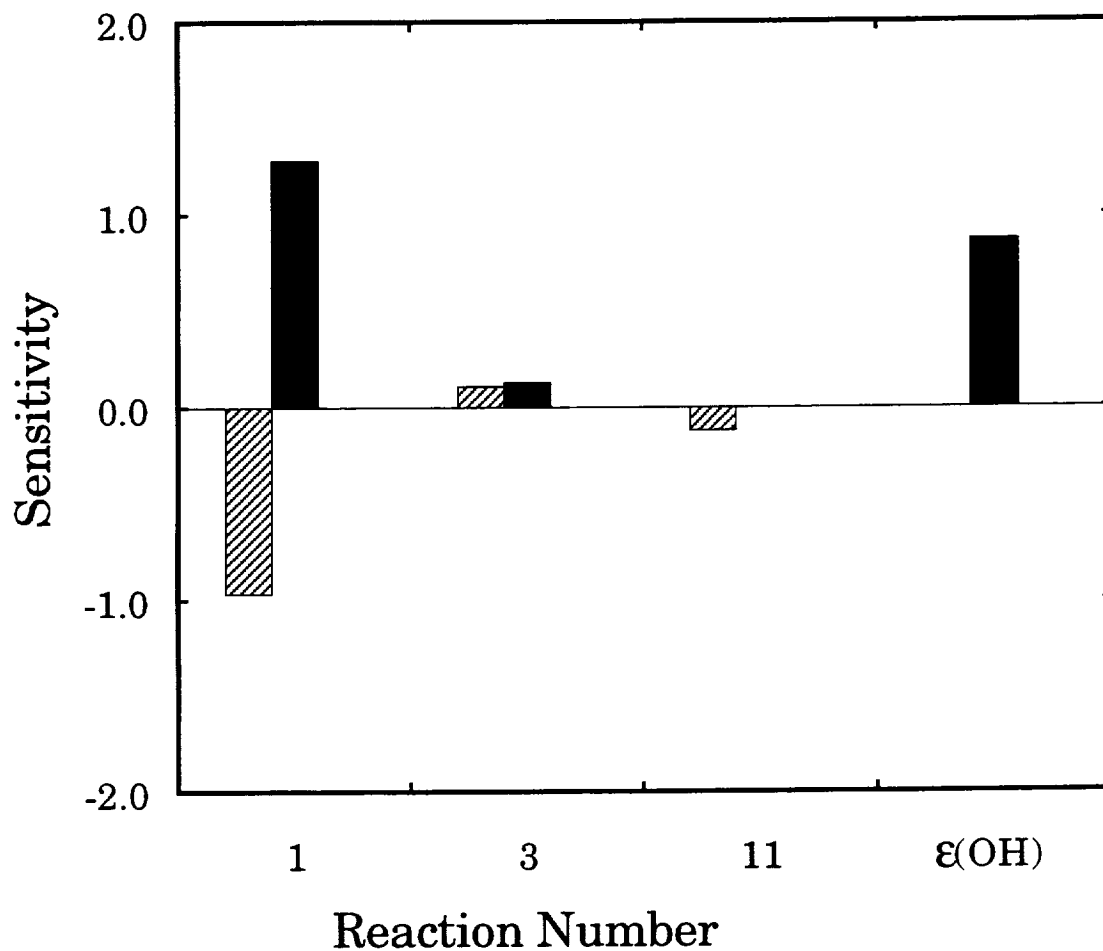
Figure I.5(a) Sensitivity spectrum of t_{50} by H-atom or C_3H_8 impurity for the experimental condition of $X_{H_2} = 0.02$, $X_{O_2} = 0.005$, $X_{Ar} = 0.975$, $T_5 = 1234$ K and $P_5 = 0.945$ atm. Ordinate is absolute sensitivity defined as $(Y' - Y_o) / Y_o$ where Y_o is the value of t_{50} without H-atom or C_3H_8 impurity. ▨ H-atom sensitivity and ■ C_3H_8 sensitivity.
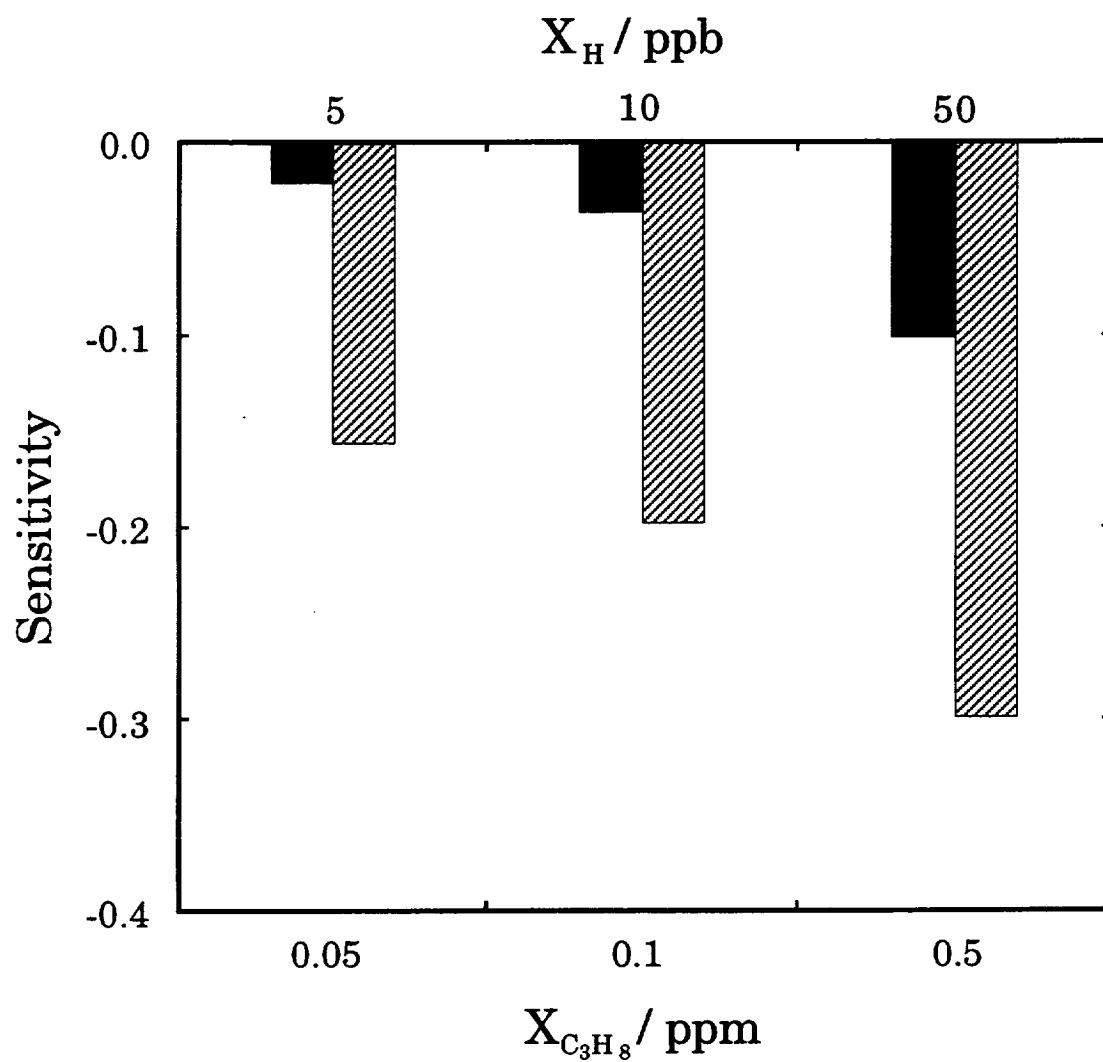
Figure I.5(b) Sensitivity spectrum of t_{50} by H-atom or C_3H_8 impurity for the experimental condition of $X_{H_2} = 0.02$, $X_{O_2} = 0.005$, $X_{Ar} = 0.975$, $T_5 = 1556$ K and $P_5 = 0.751$ atm. Ordinate is absolute sensitivity defined as $(Y' - Y_o) / Y_o$ where Y_o is the value of t_{50} without H-atom or C_3H_8 impurity. ▨ H-atom sensitivity and ■ C_3H_8 sensitivity.

Figure I.5(c) Sensitivity spectrum of t_{50} by H-atom or C_3H_8 impurity for the experimental condition of X_{H_2} = 0.01, X_{O_2} = 0.001, X_{Ar} = 0.989, T_5 = 1700 K and P_5 = 3.203 atm. Ordinate is absolute sensitivity defined as (Y' – Y_o) / Y_o where Y_o is the value of t_{50} without H-atom or C_3H_8 impurity. ▨ H-atom sensitivity and ■ C_3H_8 sensitivity.
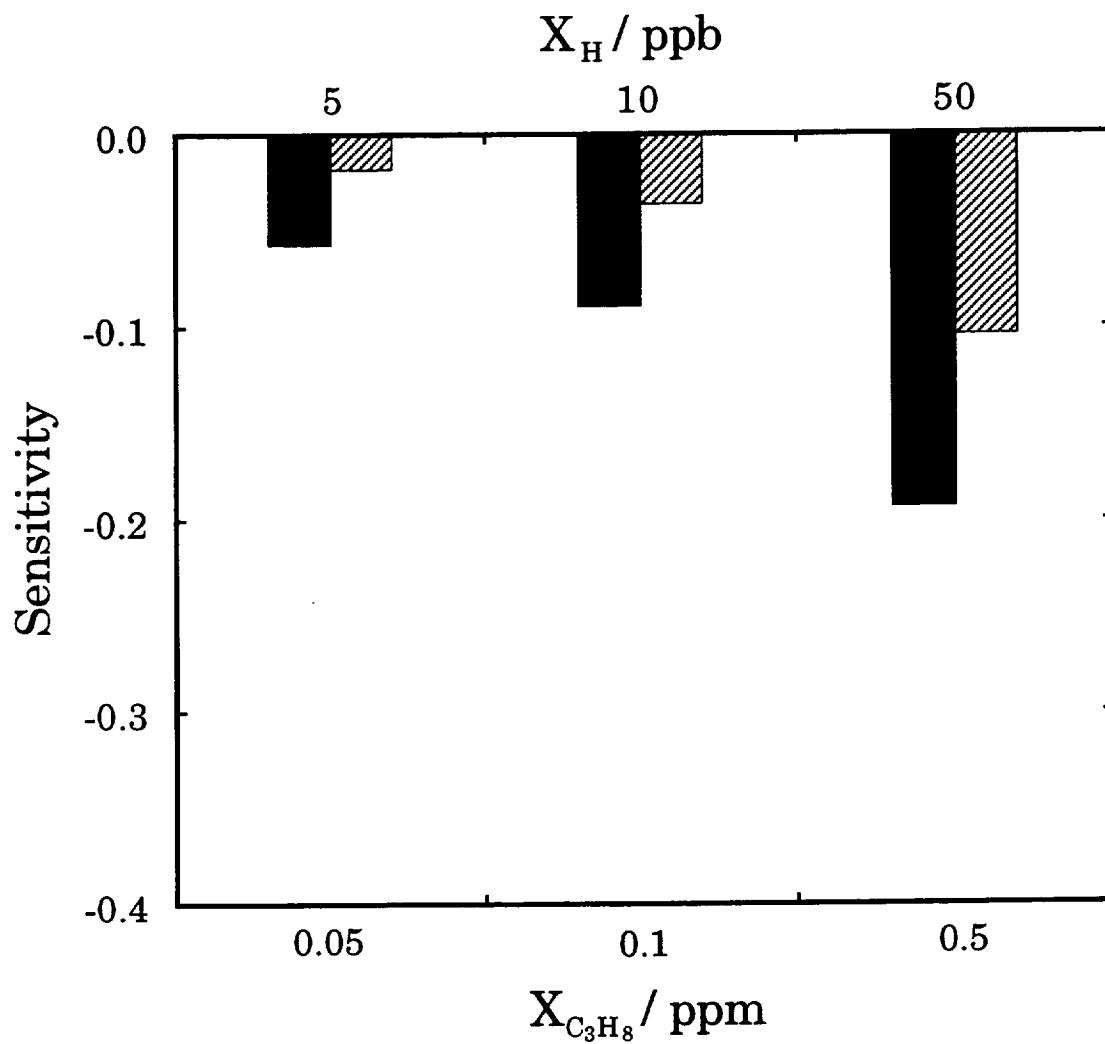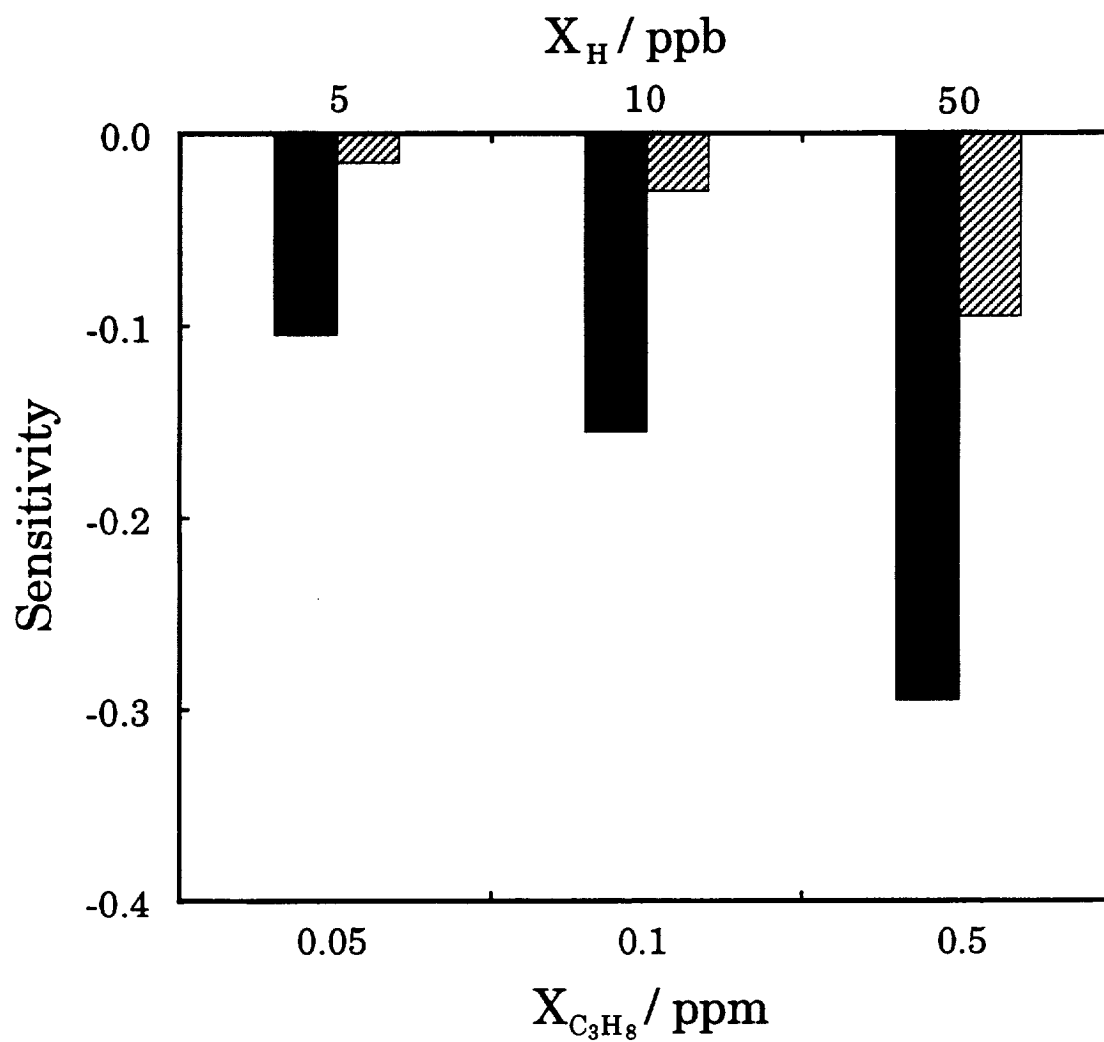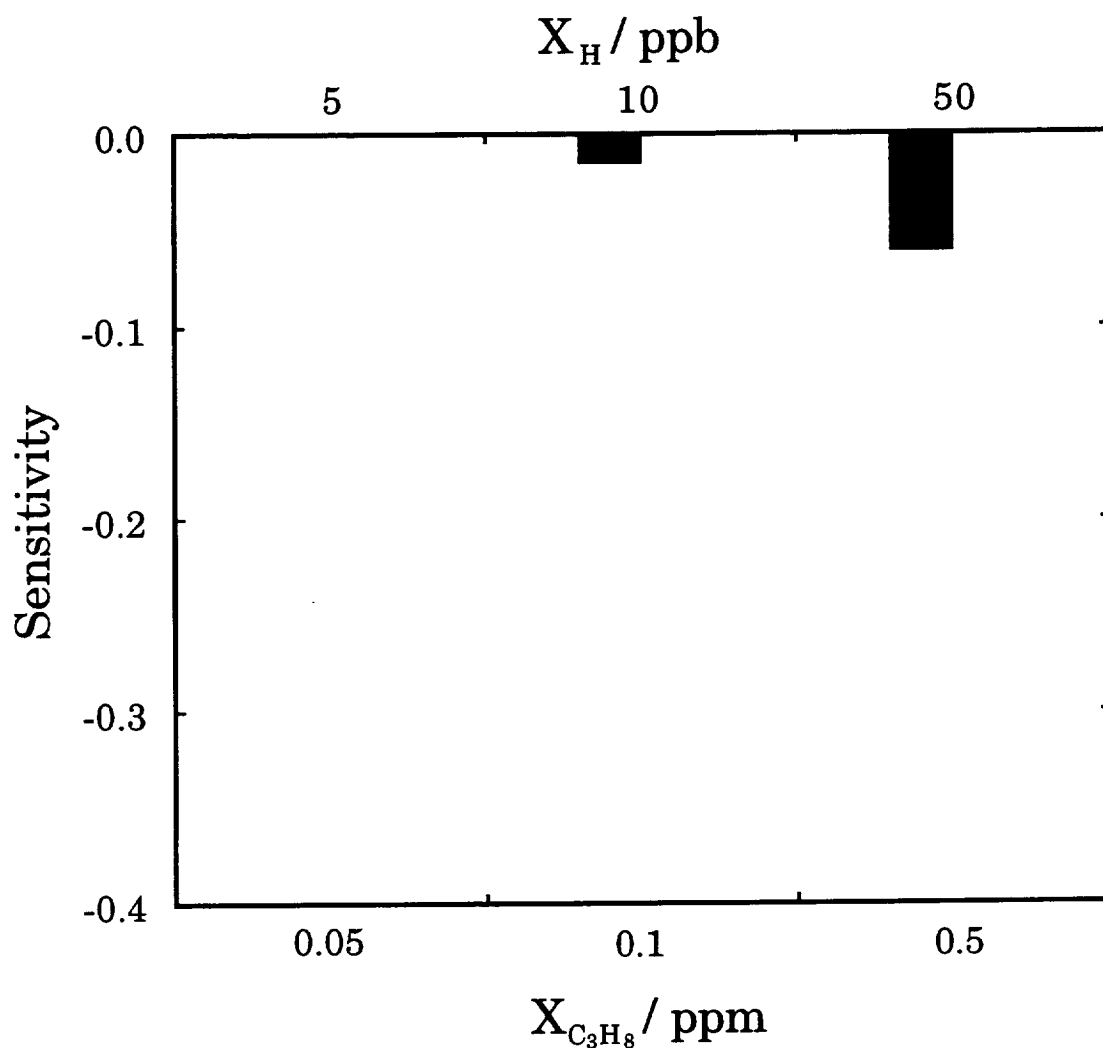
Figure I.5(d) Sensitivity spectrum of t_{50} by H-atom or C_3H_8 impurity for the experimental condition of $X_{H_2} = 0.02$, $X_{O_2} = 0.002$, $X_{Ar} = 0.978$, $T_5 = 2163$ K and $P_5 = 1.994$ atm. Ordinate is absolute sensitivity defined as (Y' $- Y_o$) / Y_o where Y_o is the value of t_{50} without H-atom or C_3H_8 impurity. ▨ H-atom sensitivity and ■ C_3H_8 sensitivity.

markedly, obviously owing to the increase of the C_3H_8 decomposition rate to produce H-atoms. At 2163 K, H-atoms are generated by the fast initiation reactions ($H + H + M = H_2 + M$ and $H + HO_2 = H_2 + O_2$) so that contaminant effects were found to be small. At 1234 K, even though the effect of C_3H_8 is not as big as at higher temperatures (1556 K and 1700 K) because of the slow decomposition of C_3H_8, the effect of H-atoms which could be produced easily from other possible contaminants (e.g., long-chain hydrocarbons such as vacuum pump oil), is great as seen in Figure I.5 (a). As an example, matching t_{50}, shortened about 10% by contaminants, requires about a 15% increase of k_1. At all conditions tested the sensitivity of NS_{max} to the added contaminants was negligible.

Based upon the sensitivity analysis for $\{k_i\}$, $\varepsilon(OH)$ and contaminants, the parameters k_1 and $\varepsilon(OH)$ were chosen for simultaneous optimization. Goodness of match to the experimentally determined NS_{max} and A_{max} was the criteria used in optimization. In the simulation, NS_{max}, the normalized slope at maximum OH growth, was generated from the time derivative of the light transmittance:

$$NS_{max} = abs\{d(I/I_o)/dt\}_{max}$$

$$= abs\{-\varepsilon(OH) \times l \times exp[-\varepsilon(OH) \times l \times C_{OH}] \times (dC_{OH}/dt)\}_{max} \qquad (8)$$

where I/I_o is the transmittance, $\varepsilon(OH)$ is the absorption coefficient of OH, l is the light path length and C_{OH} is the OH concentration. The NS_{max} is not only a function of $\varepsilon(OH)$ as seen in the above equation, but also being exclusively dependent upon k_1. This indicates that k_1 and $\varepsilon(OH)$ are coupled together on

NS_{max} and A_{max} . This coupling can also be observed in the sensitivity analyses. For instance, the sensitivities of $\varepsilon(OH)$ on NS_{max} amount to about half of the sensitivities of k_1 at the conditions given before. Thus it seems difficult to separate the effects of k_1 and $\varepsilon(OH)$ on NS_{max} and A_{max} unless a special statistical method is employed. However, if k_1 is changed by 30% with a fixed value of $\varepsilon(OH)$, the sensitivities of NS_{max} are more than three times as large as those of A_{max} . Therefore it is possible to simultaneously optimize k_1 and $\varepsilon(OH)$ without relying upon the extensive parameter optimization techniques used elsewhere [9, 33, 46, 47, 48, 49]. In the simulation the absorption coefficient of OH was varied first to match A_{max}, then k_1 was varied to match NS_{max} . This procedure was repeated several times until satisfactory matches were achieved. The reaction rate coefficient expressions of k_2 and k_3 in Table I.2 were assumed to be correct and were not subjected to the optimization, although they showed some sensitivities at T < 1700 K. For k_2, the two parameter rate coefficient expression of Sutherland et al. [31] (880 K $\leq$ T $\leq$ 2495 K) was used. Recent results from this laboratory indicate that k_2 could be best represented by an Arrhenius rather than a non-Arrhenius type expression in the temperature range of interest in this study. For k_3, a recent fit to the existing data was taken [25].

The values of k_1 obtained in this way are listed in the last column of Table I.1 and are presented in Figure I.6. The least squares fit to the data for 1050 K $\leq$ T $\leq$ 2500 K is given by

$$k_1(NS_{max}) = (7.13 \pm 0.31) \times 10^{13} \ \exp(-6957 \pm 30 \ K/T) \ cm^3 \ mol^{-1} \ s^{-1} \quad (9)$$

with uncertainties of 1-σ standard deviation. In the simulation there was a temperature rise during the course of reaction. As k_1 was determined using the OH growth early in the reaction and ε(OH) was determined using the maximum absorption rate in the reaction, the temperatures at those relative reaction times varied by less than 25 K depending upon initial conditions. The expression for the temperature dependent shape function ($g(\omega_o)$) for ε(OH) given by Hanson and coworkers [50] gave negligible change in ε(OH) during the reaction due to the increase of temperature.

As the coupling between k_1 and ε(OH) is not reflected on {t_{25}, t_{50} and t_{75}} and A_{max} , k_1 and ε(OH) were also optimized using characteristic times and A_{max} by ignoring possible contamination effect. The results are plotted in Figure I.7. The solid line represents the least squares fit to the data and is given by

$$k_1(\{t_i\}) = (7.19 \pm 0.41) \times 10^{13} \ \exp(-7015 \pm 40 \ K/T) \ cm^3 \ mol^{-1} \ s^{-1} \quad (10)$$

for 1050 K ≤ T ≤ 2500 K. The uncertainties are 1-σ standard deviation. The 1-σ standard deviation of individual points from the $k_1(NS_{max}$) and $k_1(\{t_i\})$ are ± 4% and ± 6% respectively.

C. Error Analysis

Error analyses for individual $k_1(NS_{max}$) and $k_1(\{t_i\}))$ were performed under high temperature conditions since the most probable uncertainties in the measurements of the incident shock velocity and of the pressure of the

Figure I.6 Arrhenius plot of the experimental data of $k_1(NS_{max})$. The solid line is the least squares fit to the data, $k_1(NS_{max}) = 7.13 \times 10^{13}$ exp(– 6957 K/T) $cm^3mol^{-1}s^{-1}$ (1050 K ≤ T ≤ 2500 K). Symbols are Δ for φ = 2 mixtures, □ for φ = 5 mixtures, O for φ = 10 mixtures, and ● for φ = 15 mixtures (15.0% H_2, 0.5% O_2, 84.5% Ar). The data for φ = 15 mixtures were not included in the least square fit for $k_1(NS_{max})$ (see text).
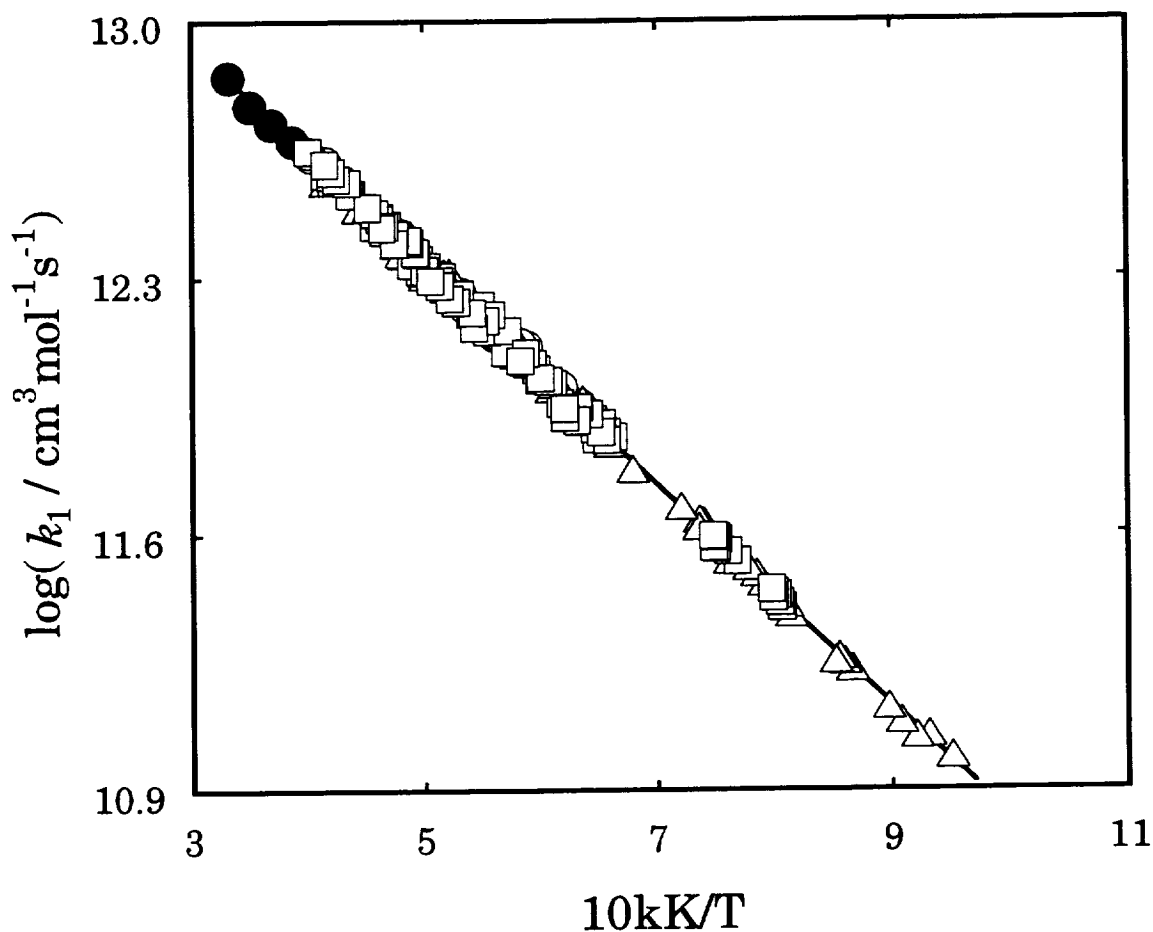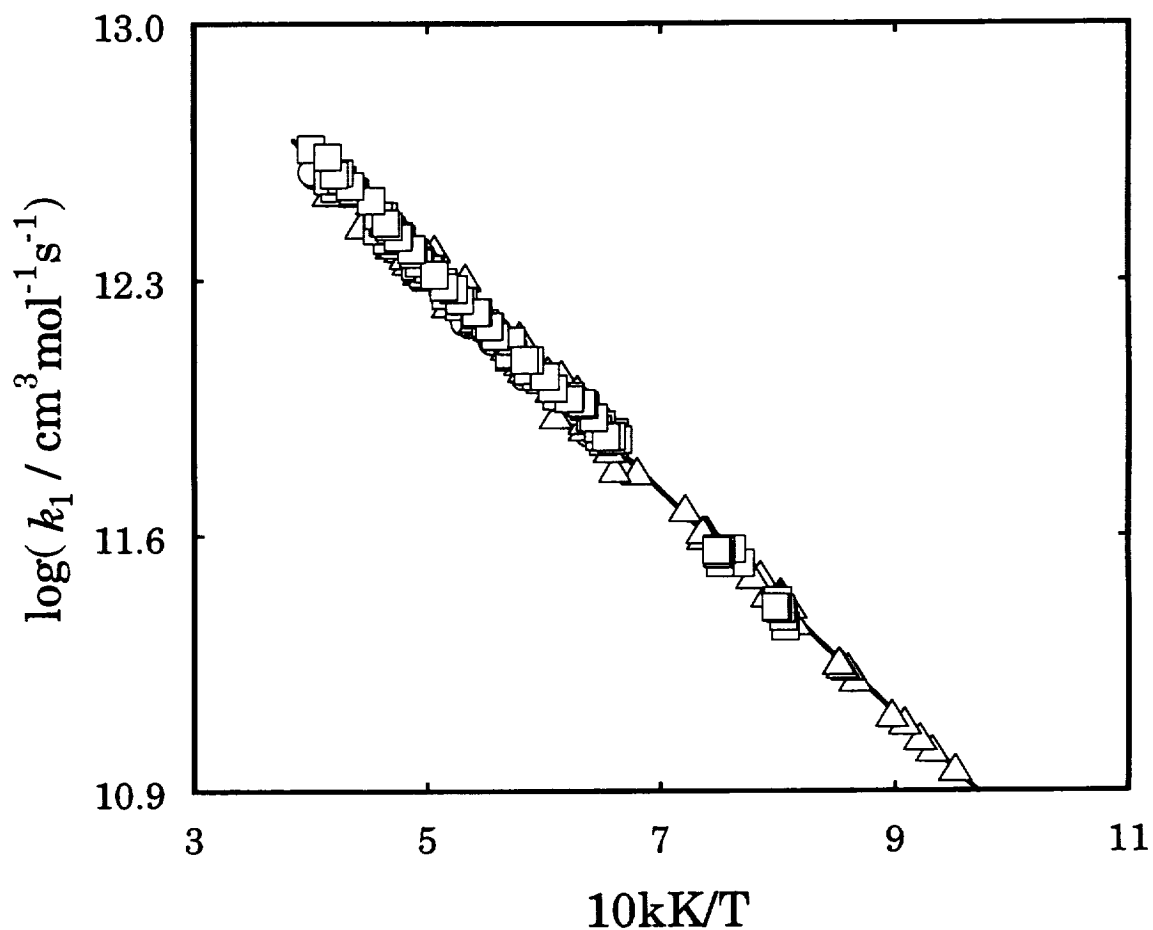
Figure I.7 Arrhenius plot of the experimental data of $k_1(\{t_i\})$. The solid line is the least squares fit to the data, $k_1(\{t_i\}) = 7.19 \times 10^{13}$ exp($-$ 7015 K/T) cm^{3}mol^{-1}s^{-1} (1050 K $\leq$ T $\leq$ 2500 K). Symbols are $\triangle$ for ϕ = 2 mixtures, $\square$ for ϕ = 5 mixtures, O for ϕ = 10 mixtures.

reflected shock region (P_5) were from the high temperature experiments. The sampling time of the oscilloscopes used in the incident shock velocity measurements was set to 0.5 µs per point. If we consider 1 µs as the maximum uncertainty in time measurement, this uncertainty propagates to 0.5% error in shock velocity, which yields 0.9% error in T_5 and 0.5% error in k_1. As described before, P_5, used for the correction of T_5, was obtained from the last pressure transducer signal. About 0.7% reading error of the signal output resulted in a 0.7% error for P_5, which produced a 0.2% error in the corrected T_5 and a 1.0% error in k_1. The error in k_1 from the initial test gas mixture pressure (P_1) was negligible. Although the possible errors introduced in the mixture preparation is small, the effect on k_1 is not ignorable and they are appropriately considered in the error propagation analysis below.

The largest error introduced to $k_1(NS_{max})$ was from NS_{max}. The maximum error in the measurement of NS_{max} was 6%, which alone generated an error of 3% in $k_1(NS_{max})$. The matching error of less than 4% for the computed to the experimental NS_{max} is within the error bounds of NS_{max} considered above. Since the coupling between $k_1(NS_{max})$ and A_{max} through $\varepsilon(OH)$ is not discernible at high temperatures as shown in the sensitivity analysis, the error to $k_1(NS_{max})$ from A_{max} evaluation was examined under the low temperature condition (1234 K) of Figure I.4 (a). Simulations indicated that a 3.0% error in A_{max} could only change the value of $k_1(NS_{max})$ by less than 0.5%.

The maximum uncertainty in taking characteristic times from experimental records was 2.0%, resulting in 2.0% error in $k_1(\{t_i\})$. Because the

characteristic times are not coupled with $\varepsilon(OH)$, errors in A_{max} do not induce any error in $k_1(\{t_i\})$. The maximum error in matching, for example, t_{50}, is 2.0% and the effect on $k_1(\{t_i\})$ is also 2.0%.

The propagation of error was computed using the following equation at a high temperature condition of Figure I.4 (d), [51],

$$\varepsilon(F) = \text{sqrt}\left\{\left(\frac{\partial F}{\partial x}\right)^2_{y,z} [\varepsilon(x)]^2 + \left(\frac{\partial F}{\partial y}\right)^2_{z,x} [\varepsilon(y)]^2 + \left(\frac{\partial F}{\partial z}\right)^2_{x,y} [\varepsilon(z)]^2 + \cdots\right\} \qquad (11)$$

where F is the individual data points of $k_1(NS_{max})$ or of $k_1(\{t_i\})$ and $x, y, z, \ldots$ are error sources. A very conservative error propagation analysis with all the possible errors mentioned above gives errors for $k_1(NS_{max}) = \pm 6.0\%$ and for $k_1(\{t_i\}) = \pm 7.5\%$. The percentage contributions to the errors for the data of $k_1(NS_{max})$ are 54% for NS_{max}, 24% for P_5 in the temperature correction, 10% for incident shock velocity, and 10% and 2% for ΔX_{O_2} and ΔX_{H_2} of the initial mixture composition, respectively. A similar distribution of the error contributions was also obtained for $k_1(\{t_i\})$.

Discussion

Figures I.2 (a) - (d) show the computed profiles (smooth lines) by using the reaction mechanism in Table I.2. At temperatures of 1556 K, 1700 K and

2163 K with different final pressures and mixture compositions, the Table I.2 reaction mechanism reproduced the experimental profiles quite well. However, as seen in Figure I.2(a) (1234 K), the simulation underpredicts the OH concentration after the peak. Only more than a factor of 10 reduction of k_6 (H + H + M = H_2 + M), which does not affect the pre-peak absorption profile at all, could bring the simulated OH concentration to the experimental level. This disagreement is possibly due to either the additional heating of the still moving gas toward the reaction zone long after the beginning of the reaction ($\sim 1ms$) so that the OH producing reactions proceeded faster while the computer simulations could not properly account for these phenomena, or it is due to the current incomplete understanding of HO_2 chemistry at these conditions. Despite this mismatch after the absorption peak at low temperatures, the k_1 values reported in this study are valid because the rapid growth of OH concentration is mostly influenced by the chain branching reaction, H + O_2 = OH + O, and in any case the matches to the pre-peak experimental profiles are excellent. This is further manifested by the exact reproduction of the timewise change of the pre-peak OH concentration.

The absorption coefficients of OH (Figure I.3) show two distinct characteristics, i. e., dependence upon temperature and pressure. They show a small positive temperature dependence, absorption coefficients being slightly high at high temperatures. The temperature dependence comes mainly from the Boltzmann fraction in the integrated absorption (S) expression and the Voigt function ($g(\omega_o)$). As temperature increases, the Boltzmann fraction decreases and the value of the Voigt function at fixed pressure increases because of the decrease of the spectral line broadening [27, 28, 29, 30].

However, the positive temperature dependence indicates that the Voigt function is a stronger function of temperature than the Boltzmann fraction. The pressure dependence of $\epsilon(OH)$ can be interpreted in terms of the spectral line broadening due to collision (collision broadening). The collision broadening width is directly proportional to the system pressure [27, 50]. As expected, $\epsilon(OH)$ decreased as pressure increases at fixed temperature. Because the Voigt function is the convolution integral of Gaussian (Doppler) and Lorentzian (collision) function [27, 28, 29, 30], its value optimized for each experiment reflects the extent of contribution by collision broadening to $\epsilon(OH)$ [52].

In Figures I.8 and I.9 the matches between the experimental and computed NS_{max} and A_{max} are seen, within the data scatter of $\pm$ 4% and $\pm$ 3%, respectively, to be excellent over the entire range of temperature and density of the various compositions of the mixtures studied. The mean deviations are $0.0 \pm 0.96\%$ for NS_{max} and $0.15 \pm 0.68\%$ for A_{max}. The uncertainties are 1-σ deviation. The optimized A_{max} could not be distinguished in the evaluation of $k_1(NS_{max})$ and $k_1(\{t_i\})$ in most cases. Figure I.10 shows the match of a characteristic time, t_{50}. The mean value of the deviation is – 0.42% with a standard deviation of 1.42%. The negative mean deviation of t_{50} denotes that the simulated t_{50}'s are slightly shorter. However, it is within noise level, especially at high temperatures. For example, at 2163 K, the measured t_{50} was 64.0 μs with an error of $\pm$ 1.0 μs or $\pm$ 2%.

The $k_1(\{t_i\})$ expression gives always slightly lower values than $k_1(NS_{max})$ over the full temperature ranges, but the differences are quite small; at 1050 K, $k_1(NS_{max}) = 9.45 \times 10^{10}$ $cm^3mol^{-1}s^{-1}$, $k_1(\{t_i\}) = 9.02 \times 10^{10}$ $cm^3mol^{-1}s^{-1}$ while

Figure I.8 Match between experimental and calculated values of NS_{max}.
The percent deviation is defined as $100 \times [NS_{max}$ (calculation) $- NS_{max}$
(experiment)$]/ NS_{max}$ (experiment). Symbols are Δ for $\phi = 2$ mixtures, $\square$
for $\phi = 5$ mixtures, and O for $\phi = 10$ mixtures.

Figure I.9 Match between experimental and calculated values of A_{max}. The percent deviation is defined as $100 \times [A_{max}$ (calculation) $- A_{max}$ (experiment)]/ A_{max} (experiment). Symbols are $\triangle$ for $\phi = 2$ mixtures, $\square$ for $\phi = 5$ mixtures, and $\bigcirc$ for $\phi = 10$ mixtures.
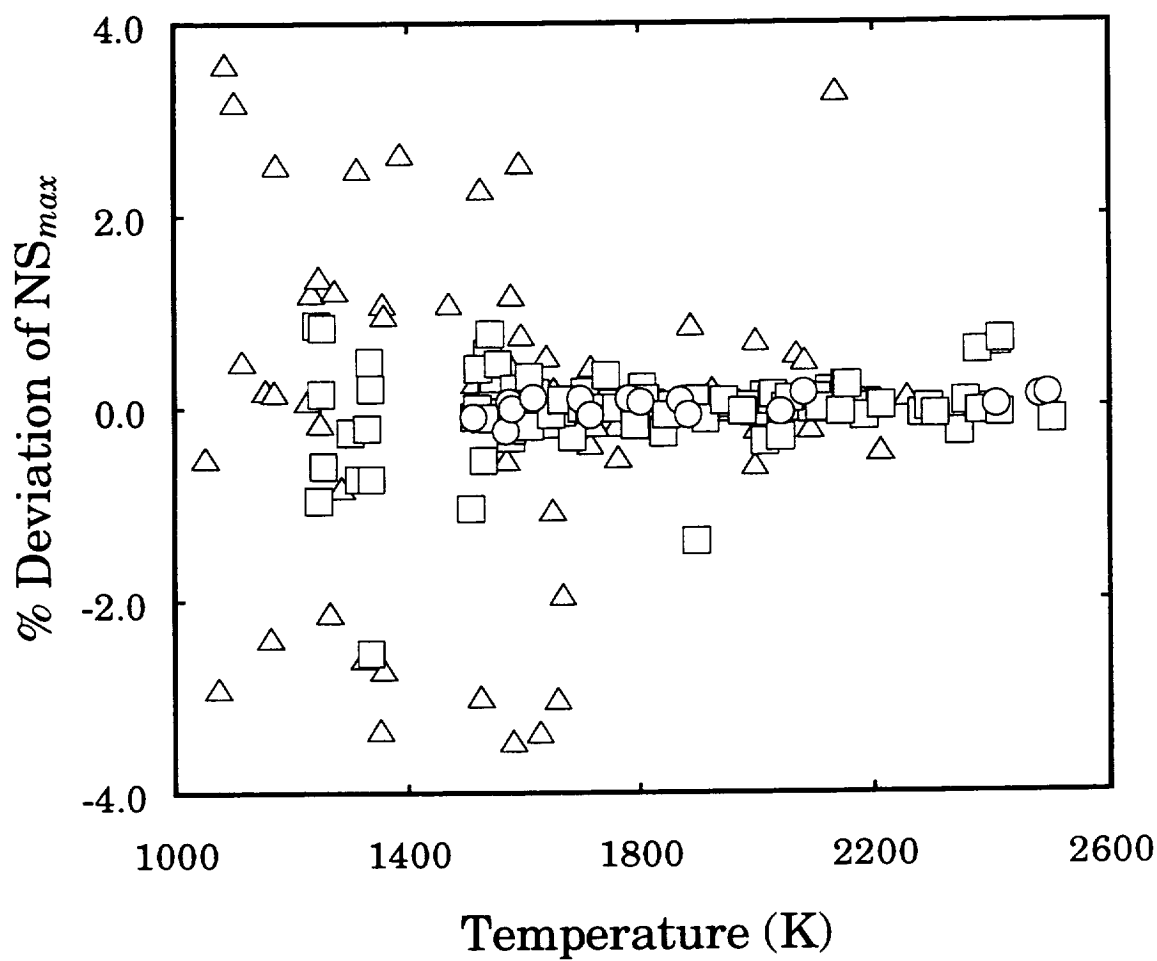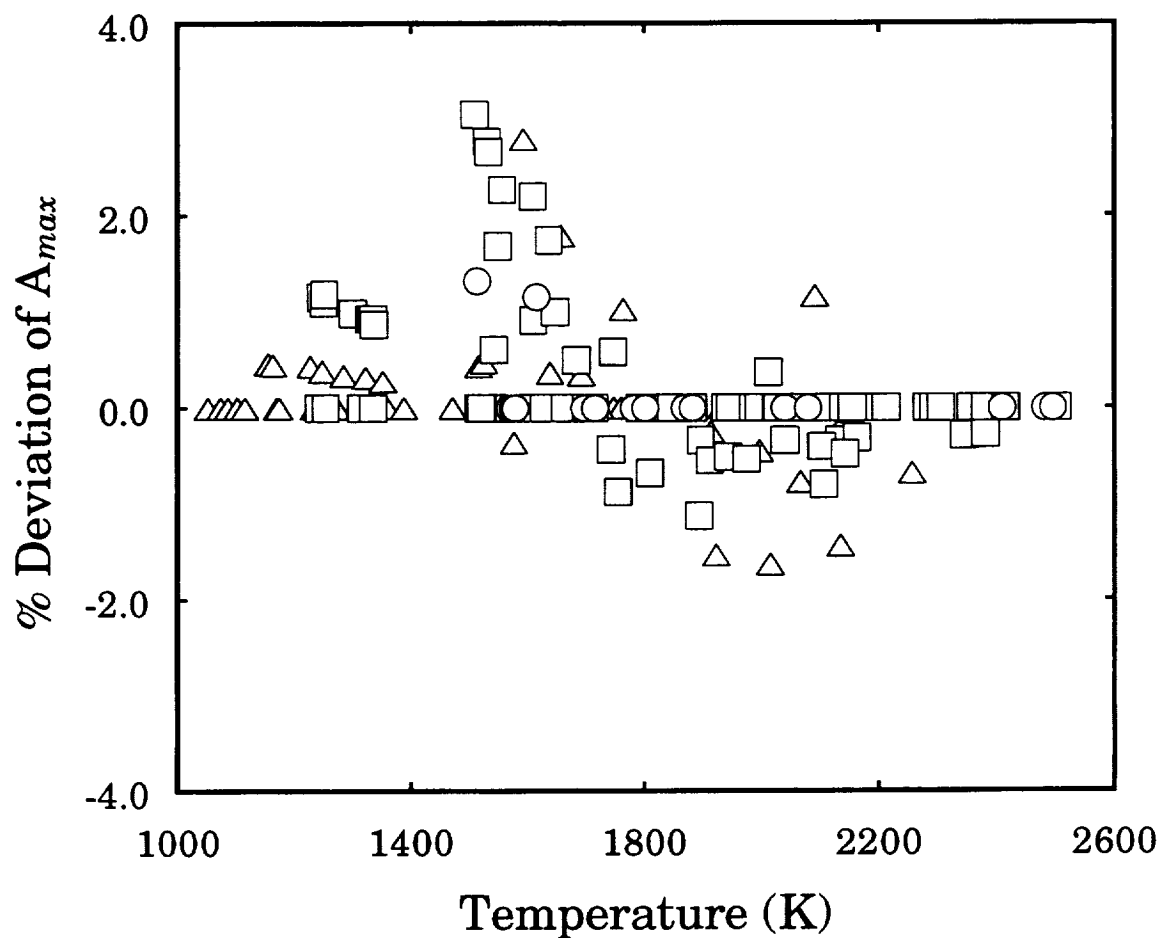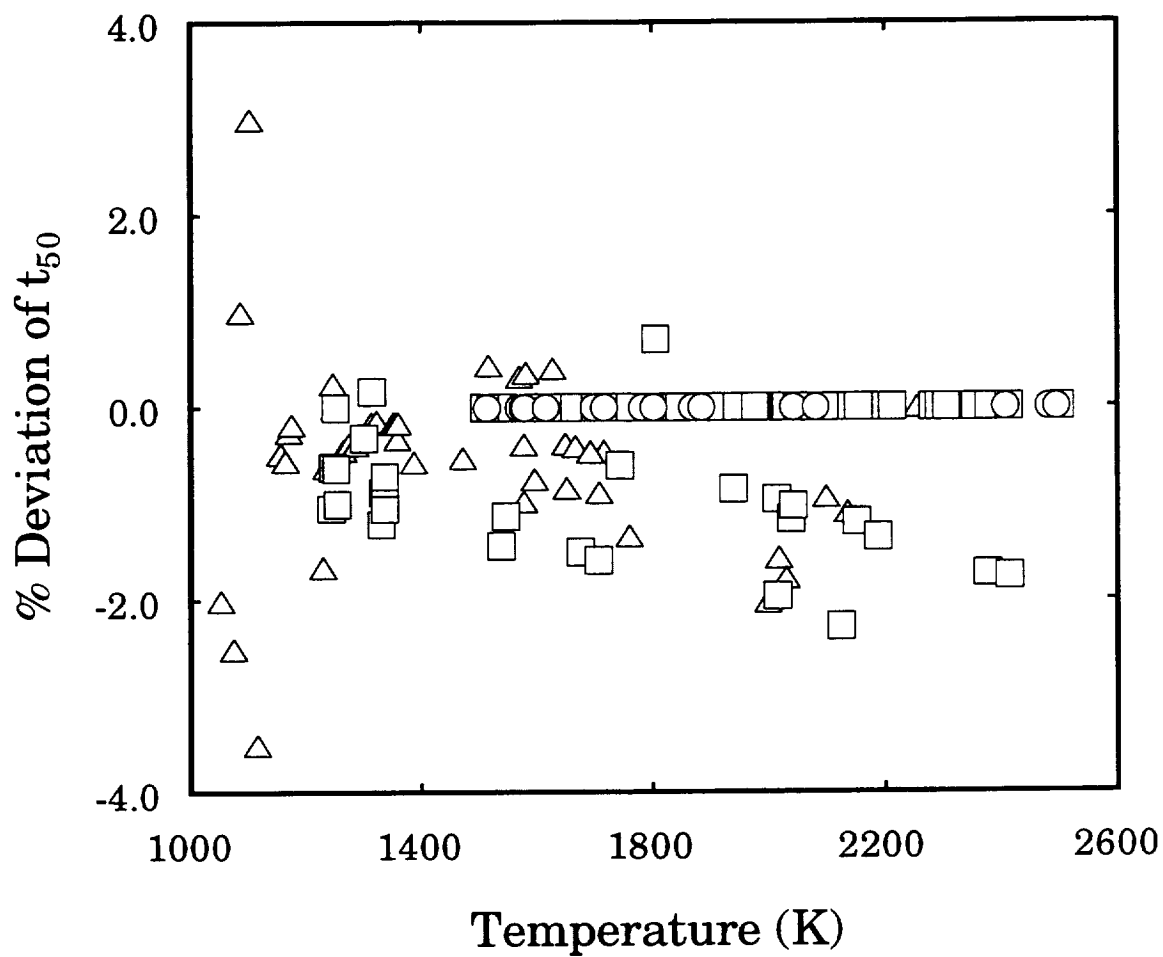
Figure I.10 Match between experimental and calculated values of t_{50}. The percent deviation is defined as $100 \times [t_{50} \text{ (calculation)} - t_{50} \text{ (experiment)}]/ t_{50} \text{ (experiment)}$. Symbols are $\triangle$ for $\phi = 2$ mixtures, $\square$ for $\phi = 5$ mixtures, and $\circ$ for $\phi = 10$ mixtures.

at 2500 K, $k_1(NS_{max}) = 4.41 \times 10^{12}$ cm^{3}mol^{-1}s^{-1}, $k_1(\{ti\}) = 4.35 \times 10^{12}$ cm^{3}mol^{-1} s^{-1}. If there were some impurities in the experimental system, the characteristic times would be shortened so that a higher $k_1(\{t_i\})$ would be resulted in, which indicates that our system was not contaminated with impurities. As the above comparison indicates, $k_1(NS_{max})$ and $k_1(\{t_i\})$ overlap each other within the mutual error limits. This confirms that our experimental results were not influenced by any possible impurities present.

The present determination of k_1, Eq.(9), is compared to the previous experimental studies in Figure I.11. Yang et al. [13] performed a single beam laser absorption study of OH radical. A reinvestigation that surplanted their previous work on the title reaction [14, 15]. An iterative optimization using eight time - difference responses (e.g., $t_{50} - t_{40}$) and an adjustable time - zero yielded a rate coefficient expression that is 5% lower at 1850 K and 5% higher at 2500 K than our expression. Yang et al. then combined their data with that of Shin and Michael and obtained a new expression that is well within our error bounds, being 4% lower at 1100 K and 2% higher at 2500 K.

Du and Hessler [11] measured the rate coefficients for reaction (1) in the temperature range of 3450 K to 5300 K by a flash absorption - shock tube technique. They combined their results with the data of Masten et al. [8], Shin and Michael [10] and Pirraglia et al. [7] and reported for the temperature range of 960 - 5300 K :

$$k_1 = (9.76 \pm 0.72) \times 10^{13} \exp(- 7474 \pm 122 \text{ K/T}) \text{ cm}^3\text{mol}^{-1}\text{s}^{-1} \qquad (12)$$
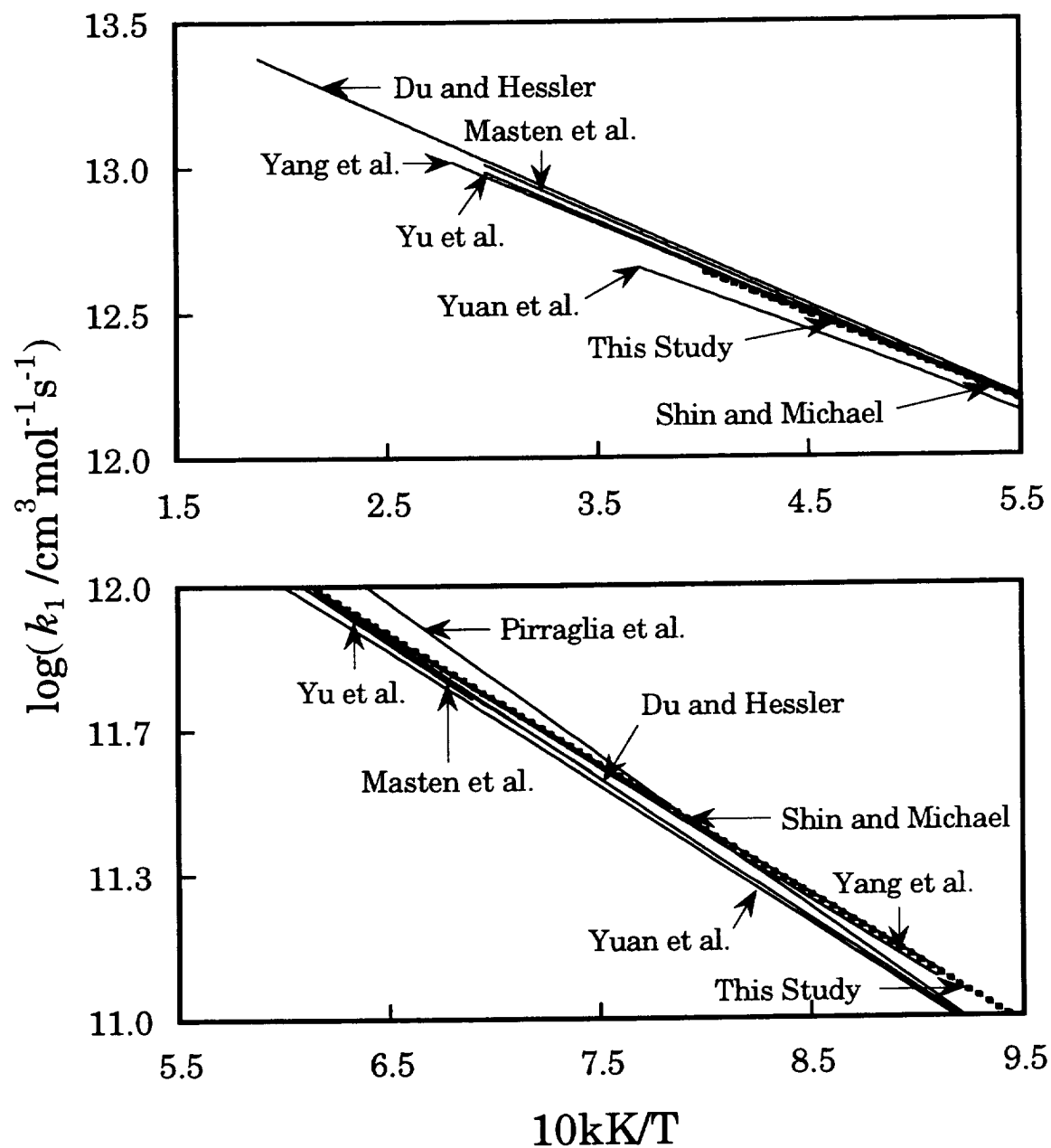
Figure I.11 Comparison of the present results for $k_1(NS_{max})$ to the previous experimental studies.

with uncertainties at the 95% confidence level. Comparing equations (9) and (12), the Du and Hessler's mean values are 16% lower at 1050 K and 11% higher at 2500 K than the present results. Since large error limits are involved in the above expression, the two expressions are in agreement within the combined experimental uncertainties over $1050K \leq T \leq 2500K$.

In their evaluation Du and Hessler introduced a profile shift parameter, x_c, that was needed to shift their calculated profiles to longer distances in order to match the experimental profiles. They associated x_c with the incubation time of H_2 dissociation, the main initiation channel at high temperature. However, we are able to model their Figure 3 experiment using the Table I.2 mechanism without resorting to the use of profile shifting. This comparison is shown in Figure I.12, where the solid line is our predicted absorption profile and the dotted lines are the upper and lower noise band of the Du and Hessler's profile. For this condition Du and Hessler used a 0.783 mm shift of their calculated profile. Our prediction is well within the noise band, although approaching the high end at long distances, where the profile is controlled by H_2 decomposition. Indeed, at all times, the profile is more sensitive to reaction (6) $(H + H + M = H_2 + M)$ than all other reactions including reaction (1) $(H + O_2 = OH + O)$. This can be seen in Figure I.12 where the upper filled boxes and the lower open boxes represent the extent of profile shift for $\pm$ 20% variations in k_1 and k_6 respectively.

Shin and Michael studied the reaction (1) by using the laser photolysis - shock tube technique by monitoring H-atom depletion in the pseudo-first-order conditions over the temperature range of 1103 - 2055 K [10]. The Arrhenius
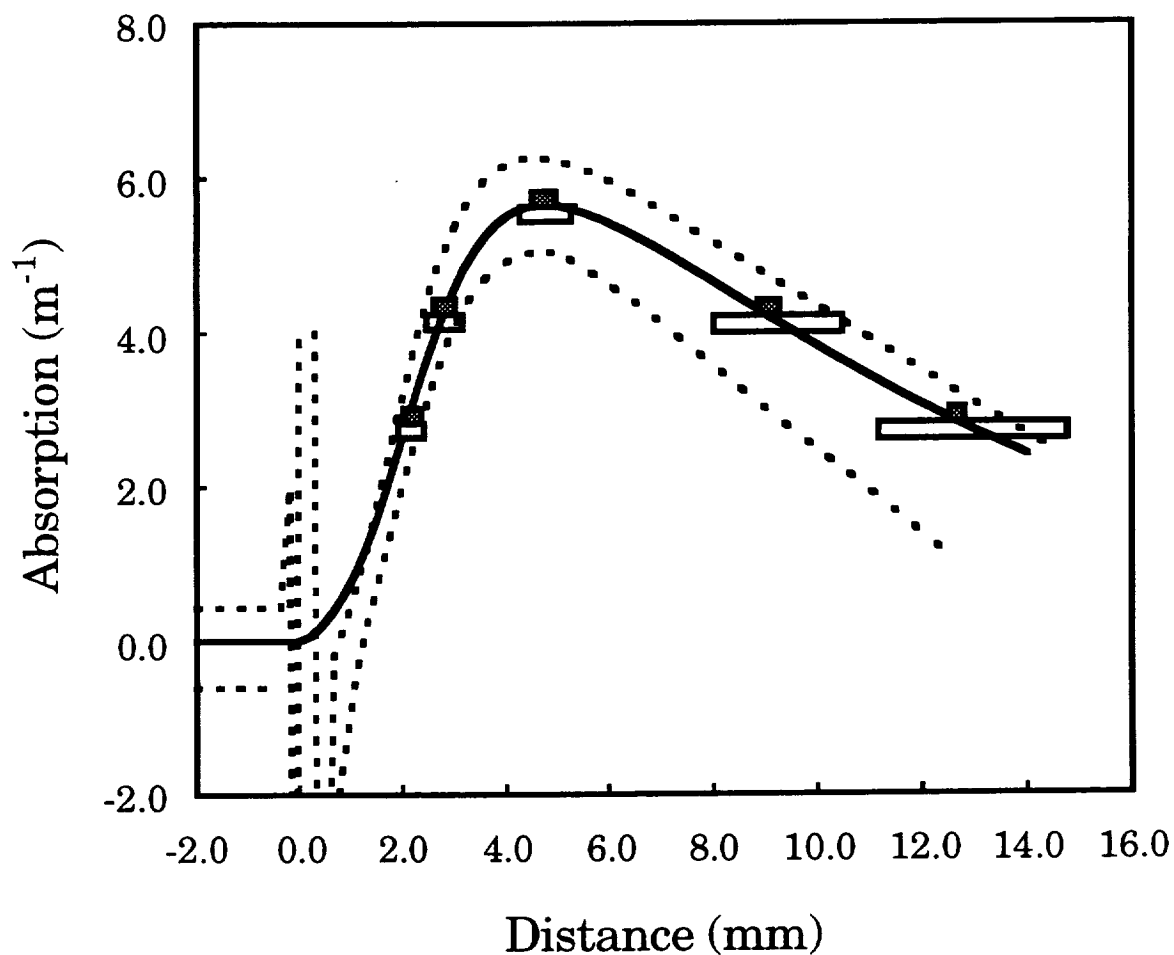
Figure I.12. Comparison of our computed profile to the experimental profile of Du and Hessler's Figure 3 condition [11]. Solid line is the absorption profile computed using the Table II reaction mechanism with $x_c = 0$ and the dotted lines are upper and lower noise band of the Du and Hessler's profile. Early part of experimental signal is dominated by shock passage transients. Filled and open boxes represent the extent of profile change for $\pm$ 20% variation of k_1(H + O_2 = OH + O) and k_6(H + H + M = H_2 + M) respectively.

expression for k_1 is given by

$$k_1 = (6.93 \pm 0.96) \times 10^{13} \exp(- 6917 \pm 193 \text{ K/T}) \text{ cm}^3 \text{ mol}^{-1} \text{ s}^{-1} \qquad (13)$$

where uncertainties are at the 1-σ level. Since they derived k_1 from the measured slope of ln(absorbance)$_t$, their results are independent of impurities, just as our determination of k_1 from the maximum slope (NS_{max}) was insensitive to impurity effects. It is important to emphasize that in Shin and Michael's experiments, corrections of T_5 and ρ_5 for boundary layer effects were made using the same basis [23, 53] as was done in the present study. As seen in Figure I.11, the k_1 values of Shin and Michael and of the present study are in quantitative agreement over the temperature range of 1103 - 2055 K.

Masten et al. [8] determined k_1 using laser absorption spectroscopy to detect OH radicals formed by heating mixtures of H_2 and O_2 diluted in Ar ($\phi =$ ~2.5, and ~5.0) behind the incident and reflected shock waves for the temperature range 1450 - 3370 K. The $R_1(5)$ line of the $A^2\Sigma^+ \leftarrow X^2\Pi$ system of OH at 306.687 nm (vacuum) was utilized to monitor OH concentration. The reported k_1 expression is given by

$$k_1 = (9.33 \pm 0.40) \times 10^{13} \exp(- 7448 \pm 86 \text{ K/T}) \text{ cm}^3 \text{ mol}^{-1} \text{ s}^{-1} \qquad (14)$$

At the extreme ends of the common temperature range this expression is 7.5% higher at 2500 K and 7.0% lower at 1450 K than the present study; however the two experiments agree with each other within the given mutual error limits, $\pm$ 10% by Masten et al. and $\pm$ 6% by this study. Even at the

extreme ends of both temperature ranges, 3370 K (Masten et al.) and 1050 K (the present study), the k_1 values agree within the combined error limits. Simulations were performed using the reaction mechanisms of Masten et al. and of Table I.2. Laminar flow and constant volume conditions were assumed for incident and reflected shock wave experiments, respectively. At their Figure 3 condition (1980 K), maximum OH concentration and the characteristic times t_{25}, t_{50} and t_{75} were simulated. Using either the Masten et al.'s or our k_1 expression resulted in identical values for $[OH]_{max}$. Furthermore, our mechanism reproduced the experimental results of Masten et al. as well as their reaction mechanism. However, our k_1 value is 2% smaller than that of Masten et al. at 1980 K. Substituting our k_1 expression into the reaction mechanism of Masten et al. and adjusting k_{11} (H + HO$_2$ = H$_2$ + O$_2$) to match characteristic times, as was done by Masten et al., a 34% increase of k_{11} was required. Next, as there is no $[OH]_{max}$ under Masten et al.'s Figure 5 condition (2898 K), the first visible appearance of plateau OH concentration and the characteristic times, t_{25}, t_{50} and t_{75} defined above were taken as simulation parameters. Again, our mechanism reproduced Masten et al.'s experimental results as well as the reaction mechanism of Masten et al. At this temperature, our k_1 value is about 10% smaller than that of Masten et al. As before, we substituted our k_1 expression and adjusted k_{11} to obtain a match. A factor of 2.5 increase of k_{11} was required. At this temperature, thermal decomposition rate coefficient of H$_2$, k_6, is an important initiation source, indeed, the sensitivities of k_6 and k_{11} are equal. However, NS_{max} is not sensitive to either k_{11} or k_6 at this condition. In essence, the difference between the k_1 expressions derived by Masten et al. and in this study are caused by secondary chemical reactions, i.e., either k_1 expression can be used

to simulate the characteristic times of both sets of experiments by carefully choosing the rates of the initiation reactions. However, the temporal behavior of the OH concentration measured in this study was well reproduced using the k_1 value determined by matching NS_{max}. Moreover, this determination was independent of any cross sensitivity upon initiation reactions. The effect of k_2 and k_3 on $k_1(NS_{max})$ were also examined under our conditions used above and was found to be negligible. Table I.2 reaction mechanism with k_2 and k_3 expressions of Masten et al. resulted in 0.6% and 1.3% changes in k_1 values at 1234 K and 2163 K though there are 3 - 20% and 3-6% differences in k_2 and k_3, respectively.

Yuan et al. published a k_1 expression determined by laser absorption of OH radicals generated by heating mixtures of hydrogen and oxygen diluted in Ar behind reflected shock waves over the temperature range 1050-2700 K [9]. Five active parameters, k_1, k_2, k_3, k_{-11}, and $\Delta_f H°_{298}(HO_2)$ were simultaneously optimized by minimizing the difference between the computed and experimental characteristic times, t_{25}, t_{50}, t_{75}, using the solution mapping method [54]. The reported non-Arrhenius type of k_1 expression is

$$k_1 = 1.59 \times 10^{17} \, T^{-0.927} \exp(-8493 \, K/T) \, cm^3 \, mol^{-1} \, s^{-1} \qquad (15)$$

with $\sigma_{\log k_1} = 0.05$. Their result is in excellent agreement with that of Schott [3], $1.22 \times 10^{17} \, T^{-0.907} \exp(-8369 \, K/T)$ for 1250 K $\leq$ T $\leq$ 2500 K. Compared to the present experimental results in the common temperature range, 1050 K $\leq$ T $\leq$ 2500 K, the k_1 values of Yuan et al. are on average about 17% smaller, but agree with each other within the combined error limits. These authors also

reported that with Masten et al.'s secondary reaction rate coefficients, k_2, k_3, and k_{11}, a slightly different expression was resulted, $1.71 \times 10^{17} \, T^{-0.932} \exp(-8498 \, K/T)$, which differs from the above equation (17) by ~3%. The effect of the secondary reaction rate coefficients on the determination of k_1 was thus not large (also see Ref. 14, 15).

Recently the data of Yuan et al. and Masten et al. were subjected to a rigorous optimization using two different model responses by Yu et al. [12], the characteristic times (t_{25}, t_{50}, t_{75}) and the time difference, Δt, defined as $\Delta t = t_{75} - t_{25}$. The data of Masten et al. yielded nearly identical k_1 expressions for both model responses while those of Yuan et al. were noticeably different, with $k_1(characteristic \ times)$ being 15% lower than $k_1(\Delta t)$ at 2150 K. There was reasonable agreement between the Yuan et al.'s $k_1(\Delta t)$ and both the Masten et al.'s k_1 expressions (which were nearly identical). An explanation for the difference between the Yuan et al.'s $k_1(characteristic \ times)$ and $k_1(\Delta t)$ was proposed based upon the effect of vibrational non-equilibrium of O_2. The high temperature data of Yuan et al. was taken at short reaction times where this effect would be most pronounced. This is akin to the explanation given by Du and Hessler for the profile shift parameter included in their study. Yu et al. suggest an expression based upon the Δt response surface that is within our error bounds, being 3% higher at 2500 K and 7% lower at 1336 K than the present study.

The possible effect of O_2 vibrational relaxation on hydrogen combustion has important implications for the performance of airbreathing hypersonic propulsion systems. Such systems would be hydrogen fueled and have

characteristic chemical reaction times much shorter than 100 µs. In order to quantify the effect of O_2 vibrational relaxation a series of experiments was run using the Yuan et al.'s Series E composition in the pressure and temperature range where the effect should be most visible, i.e. 2.4 to 3.0 atm and 1905 to 2380 K, respectively. Unlike the case of the Yuan et al.'s data we did not see a difference between the k_1 value determined using either t_{50} or Δt as the modeling criteria. Experimental values of t_{50} and Δt are shorter than predicted using the Table I.2 mechanism, on average by 2% (0.6 µs) and 5% (0.3 µs) respectively. While arbitrary time accuracy may be achieved in the simulation, differences of this scale, although they are discernible, are not particularly meaningful. Nonetheless, we can match t_{50}, Δt and NS_{max} for each experiment. At these conditions there is exquisite sensitivity to t_{50} as modeling criteria – a 0.1 µs change required a 1% change in k_1, while sensitivity to Δt was smaller. The optimized k_1 values for these experiments differ on average 4% (within our uncertainty limits) from our recommended expression (individual experiments required adjustments between – 3% and 8%). We are not required to invoke O_2 vibrational relaxation to explain our short reaction time data as both t_{50} and Δt are predicted equally well using our mechanism without additional constraints. It is worth remembering that Belles and Lauver [55] had previously shown that O_2 vibrational relaxation was not required to explain the lengthening of induction delay at short times in H_2/O_2 mixtures that had been proposed by Schott and Kinsey [56].

It is worthy to note the flash photolysis - shock tube work of Pirraglia et al. in the temperature range 962 to 1705 K, because it has been used in all of the recent studies either for comparison[8, 9, 10, 15] or to make fits for k_1 in

the form of non-Arrhenius type [8, 15] or Arrhenius type [11] by combining with their own results. In the experiments, a small amount of either NH_3 or H_2O was photolyzed in excess of O_2 and Ar and H-atom decay was monitored by ARAS. The k_1 expression reported is

$$k_1 = (1.68 \pm 0.19) \times 10^{14} \exp(-8119 \pm 139 \text{ K/T}) \text{ cm}^3 \text{ mol}^{-1} \text{ s}^{-1} \qquad (16)$$

with the mean deviation of $\pm$ 16%. The above expression for k_1 is compared to our results. The two sets of expressions agree within $\pm$ 22% over the common temperature interval with k_1 of the present study being 22% larger at 1050 K and 19% smaller at 1700 K. However, as pointed out by one of the authors in a recent review [32], the k_1 expression of Pirraglia et al. was influenced by the data at low temperatures, T < 1200 K. Careful inspection of the data (Figure 2 of Ref. 7) showed that there seemed to be two sets of data separated at 1200 K and that the above k_1 expression overpredicts the data at T < 1200 K. These two sets of data could be separately fitted into $6.76 \times 10^{13} \exp(-6829 \text{ K/T})$ cm^3 mol^{-1} s^{-1} (1206 K $\leq$ T $\leq$ 1705 K) and $1.56 \times 10^{14} \exp(-8076 \text{ K/T})$ cm^3 mol^{-1} s^{-1} (962 K $\leq$ T $\leq$ 1206 K). The former expression agrees with our results within better than 6% in the common temperature range (Figure I.13). The possible reason for the low k_1 values at lower temperatures may be due to the over-correction either for temperatures for the boundary layer effect or for the contribution from reaction (9), H + O_2 + M= HO_2 + M. It is also possible that the k_1 values actually start to decrease at temperatures below 1200 K so that the k_1 expression has a negative A-factor. Nevertheless, the upward temperature corrections ranged from 4% to 6% of the ideal shock temperatures (average 50 to 60 K) for experiments with initial pressures of
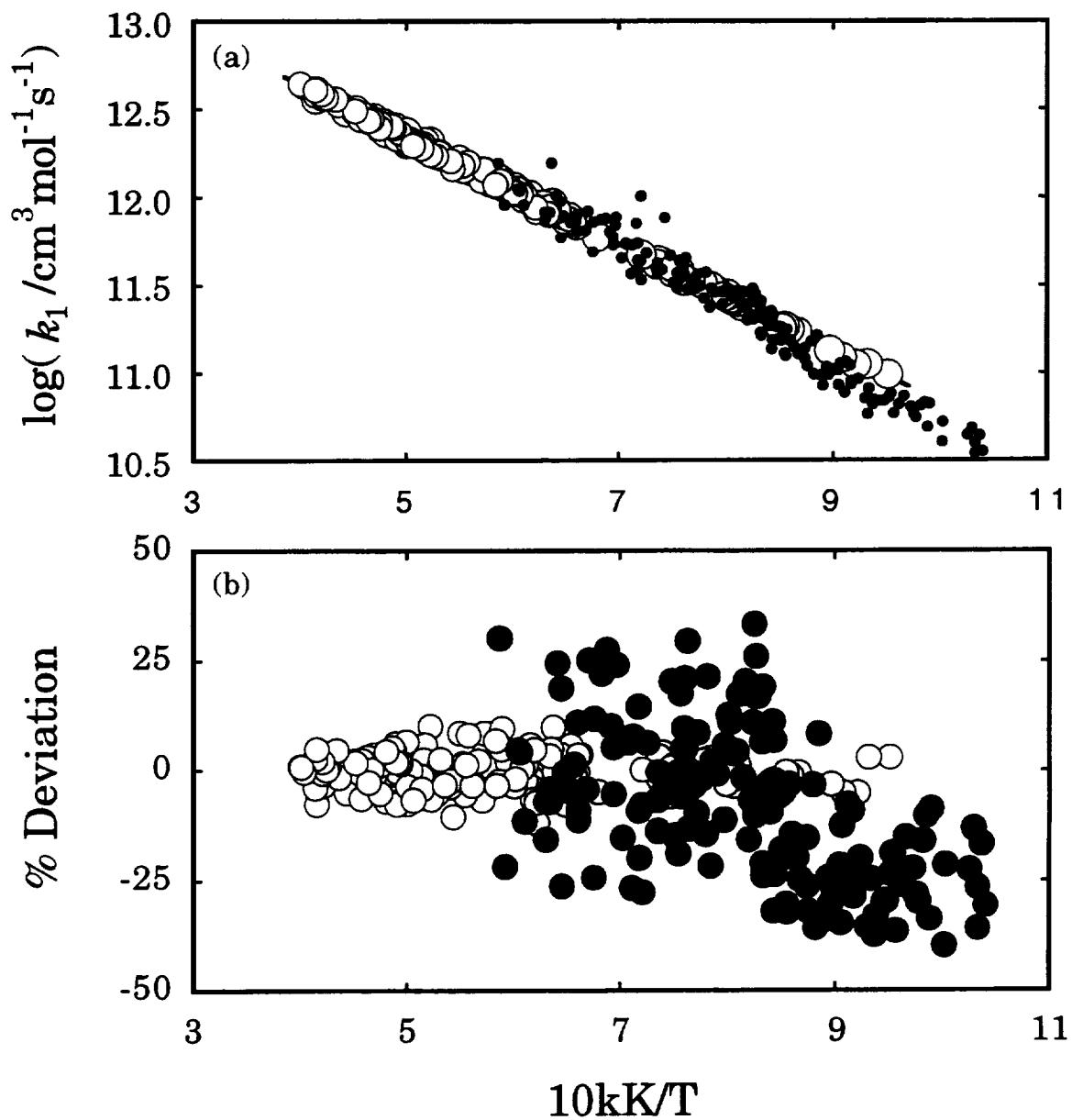
Figure I.13 Comparison between our results for $k_1(\mathrm{NS}_{max})$ with the data of Pirraglia et al. [Ref. 7]. (a) Arrhenius plot. (b) The percent deviation defined as $100 \times [k_1(\text{experiment}) - k_1(\text{fit, this study})]/ k_1(\text{fit, this study})$. Symbols are O for this study and ● for Pirraglia et al.

about 10.5 Torr and 15.5 Torr. The range of the temperature correction will vary depending upon shock tube characteristics and experimental conditions. However, a 50 to 60 K correction seems too large. If temperatures were over-corrected, then the actual temperatures would be lower so that the A-factor and the temperature dependence of the Arrhenius expression for k_1 would decrease. As temperatures are lowered by reducing over-correction, the contribution from reaction (9) to the measured overall H-atom decay constants from which k_1 values were obtained may not be ignorable. However, the influence of reaction (9) on the evaluation of k_1 values is rather small compared to increasing T^{-1} (lowering the temperatures).

The temperature dependence of the A-factor was reported by several authors: −0.907 by Schott, −0.927 by Yuan et al., −0.7 by Masten et al., 2.0 by Fujii et al. from the combination of their results with the data of Pirraglia et al.; and −0.816 by theoretical calculation of Miller [17, 18]. Miller [17] calculated the rate of the reaction (1) using quasiclassical trajectory and quantum mechanical threshold (QCT-QMT) methods and the potential energy surface of Melius and Blint [19], and attributed the negative temperature dependence to the nonstatistical "recrossing" effects especially at high temperatures. However, the results of the present work and Shin and Michael do not support this negative temperature dependence for 1100K ≤ T ≤2500K. Recently Varandas et al. [20] calculated the thermal rate coefficient of reaction (1) using the quasiclassical trajectory (QCT), quasiclassical trajectory-quantum mechanical threshold (QCT-QMT), quasiclassical trajectory-internal energy quantum mechanical threshold (QCT-IEQMT), and the improved version of QCT-IEQMT methods at five temperatures, 1000, 1750, 2000, 2500, and 3000

K. In the calculation, the fourth version of their own double many-body expansion (DMVE IV) potential energy surface for the ground state of HO_2, which reproduces the most accurate estimates of the experimental dissociation energy, equilibrium geometry, and quadratic force constants [57], was utilized. The results from the QCT-QMT methods gave best agreement with the present study within computational error bounds and are plotted in Figure I.14. Our k_1 value is 4% smaller at 3000 K and 12% smaller at 1000 K where the minimum number of trajectories was calculated because of the computational burden. The Arrhenius expression for k_1 from QCT-QMT methods given by Varandas et al. is $k_1 = (7.19 \pm 1.11) \times 10^{13} \exp(- 6943$ K/T$)$, which is very similar to equation (9) of the present study.

There exists reasonable agreement between this study and most of the recent evaluations of k_1 [7, 10-13, 58] so it is possible to achieve a consensus expression, shown in Figure 15, that is given by:

$$k_1 = 7.82 \times 10^{13} \exp(- 7105 \text{ K/T}) \text{ cm}^3 \text{ mol}^{-1} \text{ s}^{-1} \tag{17}$$

over the temperature range 960 to 5330 K, with an uncertainty of 6%. We developed this expression in the following fashion. The expressions of Pirraglia et al., Shin and Michael, Du and Hessler, Yu et al., Yang et al. and the present study were converted to a series of "data points" evenly spaced in 1/T over each of their temperature ranges. A weighted least squares fit was then obtained with the weighting factor being the inverse of the uncertainty limits for the Arrhenius expressions reported in the individual studies. The data of Pirraglia et al. and Shin and Michael were used to develop the Du and Hessler's
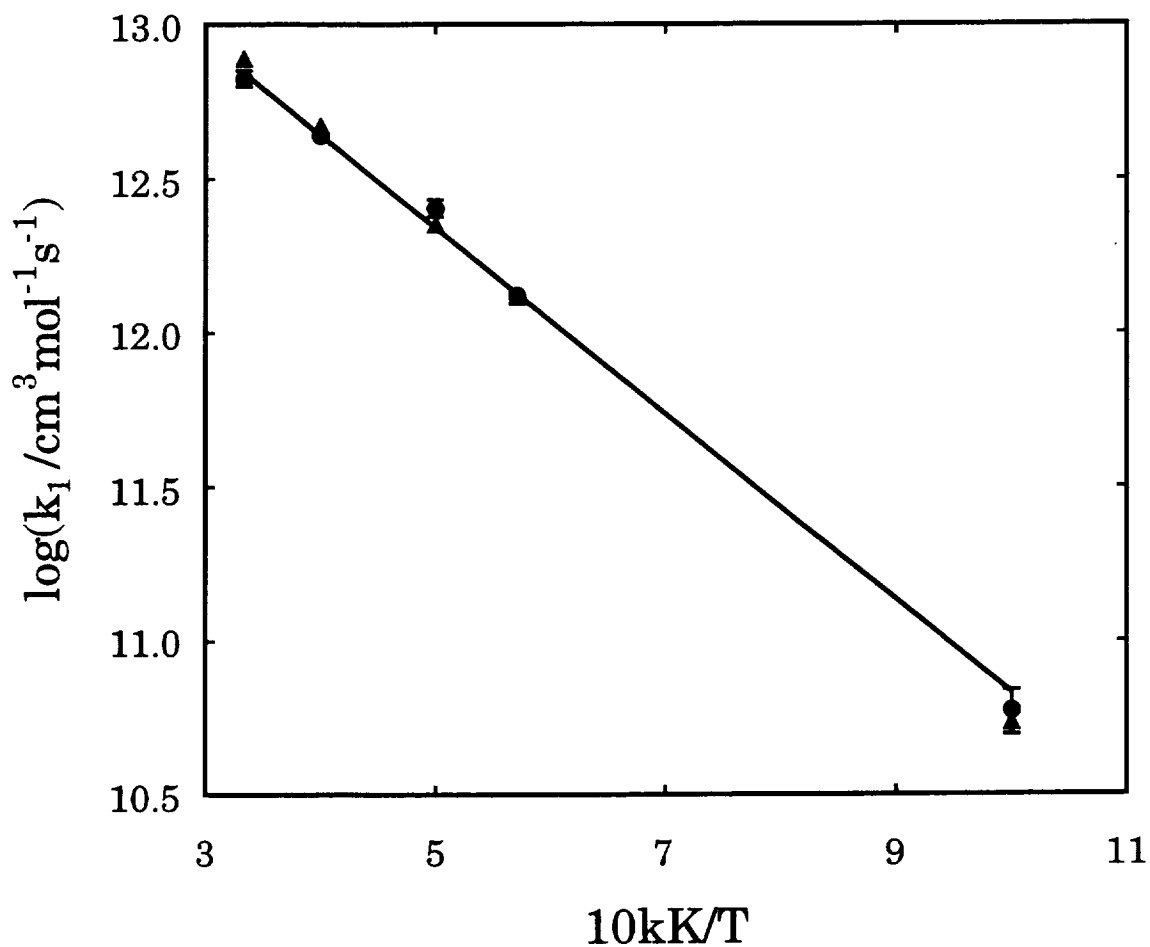
Figure I.14 Comparison of our results for $k_1(NS_{max})$ with the experimental results of Masten et al. [Ref. 8] and the theoretical calculation of Varandas et al. [Ref. 20]. The solid line represents $k_1(NS_{max})$ expression. Symbols are ▲ for Masten et al. and ● for Varandas et al.
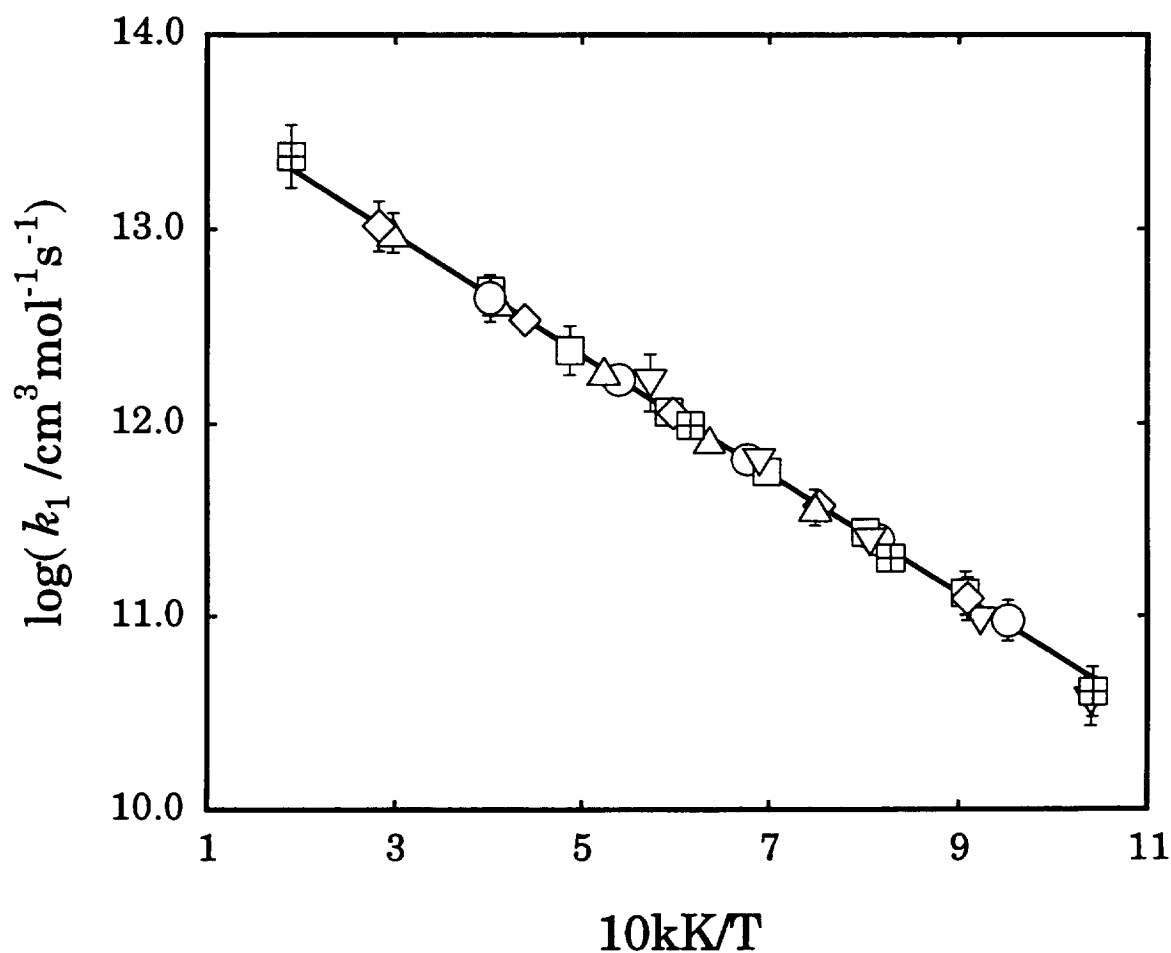
Figure 15. Consensus expression for k_1. Solid line is the consensus expression, $k_1(NS_{max}) = 7.26 \times 10^{13} \exp(- 6985 \text{ K/T})$ $\text{cm}^3 \text{mol}^{-1} \text{s}^{-1}$ (960 K $\leq$ T $\leq$ 5330 K). Symbols are: ∇, Pirraglia et al.; $\boxplus$, Du and Hessler; $\square$, Shin and Michael; $\triangle$, Yu et al.; $\diamondsuit$, Yang et al.; $\bigcirc$, This Study. Uncertainty limits for the individual expressions are shown for the highest and lowest temperature points.

expression and the data of Shin and Michael were used to develop the Yang et al.'s expression. Accordingly, their weighting factors were reduced to correct for this over representation. The weighting factors used to extract a consensus expression were 2 for Shin and Michael, 14 for Yu et al., 3 for Pirraglia et al., 8 for Yang et al., 5 for Du and Hessler, 40 for this study, respectively. An Arrhenius expression was assumed.

Conclusions

The rate coefficient of reaction (1), $H + O_2 = OH + O$ was determined by using the OH laser absorption spectroscopic method behind reflected shock waves over the temperature range 1050 - 2500 K and pressure range from about 0.7 atm to about 4.0 atm. Eight different compositions of mixtures of ϕ = 2, 5 and 10 were used in the study. Two different methods utilizing the absorption maximum (A_{max}) and the normalized maximum slope (NS_{max}) and A_{max} and the characteristic times ($\{t_i\}$) employed in the evaluation of k_1 yielded almost identical results. The recommended expression for k_1 is from the normalized maximum slope analysis and is given by

$$k_1 = (7.13 \pm 0.31) \times 10^{13} \exp(- 6957 \pm 30K/T) \text{ cm}^3 \text{ mol}^{-1} \text{ s}^{-1} \qquad (18)$$

with uncertainties of 1-σ level. This expression is in quantitative agreement with that of Shin and Michael and is very similar to the computational results of Varandas et al. A complete comparison was given between the results of

the present study and those of recent experimental studies. The experimental data for k_1 were best fitted using the Arrhenius type rate coefficient expression. Therefore, in the temperature range of the current study, which is relatively wide, we support the Arrhenius type expression for k_1 although more data, especially below 1000 K, are needed to confirm the curvature.

Critical review of the recent k_1 determinations yields a consensus expression given by:

$$k_1 = 7.82 \times 10^{13} \exp(-7105 \text{ K/T}) \text{ cm}^3 \text{ mol}^{-1} \text{ s}^{-1} \qquad (19)$$

over the temperature range 960 to 5300 K.

The inverse reactant density dependence of k_1 at 2000 K, which was suggested by Schott, could not be found even though the reactant densities were varied ten-fold.

References

1. Warnatz, J. In *Combustion Chemistry*; Gardiner, W. C., Jr., Ed.; Springer-Verlag: New York, 1984; Chapter 5.

2. Baulch, D. L.; Drysdale, D. D.; Horne, D. G.; Lloyd, A. C. *Evaluated Kinetic Data for High Temperature Reactions*; Butterworths: London, 1972; Vol. 1.

3. Schott, G. L. *Combust. Flame* **1973**, *21*, 357.

4. Cohen, N.; Westberg, K. R. *J. Phys. Chem. Ref. Data* **1983**, *12*, 531.

5. Cohen, N. "A Brief Review of the Kinetics of H_2-O_2 Reactions", Aerospace Report No. ATR-89 (8412) - 3; Aerophysics Laboratory: El Segundo, CA, September 1989.

6. Frank, P.; Just, Th. *Ber. Bunsen-Ges. Phys. Chem.* **1985**, *89*, 181.

7. Pirraglia, A. N.; Michael, J. V.; Sutherland, J. W.; Klemm, R. B. *J. Phys. Chem.* **1989**, *93*, 282.

8. Masten, D. A.; Hanson, R. K.; Bowman, C. T. *J. Phys. Chem.* **1990**, *94*, 7119.

9. Yuan, T.; Wang, C.; Yu, C. L.; Frenklach, M.; Rabinowitz, M. J. *J. Phys. Chem.* **1991**, *95*, 1258.

10. Shin, K. S.; Michael, J. V. *J. Chem. Phys.* **1991**, *95*, 262.

11. Du, H.; Hessler, J. P. *J. Chem. Phys.* **1992**, *96*, 1077.

12. Yu, C. -L.; Frenklach, M.; Masten, D. A.; Hanson, R. K.; Bowman, C. T. *J. Phys. Chem.* **1994**, *98*, 4770.

13. Yang, H.; Gardiner, W. C., Jr.; Shin, K. S.; Fujii, N. *Chem. Phys. Lett.* **1994**, *231*, 449.

14. Fujii, N.; Shin, K. S. *Chem. Phys. Lett.* **1988**, *151*, 461.

15. Fujii, N.; Sato, T.; Miyama, H.; Shin, K. S.; Gardiner, W. C., Jr. *Seventeenth International Symposium on Shock Waves and Shock Tubes*; Kim, Y. W., Ed.; American Institute of Physics: New York, 1989; p 456

16. Schott, G. L. Eastern States Section Combustion Institute Meeting, Orlando, FL., December 1990.

17 Miller, J. A. *J. Chem. Phys.* **1981**, *74*, 5120.

18. Miller, J. A. *J. Chem. Phys.* **1986**, *84*, 6170.

19. Melius, C. F.; Blint, R. *J. Chem. Phys. Lett.* **1979**, *64*, 183.

20. Varandas, A. J. C.; Brandão, J.; Pastrana, M. R. *J. Chem. Phys.* **1992**, *96*, 5137.

21. Gardiner, W. C., Jr.; Walker, B. F.; Wakefield, C. B. In *Shock Waves in Chemistry*; Lifshitz, A., Ed., Marcel Dekker: New York, 1981; Chapter 7.

22. McBride, B. J.; Gordon, S.; Reno, M. A. "Coefficients for Calculating Thermodynamic and Transport Properties of Individual Species". NASA TM-4513; National Aeronautics and Space Administration: Washington D. C., 1993.

23. Gardiner, W. C., Jr. *Ber. Bunsen-Ges. Phys. Chem.* **1986**, *90*, 1024.

24. Michael, J. V.; Sutherland, J. W. *Int. J. Chem. Kinet.* **1986**, *18*, 409.

25. Oldenborg, R. C.; Loge, G. W.; Harradine, D. M.; Winn, K. R. *J. Phys. Chem.* **1992**, 96, 8426.

26. Hindmarsh, A. C. "Towards a Systematic Collection of ODE Solvers". Presented at the 10th IMACS World Congress on System Simulation and Scientific Computation, Montreal, August 1982.

27. Smith, M. A. H.; Rinsland, C. P.; Fridovich, B.; Rao, K. N. In *Molecular Spectroscopy: Modern Research*; Rao, K. N., Ed.; Academic Press: New York, 1985; Vol. 3, Chapter 3.

28. Mitchell, A. C. G.; Zemansky, M. W. *Resonance Radiation and Excited Atoms*; Cambridge University Press: London, 1971.

29. Penner, S. S. *Quantitative Molecular Spectroscopy and Gas Emissivities*; Addison-Wesley: Reading, Mass., 1959.

30. Flygare, W. H. *Molecular Structure and Dynamics*; Prentice-Hall: Englewood Cliffs, NJ, 1978; Chapter 7.

31. Sutherland, J. W.; Michael, J. V.; Pirraglia, A. N.; Nesbitt, F. L.; Klemm, R. B. *Twenty-First Symposium (International.) on Combustion*; The Combustion Institute: Pittsburgh, 1986; p 929.

32. Michael, J. V. *Prog. Energy Combust. Sci.* **1992**, *18*, 327.

33. Frenklach, M.; Wang, H.; Rabinowitz, M. J. *Prog. Energy Combust. Sci.* **1992**, *18*, 47.

34. Dixon-Lewis, G. *Combust. Sci. Technol.* **1983**, *34*, 1.

35. Albers, E. A.; Hoyermann, K.; Wagner, H. Gg.; Wolfrum, J. *Thirteenth Symposium (International) on Combustion*; The Combustion Institute: Pittsburgh, 1971; p 81.

36. Larsson, M. *Astron. Astrophys.* **1983**, *128*, 291.

37. Whiting, E. E.; Schadee, A.; Tatum, J. B.; Hougen, J. T.; Nicholls, R. W. *J. Molecular Spectroscopy* **1980**, *80*, 249.

38. Schadee, A. *J. Quant. Spectrosc. Radiat. Transfer* **1978**, *19*, 451.

39. Smith, G. P.; Crosley, D. R. *Eighteenth Symposium (International) on*

Combustion; The Combustion Institute: Pittsburgh, 1981; p 1511.

40. Goldman, A.; Gillis, J. R. *J. Quant. Spectrosc. Radiat. Transfer* **1981**, *25*, 111.

41. Crosley, D. R.; Lengel, R. K. *J. Quant. Spectrosc. Radiat. Transfer* **1975**, *15*, 579.

42. Lewis, G. N.; Randall, M. In *Thermodynamics*; Pitzer, K. S., Brewer, L., Revised,; McGraw-Hill: New York, 1961; Chapt. 27.

43. Herzberg, G. In *Molecular Spectra and Molecular Structure: I. Spectra of Diatomic Molecules*; Van Nostrand: Princeton, 1950; Chapter 3.

44. Gardiner, W. C., Jr. *J. Phys. Chem.* **1977**, *81* 2367.

45. Frenklach, M.; Bornside, D. E. *Combust. Flame* **1984**, *56*, 1.

46. Frenklach, M. In *Combustion Chemistry*; Gardiner, W. C., Jr., Ed.; Springer-Verlag: New York, 1984; Chapter 7.

47. Frenklach, M.; Rabinowitz, M. J. "Optimization of large reaction systems", In *Extended Abstracts of Twelfth IMACS World Congress on Scientific Computation*; Vichnevetsky, R., Borne, P., Vignes, J., Eds.; Gerfidn: Cedex, France, 1988; Vol. 3, p 602.

48. Hwang, S. M. "Shock Tube and Modeling Study of Methyl Radical Self-Reactions". Ph. D. Thesis, University of Texas, Austin, 1988.

49. Hwang, S. M.; Rabinowitz, M. J.; Gardiner, W. C., Jr. *Chem. Phys. Lett.* **1993**, *205*, 157.

50. Rea, E. C., Jr.; Chang, A. Y.; Hanson, R. K. *J. Quant. Spectrosc. Radiat. Transfer* **1987**, *37*, 117.

51. Shoemaker, D. P.; Garland, C. W.; Steinfeld, J. I. In *Experiments in*

Physical Chemistry; McGraw-Hill: New York, 1974; Chapter 2.

52. Hwang, S. M.; Ryu, S. O.; Rabinowitz, M. J. "Spectral line broadening of the $P_1(5)$ line of the $A^2\Sigma^+ \leftarrow X^2\Pi$ transition of OH at high temperatures", Manuscript in preparation.

53. Michael, J. V.; Fisher, J. R. *Seventeenth International Symposium on Shock Waves and Shock Tubes*; Kim, Y. W., Ed.; American Institute of Physics: New York, 1989; p 210

54. Frenklach, M. In *Complex Chemical Reaction Systems, Mathematical Modelling and Simulation*; Warnatz, J., Jäger, W., Eds.; Springer-Verlag: Berlin, 1987; p 2.

55. Belles, F. E.; Lauver, M. R. *Tenth Symposium (International) on Combustion*; The Combustion Institute: Pittsburgh, 1965; p 285.

56. Schott, G. L.; Kinsey, J. L. *J. Chem. Phys.* **1958**, *29*, 1177.

57. Pastrana, M. R.; Quintales, L. A. M.; Brandão, J.; Varandas, A. J. C. *J. Phys. Chem.* **1990**, *94*, 8073.

58. "..., facies non omnibus una, nec diversa tamen, qualem decet esse sororum" - Ovid, Metamorphoses 2.13-14.
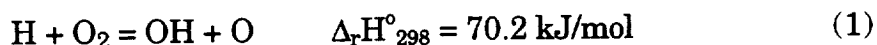
# Chapter II. O + H$_2$ = OH + H Reaction

Introduction

The reaction between oxygen atoms and hydrogen molecules

$$O + H_2 = OH + H \qquad \Delta_r H^{\circ}_{298} = 7.8 \text{ kJ/mol} \qquad (2)$$
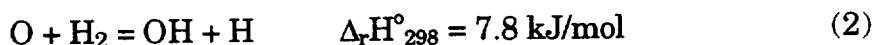
which is slightly endothermic, is the second most important chain branching step after the reaction of

$$H + O_2 = OH + O \qquad \Delta_r H^{\circ}_{298} = 70.2 \text{ kJ/mol} \qquad (1)$$

in the H$_2$/O$_2$ system. Although it was reported that flame propagation and ignition were not sensitive to the rate coefficients of reaction (2) [1], reaction (2) furnishes a reactive chain center (H-atom) directly, and also indirectly to the primary chain branching step, reaction (1), through

$$OH + H_2 = H_2O + H \qquad \Delta_r H^{\circ}_{298} = -62.8 \text{ kJ/mol} . \qquad (3)$$
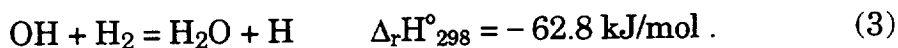
Because of the reason stated above, reaction (2) has been an interesting subject of research for many authors. Numerous experimental and theoretical investigations have been performed to determine the rate coefficients of

reaction (2). It is generally well known that the rate coefficients of this reaction, k_2, can be represented by a curved non-Arrhenius type expression. The reaction rates are enhanced due to quantum mechanical tunneling [2] at low temperatures and due to the participation of the vibrationally enhanced reaction, $O(^3P) + H_2(v \geq 1)$ [3] at high temperatures. However, the extent of the curvature, especially, the vibrational enhancement at high temperatures is still not known well.

Currently there are three reviews available for the rate coefficient information of reaction (2). Low temperature data obtained using discharge-flow systems and a few high temperature shock tube data up to 1972 were reviewed by Baulch et al. [4]. The recommended k_2 expression in the temperature range of 400 - 2000 K is

$$k_2 = 1.8 \times 10^{10} \, T^{1.0} \, \exp(-4480 \, K/T) \, cm^3 \, mol^{-1} \, s^{-1} \qquad (4)$$

with the suggested error limits of $\pm$ 30%. Cohen and Westberg [5] reviewed k_2 data available up to 1983 and recommended

$$k_2 = 1.1 \times 10^4 \, T^{2.8} \, \exp(-2980 \, K/T) \, cm^3 \, mol^{-1} \, s^{-1} \qquad (5)$$

for temperatures from 298 to 2500 K. The uncertainty was $\sigma_{\log(k_2)} = \pm \, 0.3$ at 298 K and at 1600 K and above. Because of the uncertainty and scatter in the data above 900 K, they suggested that an Arrhenius expression, $k_2 = 7 \times 10^{13} \exp(-5400 \, K/T) \, cm^3 mol^{-1} s^{-1}$ described the data better at high temperatures (T > 1000 K). Warnatz [1] recommended the following k_2 expression which

differed only slightly from that of Baulch et al. (300 K ≤ T ≤ 2500 K).

$$k_2 = 1.5 \times 10^7 \, T^{2.0} \exp(- 3800 \, K/T) \, cm^3 \, mol^{-1} \, s^{-1} \qquad (6)$$

Recent experimental results and one theoretical estimation for k_2 are listed in Table II.1.

From the rate coefficient expressions in the three reviews and in Table II.1, it is easily seen that the k_2 values at combustion temperatures are widely different. For example, at 2000 K they are (in units of $cm^3mol^{-1}s^{-1}$): 8.97×10^{12} (Warnatz, Ref. 1); 3.83×10^{12} (Baulch et al., Ref. 4); 4.34×10^{12} (Cohen and Westberg, Ref. 5); 6.93×10^{12} (Schott et al., Ref. 6); 7.24×10^{12} (Pamidimukkala and Skinner, Ref. 7); 6.07×10^{12} (Sutherland et al., Ref. 8); 6.80×10^{12} (Sutherland et al., extended temperature fit, Ref. 8); 7.04×10^{12} (Natarajan and Roth, Ref. 9); 6.55×10^{12} (Natarajan and Roth, extended temperature fit, Ref. 9); 7.25×10^{12} (Shin et al., Ref. 10); 6.89×10^{12} (Davidson and Hanson, Ref. 11); and 7.74×10^{12} (Garrett et al., Ref. 12). The discrepancies worsen as the temperature increases. Also, in the Arrhenius expressions at high temperatures, the values of the A-factor ($cm^3mol^{-1}s^{-1}$) range from 1.87×10^{14} to 8.13×10^{14} and the temperature dependence from 6854 to 9540 K, respectively. Furthermore, in the extensive study by Sutherland et al. [8], the difference between the values from the high temperature fit and the extended temperature fit, which incorporated low temperature data, becomes large as temperature increases. This invokes the question about the extent of curvature of the non-Arrhenius expression of k_2.

Table II.1. Results of the previous studies for $k_2{}^a$

A (cm³mol⁻¹s⁻¹)	n	θ (K)	T range (K)	Reference
2.20×10^{14}	0.00	6916	1400 - 1900	6
2.30×10^{14}	0.00	6916	1919 - 2781	7
1.87×10^{14}	0.00	6854	880 - 2495	8
4.34×10^{13}	0.00	5249	504 - 923	8
5.06×10^{4}	2.67	3165	297 - 2495	8^b
3.72×10^{6}	2.17	4080	1713 - 3532	9
3.87×10^{4}	2.70	3150	300 - 3530	9^c
7.90×10^{14}	0.00	9382	1790 - 2250	10
8.13×10^{14}	0.00	9540	2120 - 2750	11
2.89×10^{14}	0.00	7240	1400 - 1900	12

^{a} Rate coefficient expression is in the form of $k_2 = A\,T^n\,\exp(-\theta/T)$.

^{b} Extended temperature fit using the results of their own and low temperature data (277 - 471 K) of Presser and Gordon [13].

^{c} Extended temperature fit using the results of their own and those of Sutherland et al. [8] and low temperature data (277 - 471 K) of Presser and Gordon [13].

In this study a series of experiments was performed at high temperatures in order to answer the two questions described above, i.e., what the absolute values of k_2 are; and how adequate the non-Arrhenius type expression for k_2 is.

Experimental Section

The experimental set up and methods are the same as described in Chapter I. A mixture composition of $X_{H_2}=0.0005$, $X_{O_2}=0.005$, and $X_{Ar}=0.9945$ was selected for investigation based on the sensitivity analysis (see Computer Simulation).

Results

A typical hydroxyl radical absorption profile is shown in Figure II.1. The rapid rise of the signal after an induction period is due to the exponential growth of OH by the chain branching and chain propagating reactions. Depending upon experimental conditions the OH concentration reaches a partial equilibrium or a maximum.

As in the previous study of the $H_2/O_2/Ar$ system for k_1 (see Chapter I), a set of experimental observables, {t_{50}, A_{max} and NS_{max}} were obtained from
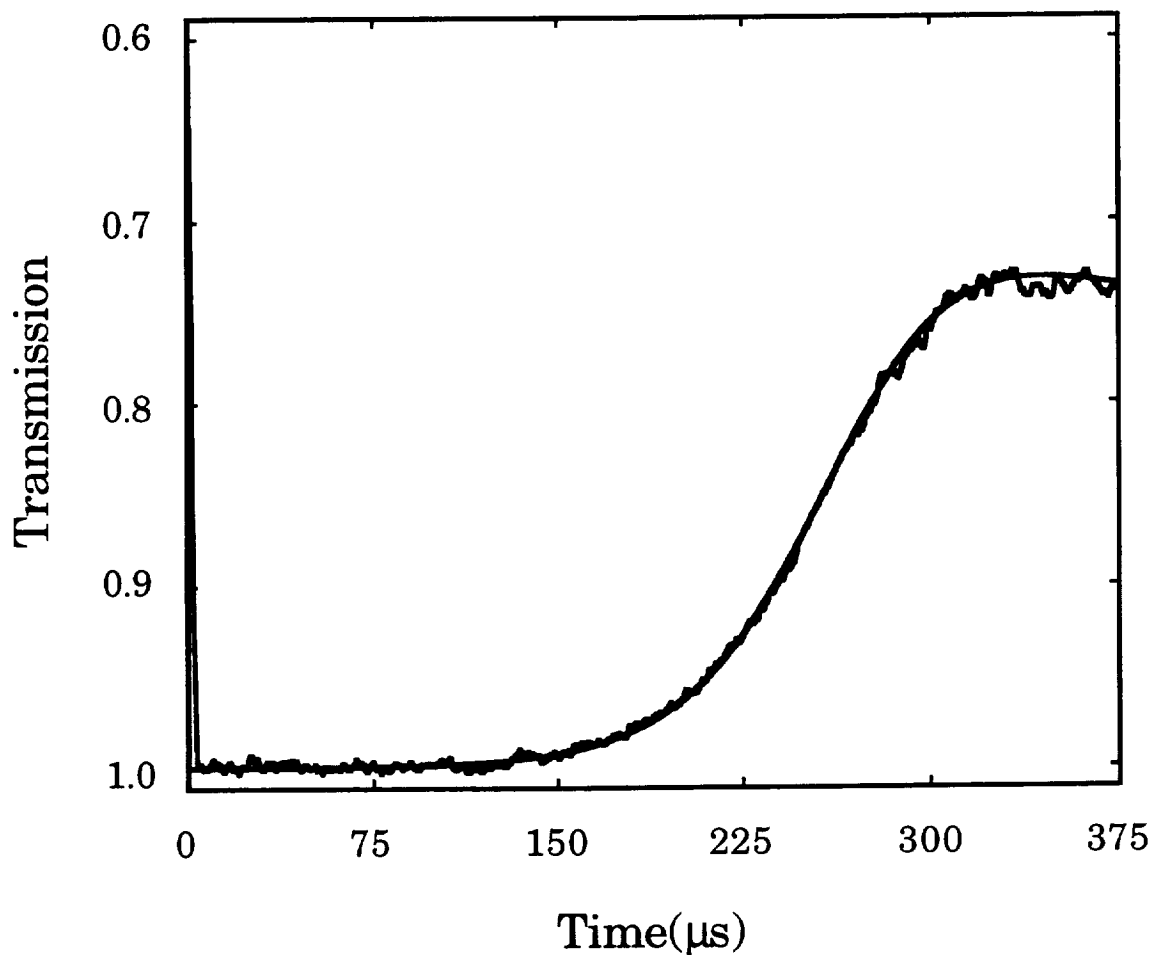
Figure II.1 A typical experimental record of OH absorption for the experimental condition of X_{H_2} = 0.0005, X_{O_2} = 0.005, X_{Ar} = 0.9945, T_5 = 1898 K and P_5 = 1.826 atm. Characteristic time (t_{50}), A_{max}, and NS_{max} were chosen as simulation parameters. The initial peak is the schlieren signal corresponds to passage of the reflected shock front. The smooth line indicates the computed OH absorption profile using the Table II.3 reaction mechanism and the OH absorption coefficient obtained from self-calibration at the maximum absorption (A_{max}).

82

each experimental record to represent the rate of the reaction progress and used for optimization targets of k_2. The definitions of the observables are: A_{max} is the absorption maximum, $(1 - I/I_o)_{max}$, t_{50} is the characteristic time at which the light absorption has reached 50% of A_{max}, NS_{max} is the normalized maximum slope of OH growth, respectively.

Table II.2 shows the experimental conditions and results. The temperature ranged from 1424 K to 2427 K and the pressures were kept around 1.9 atm. Temperature corrections for the boundary layer effects always increased T_5 from the ideal shock temperature by an average about 1.4 %. Contrary to the results reported by Michael and Sutherland [14], the dependence of the ideal shock temperature and the initial pressure (P_1) upon the extent of T_5 correction could not be observed.

A. Computer Simulation

Computer simulations were performed using the detailed reaction mechanism and rate coefficient expressions in Table II.3. The reverse reaction rate coefficients were automatically computed from the principle of detailed balancing. NASA thermodynamic data [15] were used to calculate the shock parameters and the equilibrium constants. The LSODE integrator [16] was utilized to solve a set of stiff differential equations describing chemical kinetics under assumed constant density conditions, calculated for the reflected shock waves [17].

Table II.2 Experimental Conditions and Results of $k_2{}^a$

T_5	P_5	A_{max}	NS_{max}	t_{50}	$k_2{}^b/10^{12}$	$k_2{}^c/10^{12}$
$X_{H_2}=0.0005$, $X_{O_2}=0.005$, $X_{Ar}=0.9945$ ($\phi=0.05$)						
1424	1.801	0.198	850	797	1.50	1.50
1430	1.813	0.190	865	795	1.55	1.58
1449	1.837	0.198	951	756	1.54	1.62
1528	1.903	0.238	1444	558	2.28	2.14
1529	1.912	0.238	1448	592	1.96	1.99
1559	1.967	0.235	1579	505	2.29	2.36
1564	1.964	0.263	1725	508	2.23	2.30
1671	1.829	0.259	1990	422	2.94	3.04
1691	1.844	0.247	2086	382	3.25	3.31
1715	1.887	0.220	1774	371	3.19	3.19
1732	1.942	0.257	2258	335	3.58	3.40
1769	1.898	0.295	2601	322	3.65	3.71
1898	1.826	0.269	2685	252	5.00	4.70
1948	1.903	0.280	3260	225	5.26	5.59
1951	1.900	0.259	2925	219	5.29	5.40
2093	2.008	0.294	4215	160	7.14	7.36
2123	1.928	0.305	4040	157	7.40	6.79
2127	1.935	0.306	4271	157	7.44	7.77
2285	2.004	0.318	5078	125	9.12	8.83
2334	1.950	0.299	4886	118	9.90	9.90
2350	1.964	0.300	5018	114	10.1	9.94
2370	1.993	0.305	5374	109	10.4	10.8
2405	2.050	0.297	5339	101	10.9	10.9
2416	2.041	0.301	5281	98	10.8	10.3
2427	2.064	0.296	5382	94	11.1	11.3

^{a} Units are K for T_5, atm for P_5, μs for t_{50} and $cm^3\ mol^{-1}\ s^{-1}$ for k_2.

^{b} $k_2(t_{50})$

^{c} $k_2(NS_{max})$

Table II.3 Reaction Mechanism for $k_2{}^a$

	Reaction	A	n	θ	Reference
1.	$H + O_2 = OH + O$	7.13E+13	0.0	6957	*Chapter I*
2.	$O + H_2 = OH + H$	1.88E+14	0.0	6897	*This study*
3.	$OH + H_2 = H_2O + H$	2.14E+08	1.52	1736	19
4.	$O + H_2O = OH + OH$	4.51E+04	2.70	7323	20
5.	$O + O + M = O_2 + M$ Ar=1.0, H_2=2.9, O_2=1.2, H_2O=18.5	1.00E+17	−1.0	0	21
6.	$H + H + M = H_2 + M$ Ar=1.0, H_2=4.0, H_2O=12.0, H=26.0	6.40E+17	−1.0	0	21
7.	$H + O + M = OH + M$ Ar=1.0, H_2O=5.0	6.20E+16	−0.6	0	22
8.	$H + OH + M = H_2O + M$ Ar=1.0, H_2=2.5, H_2O=16.25	8.40E+21	−2.0	0	21
9.	$H + O_2 + M = HO_2 + M$ Ar=1.0, H_2=3.33, O_2=1.33, H_2O=21.3	7.00E+17	−0.8	0	21
10.	$HO_2 + H = OH + OH$	2.20E+14	0.0	710	23
11.	$HO_2 + H = H_2 + O_2$	2.50E+13	0.0	350	1
12.	$HO_2 + H = H_2O + O$	5.00E+12	0.0	710	23
13.	$HO_2 + O = O_2 + OH$	2.00E+13	0.0	0	1
14.	$HO_2 + OH = H_2O + O_2$	2.00E+13	0.0	0	1
15.	$HO_2 + HO_2 = H_2O_2 + O_2$	1.06E+11	0.0	−855	24
16.	$H_2O_2 + M = OH + OH + M$ Ar=0.67, O_2=0.78, H_2O=6.0	1.20E+17	0.0	22900	21
17.	$H_2O_2 + H = HO_2 + H_2$	1.70E+12	0.0	1900	1
18.	$H_2O_2 + H = H_2O + OH$	1.00E+13	0.0	1805	1
19.	$H_2O_2 + O = HO_2 + OH$	2.80E+13	0.0	3225	24
20.	$H_2O_2 + OH = H_2O + HO_2$	7.00E+12	0.0	720	1

^{a} Rate coefficients are in the form $k = A\, T^n \exp(-\theta / T)$.
Units are cm^3, K, mol, and s.

The local logarithmic response sensitivities defined below [18] was computed at a typical mid-temperature experimental condition presented in Figure II.1.

$$S_{ij} = ln(R'_j / R_j) / ln(P'_i / P_i) \qquad (7)$$

where $P_i=\{k_i\}$ and $R_j = \{t_{50}$ and $NS_{max}\}_j$. Figure II.2 shows the sensitivities for t_{50} and NS_{max} by raising the $\{k_i\}$ by a factor of 2. Reactions (1), (2), (3), and (11) were sensitive to characteristic time and reactions (1), (2), (3) and (4) were sensitive to NS_{max}. Similar sensitivities were also observed for other reaction conditions. Even if reaction (2) has the highest sensitivity, it was difficult to isolate the effect of reaction (2) only on the changes of characteristic time and NS_{max}. For the very lean condition (for example, $\phi = 0.025$), isolation of the contribution from reaction (2) could be obtained because the sensitivity of reaction (2) for t_{50} and NS_{max} was about twice as big as those of the next highest one. However, in this lean mixture t_{50} was extremely prone to contaminant effects. Therefore, the $X_{H_2}=0.0005$, $X_{O_2} = 0.005$, $X_{Ar}=0.9945$ mixture ($\phi = 0.05$) was chosen to study k_2. In the computer simulation, k_2 values and $\varepsilon(OH)$ were varied to match t_{50}, A_{max} and NS_{max} assuming that expressions of k_1 from our previous extensive study, k_3 and k_4 from the recent critical reviews by Oldenborg et al. [19] and Michael [20], respectively, and k_{11} recommended by Warnatz [1] were correct. Especially, the effect of k_{11} on the evaluation of k_2 was thoroughly searched because there are large discrepancies among the existing data at high temperatures (see Discussion). As was pointed out in Chapter I, the coupling between $\{t_i\}$ and $\varepsilon(OH)$ was found to be small. Therefore, first, A_{max} was
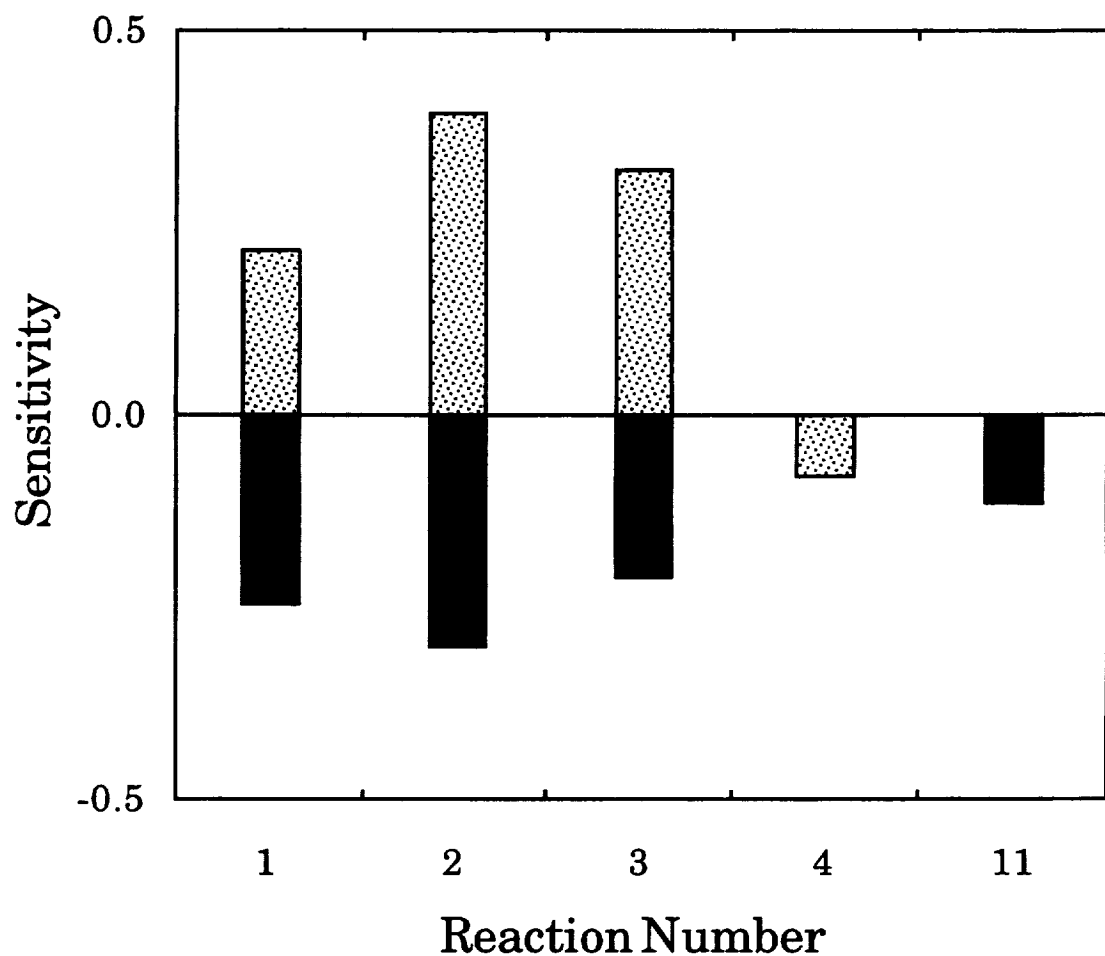
Figure II.2 Sensitivity spectrum for the experimental condition of X_{H_2} = 0.0005, X_{O_2} = 0.005, X_{Ar} = 0.9945, T_5 = 1898 K and P_5 = 1.826 atm. Ordinate is logarithmic sensitivity defined in the text. Sensitivities are for 200% increase to Table II.3 values. Reaction numbers are listed in Table II.3. ■ for t_{50} sensitivity and ▨ for NS_{max} sensitivity.

C-2

matched with ε(OH) and then t_{50} and NS_{max} were matched by varying k_2 only.

The values of k_2 obtained using t_{50} and NS_{max} are listed in the last two columns of Table II.2 and are presented in Figure II.3. The least squares fit to the combined data gives

$$k_2 = (1.88 \pm 0.07) \times 10^{14} \exp(-6897 \pm 53 \text{ K} / \text{T}) \text{ cm}^3 \text{ mol}^{-1} \text{ s}^{-1} \qquad (8)$$

with the uncertainties of 1- σ standard deviation. The 1- σ level deviation of the individual points from the fitted line is ± 6%.

B. Error Analysis

The sampling time of the oscilloscopes used in the shock speed measurement was set to 0.5 μs per point. Thus the maximum allowable uncertainty in the time measurement is 1.0 μs. An 1.0 μs uncertainty causes a 0.5% error in the shock speed, which yields a 0.9% error in T_5 and a 0.5% error in k_2. As described previously, P_5, used in the correction of T_5, was obtained from the last pressure transducer signal. A 0.7% reading error of the voltage output gave a 0.7% error for P_5, which in turn produced a 0.2% error in the corrected T_5 and an 1.0% error in k_2. The error in k_2 from the maximum of ± 0.2% reading uncertainty of the initial pressure (P_1) was negligible. Although the possible errors introduced in the mixture preparation were small, the effect on k_2 was not ignorable. They were appropriately considered in the error propagation analysis. The errors in taking t_{50} and NS_{max} from the experimental records were 2.0% and 6.0%, respectively, and these errors in
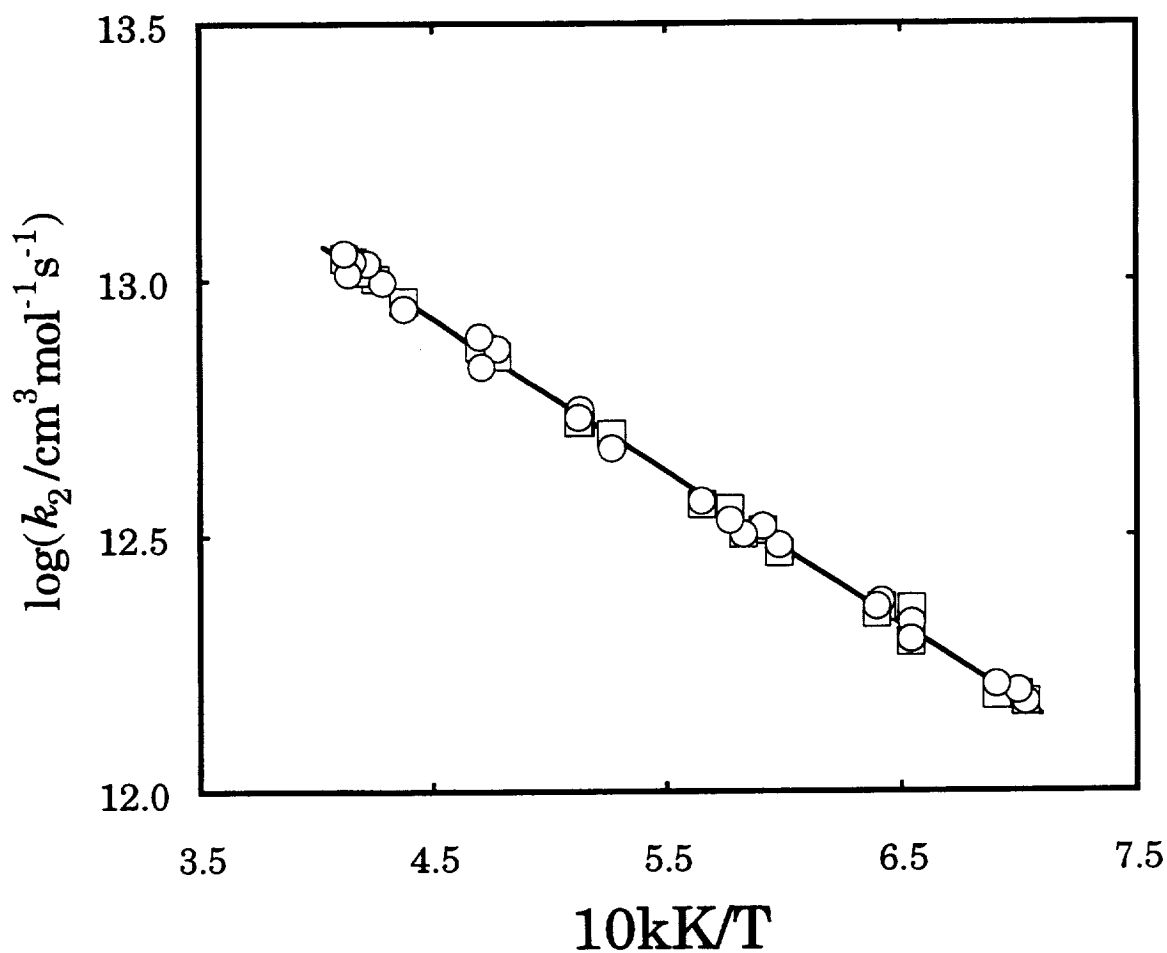
Figure II.3   Arrhenius plot of the experimental data of k_2. O are $k_2(NS_{max})$, $\square$ are $k_2(t_{50})$. the solid line is the least squares fit to the combined NS_{max} and t_{50} data, $k_2 = 1.88 \times 10^{14}$ exp(− 6897 K/T) $cm^3mol^{-1}s^{-1}$ (1420 K ≤ T ≤ 2430 K).

turn produced 5.0% and 6.0% errors in k_2, respectively. As seen in Figure II.4 and Figure II.5, the maximum errors in matching both t_{50} and NS_{max} are less than 3%.

Again, the error propagation was computed using equation (12) in the Chapter I. Considering all the errors, including the data scatter and the matching error, a maximum allowable error of $\pm$ 10% results for the k_2 expression.

Discussion

A computed profile (smooth line) is shown in Figure II.1. The reaction mechanism and the rate coefficient expressions in Table II.3, especially the combination of k_1, k_2, k_3, k_4 and k_{11}, reproduced the experimental profile quite well. The same level of matching is obtained for other experimental conditions. In Figures II.4 and II.5 the matches between experimental and computed t_{50} and NS_{max} are shown, within the scatter of $\pm$ 3.0% for both t_{50} and NS_{max}. Considering 2.0% and 6.0% for extracting t_{50} and NS_{max}, respectively, from experimental records, the matches are excellent. In the optimization of k_2 using t_{50} and NS_{max}, A_{max} was always matched exactly to the experimental values. Matching A_{max} resulted in a self-calibration of the absorption profile.

The present determination of k_2, Eq.(8), is compared to the previous studies in Figure II.6. Schott et al. [6] determined the ratio of k_2/k_1 by
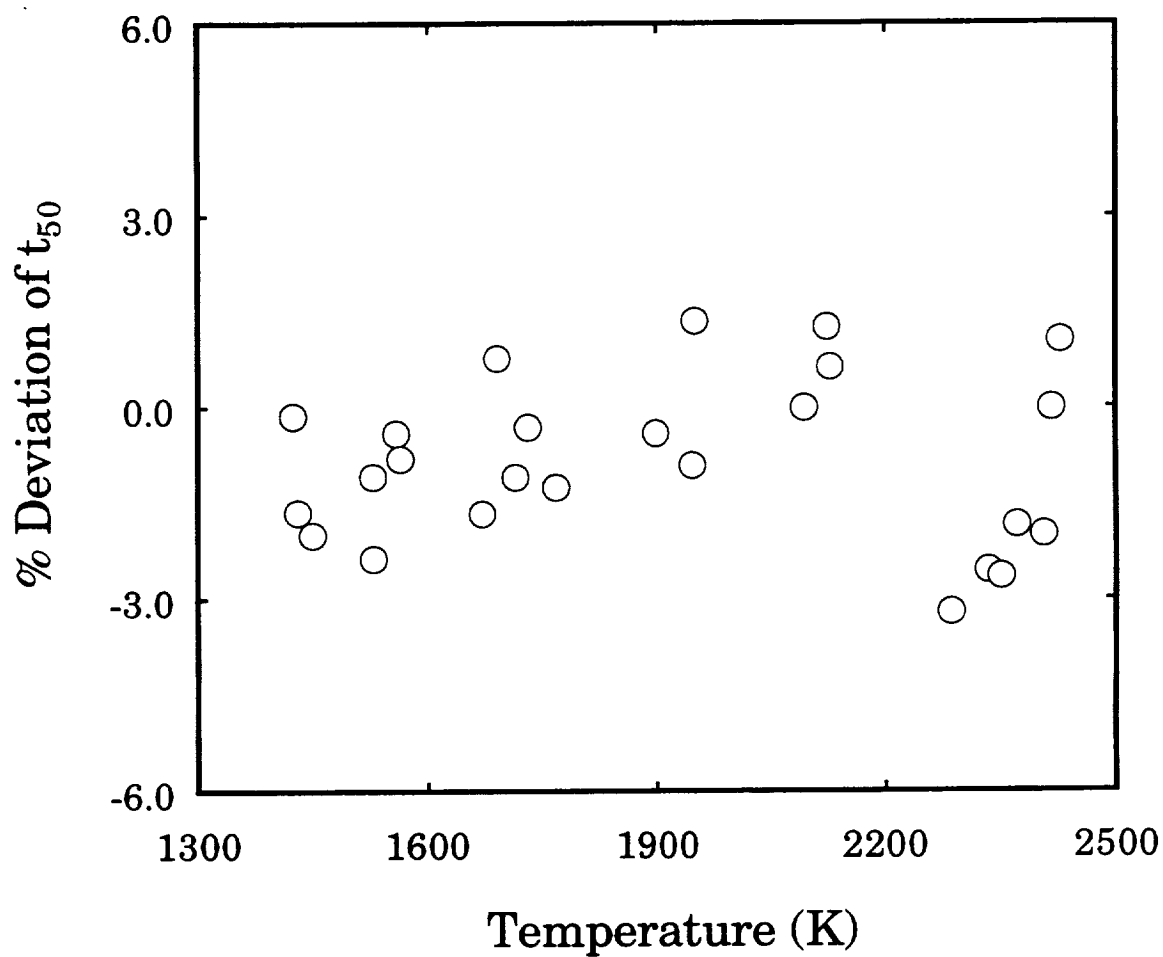
Figure II.4   Matches of the computed t_{50} to the experimental data.   In computation, Table II.3 reaction mechanism and rate coefficients with k_2 values in Table II.3 were used.   The percentage deviation is defined as 100 × {t_{50}(calculation) − t_{50}(experiment)} / t_{50}(experiment).
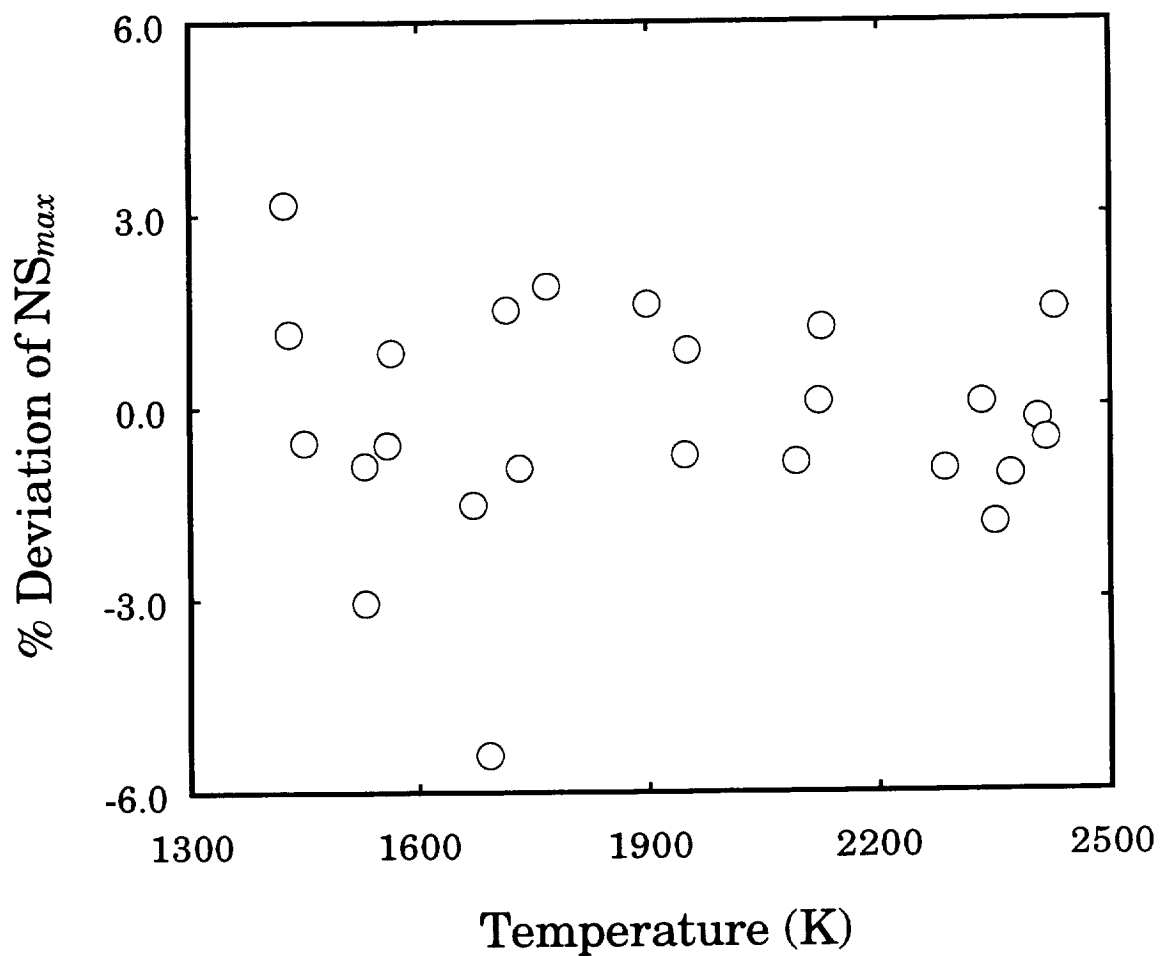
Figure II.5 Matches of the computed NS_{max} to the experimental data. In computation, Table II.3 reaction mechanism and rate coefficients with k_2 values in Table II.3 were used. The percentage deviation is defined as 100 $\times$ {NS_{max}(calculation) $-$ NS_{max}(experiment)} / NS_{max}(experiment).
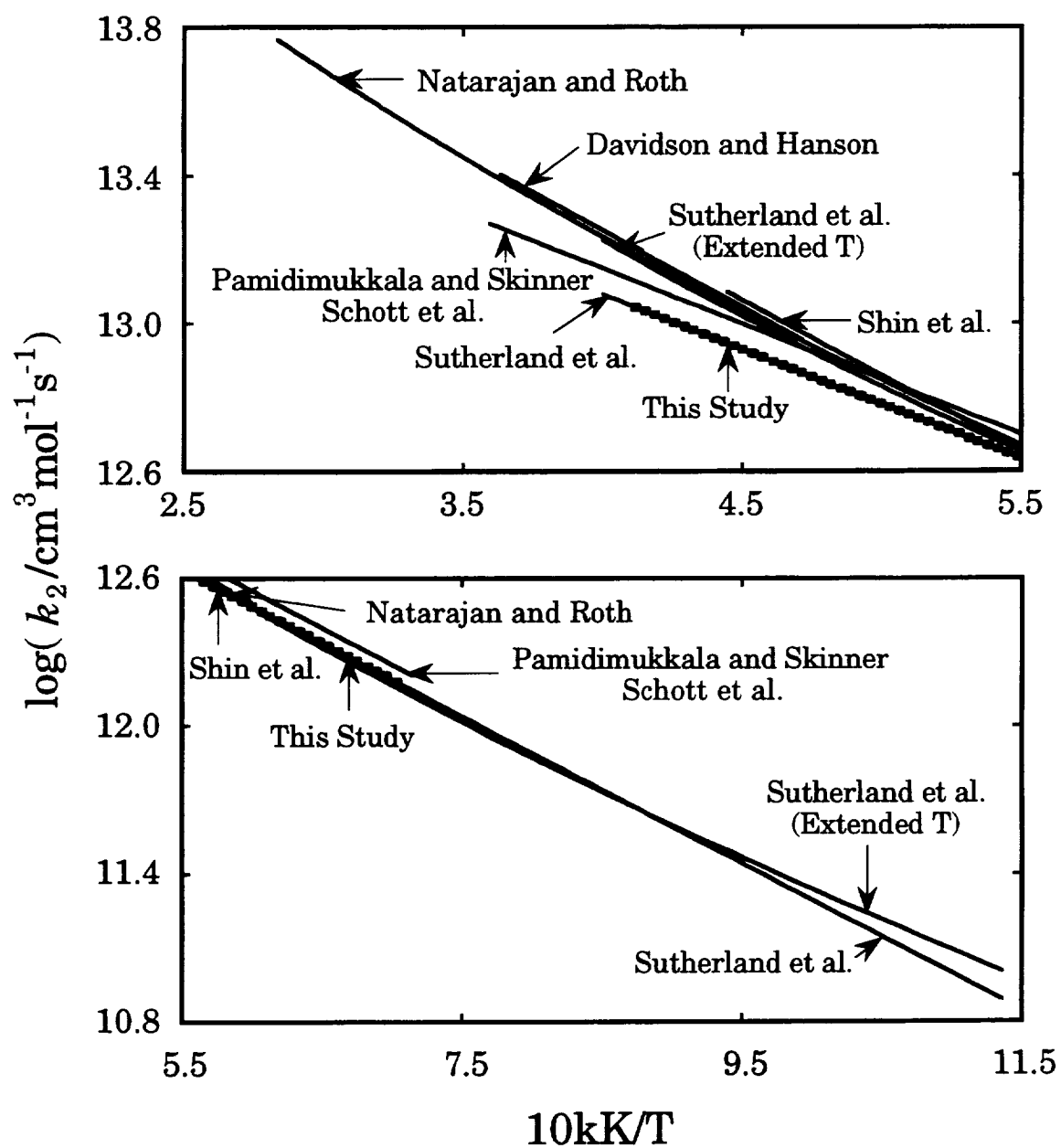
Figure II.6 Comparison of the present results for k_2 to the previous studies.

measuring the O-atom concentration during the incident shock-wave initiated combustion of rich $H_2/O_2/CO/CO_2/Ar$ mixtures (ϕ = 3.0, 5.0 and ~ 8.1) for the conditions of 1400 K ≤ T_2 ≤ 1900 K and 0.25 atm ≤ P_2 ≤ 1.73 atm. Light emission intensity from $CO + O \rightarrow CO_2^* + h\nu$ was monitored. [O] was calibrated against the partial equilibrium transmitted light intensity, I_{PE} and $[O]_{PE}$, obtained with H_2/O_2 = 1 mixture. The spike O-atom concentration, $[O]_S$, calculated from each experiment with the aid of calibration experiments mentioned above, was simulated by varying k_2 / k_1. The results are presented as

$$k_2 = 2.2 \times 10^{14} \exp(- 6916 \text{ K} / \text{T}) \text{ cm}^3 \text{ mol}^{-1} \text{ s}^{-1} \tag{9}$$

with uncertainties of ± 25%. The values of k_2 from the present study are smaller than Eq. (9) by ca. 13% in the temperature interval 1400 - 1900 K, but they agree with each other within the combined error bounds. Because calculation of the temperature at $[O]_S$ for each experiment was not possible from the information given in Ref. 6, the source(s) of these discrepancies could not be found.

Pamidimukkala and Skinner [7] determined k_2 by measuring [O] with atomic resonance absorption spectroscopy in reflected shock heated $H_2/N_2O/Ar$ mixtures over the temperature range 1919 - 2781 K. The k_2 expression reported is given by

$$k_2 = 2.3 \times 10^{14} \exp(- 6916 \text{ K} / \text{T}) \text{ cm}^3 \text{ mol}^{-1} \text{ s}^{-1}. \tag{10}$$

Since Eqns. (9) and (10) are basically identical, although the experimental temperature range is different, they are plotted as a single line in Figure II.6. In the data analysis for deriving k_2 values, the converted O-atom concentration profiles from absorption traces with the pre-determined calibration curve were simulated using the reaction mechanism which was composed of 11 reactions. In the temperature range 1900 - 2400 K, Eq.(10) yielded about 20% higher values than the present results.

Frank and Just [25] measured k_2 using atomic resonance absorption spectroscopy to monitor H-atoms formed in the shock heated $N_2O/H_2/Ar$ mixtures and suggested that the k_2 values of Pamidimukkala and Skinner should be reduced by 20%. The k_2 expression reported by Frank and Just is

$$k_2 = 1.85 \times 10^{14} \exp(- 6976 \text{ K} / \text{T}) \text{ cm}^3 \text{ mol}^{-1} \text{ s}^{-1}. \qquad (11)$$

The present results (Eq.(8)) agree with Eq.(11) within our experimental uncertainties in the common temperature range, Eq.(11) being smaller by 8% at 1700 K and 6% at 2400 K.

Sutherland et al. [8] determined k_2 by two different experimental methods: the flash photolysis-shock tube technique(FP-ST) combined with atomic resonance absorption spectroscopy over the temperature range 880 K to 2495 K, and the flash photolysis - resonance fluorescence (FP-RF) technique from 504 K to 923 K. O-atoms were produced by the flash photolysis of NO in the pseudo-first-order condition([O] << [H_2]). The values of k_2 were determined from subsequent O-atom decay through the relationship of the Beer-Lambert

law, i.e., $ln\{ln(I/I_o)\} = -k_{1st}\,t + C$ and $k_{1st} = k_2\,[H_2]$. The results of the FP-ST work were presented in two-parameter Arrhenius form,

$$k_2 = (1.87 \pm 0.12) \times 10^{14}\, \exp(-\,6854 \pm 85\; K\,/\,T)\; cm^3\, mol^{-1}\, s^{-1}. \quad (12)$$

For the FP-RF work, the Arrhenius expression is given by

$$k_2 = (4.34 \pm 0.25) \times 10^{13}\, \exp(-\,5249 \pm 36\; K\,/\,T)\; cm^3\, mol^{-1}\, s^{-1}. \quad (13)$$

The errors are given as one standard deviation. Examining Eq.(12) and Eq.(13) reveals that the $O(^3P) + H_2$ reaction shows Arrhenius behavior for each temperature range. The two expressions above were then combined with the low temperature results (297 K $\leq$ T $\leq$ 471 K) of Presser and Gordon [13] and presented with a three-parameter non-Arrhenius fit,

$$k_2 = 5.06 \times 10^4\, T^{2.67}\, \exp(-\,3165\; K\,/\,T)\; cm^3\, mol^{-1}\, s^{-1} \quad (14)$$

with the estimated error of about $\pm$ 30% over the entire temperature range from 297 to 2495 K. In the temperature range of the FP-ST work, the non-Arrhenius expression (Eq.(14)) gives 30% higher value at 880 K and 40% at 2495 K than Eq.(13) (Figure II.7). This increasing discrepancy toward the high temperatures indicates that Eq.(14) overemphasized the low temperature results of Presser and Gordon. As seen in Figures II.6 and 7, the results of the present study agree remarkably well with Eq.(12), Sutherland et al.'s high temperature shock-tube results.
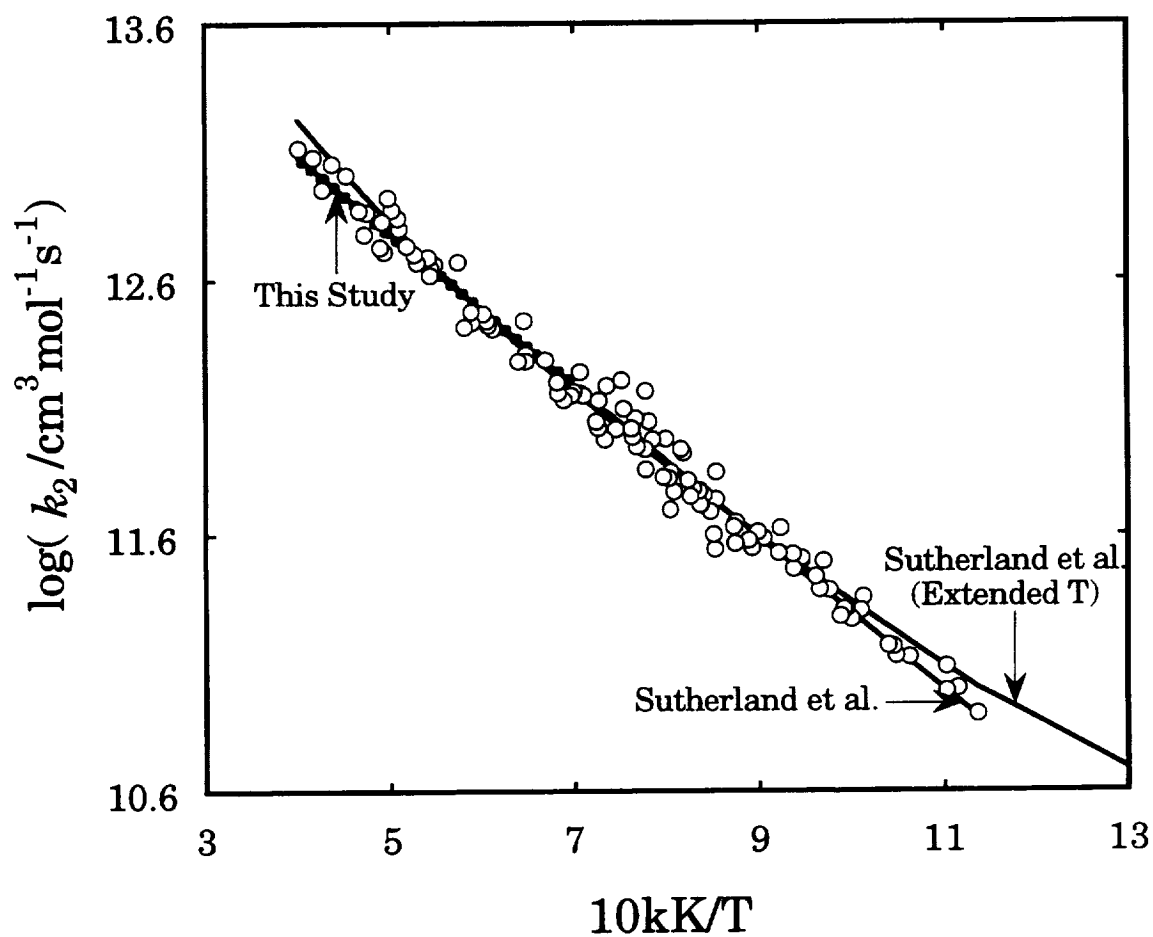
Figure II.7 Comparison of the present rate coefficient fit of k_2 with the experimental data, high and extended temperature fits of Sutherland et al. [Ref. 8]. o is the experimental data of Sutherland et al.

Natarajan and Roth [9] studied reaction (2) behind reflected shock waves in the temperature range of 1713 - 3532 K at total pressures of about 1.4 - 2.0 atm by atomic resonance absorption spectroscopy using $N_2O/H_2/Ar$ mixtures. The time dependent O- and H-atom concentrations were monitored. A reaction mechanism of 13 reactions with appropriate rate coefficient expressions was used in the simulation of the experimental profiles. Through sensitivity and reaction flux analyses, thermal decomposition of N_2O and reaction (2) were identified as the most important reactions and accordingly those two rate coefficients were varied to match the experimental profiles. The rate coefficient of N_2O thermal decomposition, $k(N_2O + M)$, was varied within the uncertainty limits of ± 20%. The results were presented by a non-Arrhenius expression,

$$k_2 = 3.72 \times 10^6 \, T^{2.17} \exp(- 4080 \, K/T) \, cm^3 \, mol^{-1} \, s^{-1} \qquad (15)$$

with uncertainties of ± 9%. Although the values of Eq.(15) agree with the present results within the mutual error limits at T < 2100 K, Eq.(15), likewise Eq.(14), gives higher values towards the high temperatures. For example, at 2400 K, it is 37% higher. The discrepancy between our results (Eq.(8)) and Sutherland et al.'s extended temperature fit (Eq.(14)) was resulted from pure fitting error whereas the 37% discrepancy between Eq.(8) and Eq.(15) is real. We repeated simulations for the maximum O-atom concentration, $[O]_{max}$, and the time to reach $[O]_{max}$, t_{max}, using their reaction mechanism and rate coefficient expressions for conditions at 1713 K (Figure 2(a)), 2171 K (Figure 2(b)), and 2719 K of Ref. 9 where t_{max} and $[O]_{max}$ are listed. The value of k_2 was fixed to that reported by Natarajan and Roth and $k(N_2O + M)$ was varied

to match $[O]_{max}$ exactly and compared t_{max}. For their Figure 2(a) and (b) conditions, about 8% increase of k(N$_2$O + M) resulted in reasonable matches to the t_{max} values by considering ± 10 μs error on time zero of their experiments. However, at 2719 K, it was necessary to reduce k(N$_2$O + M) by 35%, which is clearly outside the error limits given for k(N$_2$O + M). When we matched t_{max} values exactly and examined the resultant maximum O-atom concentrations, the agreement was not much improved. Substituting their reaction mechanism with our Table II.3 mechanism did not improve the matches. The only difference in the simulations is the thermodynamic properties of the species involved. Because the thermodynamic properties of the species used are well known, there would be no difference in computing the shock parameters and equilibrium constants. Frank and Just [25] used exactly the same method as Natarajan and Roth and reported even lower values of k_2 than those of the present study and Sutherland et al. Therefore, the discrepancies at high temperatures may be due to the calibration error for the absorption cross sections of O- and H-atoms used in extracting [H] and [O] in the experiment of Natarajan and Roth.

Shin et al. [10] determined k_2 by different experimental technique than atomic resonance absorption spectroscopy for O- or H-atoms. A laser absorption spectroscopic method was used to detect the OH radicals generated by reflected shock heating of lean H$_2$/O$_2$/Ar mixtures. The maximum slope measured from each experimental absorption record was converted to the maximum growth rate of OH, $(d[OH]/dt)_{max}$, with the absorption coefficient of OH, which was obtained by self-calibrating the observed signal at partial equilibrium and the partial equilibrium OH concentration($[OH]_{PE}$) computed

with a reaction mechanism of 9 reactions. In the computer simulation, k_2 values were adjusted to match the experimental $(d[OH]/dt)_{max}$. The reported k_2 expression is

$$k_2 = 7.9 \times 10^{14} \exp(-9382\ K\ /\ T)\ cm^3\ mol^{-1}\ s^{-1} \qquad (16)$$

with the data scatter of $\pm$ 15% over the temperature range 1790 to 2250 K. Although Eq.(16) agrees with the present study within the combined error limits ($\pm$ 27%) at temperatures below 2100 K, it gives about a 40% higher value at 2250 K. The partial equilibrium concentration of OH computed from the reaction mechanism of Shin et al. is close to that of the Table II.3 mechanism. The maximum OH growth rate should be independent of possible contaminants and of the absolute value of the absorption coefficient used in the simulation and experimental data evaluation because the self-calibration scheme was applied to both cases. We checked whether the high k_2 values of Shin et al. came from the reaction rate coefficients used in their reaction mechanism in the following way: An experimental condition, T=2250 K and P=1.4 atm, was chosen arbitrarily and $(d[OH]/dt)_{max}$ and A_{max} (instead of A_{PE}) were calculated with their reaction mechanism. These two values were assumed to represent the experimental data. The rate coefficients k_1, k_3, and k_4 were then replaced by those in the Table II.3 mechanism and the $(d[OH]/dt)_{max}$ was recalculated while keeping A_{max} the same as before. The maximum OH growth rate decreased by only 1.4%. This indicated that the difference between the reaction mechanism of Shin et al. and that of the present study is the k_2 expression itself. Unfortunately, we were not able to find the source(s) of these discrepancies because of the lack of information

given in their paper.

Recently, Yang et al. [26] repeated the experiments to determine k_2 values using the improved OH laser absorption technique used by Shin et al [10] behind the reflected shock waves; this time the laser wave-length was fixed by an intracavity assembly (ICA). Besides the same H_2/O_2 mixture as used before (1750 K - 2250 K), a 0.05% N_2O, 0.1% H_2, and 99.85% Ar mixture (1600 K - 2140 K) was also used. Again the maximum OH growth rate was modeled using the reaction mechanism of 14 reactions, including N_2O reactions. The new reaction rate coefficient expression for k_2 reported was

$$k_2 = 3.63 \times 10^{14} \exp(- 7818 \text{ K} / \text{T}) \text{ cm}^3 \text{ mol}^{-1} \text{ s}^{-1} \qquad (17)$$

with uncertainties of $\pm$ 15% from 1600 to 2250 K. Eq.(17) agrees with Eq.(8) within the combined error limits, Eq.(17) being larger than Eq.(8) by 6% at 1600 K and by 26% at 2250 K. However, as shown in their sensitivity analysis for experiments with the $N_2O/H_2/Ar$ mixture, $k(N_2O + M)$ has the highest sensitivity on $(d[OH]/dt)_{max}$ (Figure 2(b) in Ref. 26). Therefore, we examined the effect of $k(N_2O + M)$ on the evaluation of k_2 in the following manner. We assumed the Table 1 reaction mechanism of Yang et al., the OH absorption coefficient of Shin et al.(Ref. 10) correctly regenerated the experimental $(d[OH]/dt)_{max}$ and A_{max} at the condition of Figure 2(b) of Ref. 26 (1850 K, 1.53 atm). Then the k_2 expression of Eq.(17) was replaced by our results (Eq.(8)) and $k(N_2O + M)$ and $\varepsilon(OH)$ were varied to match $(d[OH]/dt)_{max}$ and A_{max}. Little change in $\varepsilon(OH)$ was necessary but $k(N_2O + M)$ had to be increased by 10%. The $k(N_2O + M)$ used in the Table 1 mechanism of Ref. 26 is about 7% small at

1850 K compared to that of Frank and Just [25], which had a ± 20% uncertainty limit. In other words, if we use Frank and Just's k(N_2O + M) and increase it by only 3%, our k_2 value also predicts the experimental observations at this temperature quite well. Furthermore, reaction flux analyses show that about 40% of the OH formed at the time of $(d[OH]/dt)_{max}$ is from the reaction of N_2O + H = N_2 + OH and the rate coefficient of this reaction is unknown at high temperatures (See Figure 16, p.404 of Ref. 27). At 2140 K, Eq.(17) is 24% higher than Eq.(8) and it was necessary to raise k(N_2O + M) of Frank and Just by 14% to obtain a satisfactory match. A 14% variation of k(N_2O + M) is still within its error limit, but seems too large. Obviously, high experimental $(d[OH]/dt)_{max}$ caused a high k_2 value. Again, it was not possible to determine the cause of this difference because the experimental conditions were not given for their oscillogram.

Davidson and Hanson [11] performed experiments to measure the rate coefficient of reaction (2). Mixtures of NO/N_2O/H_2/Ar were first shock-heated and then photolyzed with an ArF excimer laser. The pyrolysis of N_2O and the photolysis of NO were utilized to produce O-atoms under near identical conditions. The measured O-atom profiles by atomic resonance absorption spectroscopy were used to derive the k_2 values. Since the experiment with O-atom generation by NO photolysis was done under pseudo-first-order conditions, the slope of $ln\{ln(I/I_o)\}_t$ was equated to $k_2[H_2]$ and subsequently k_2 was evaluated with known $[H_2]$. The Arrhenius expression for k_2 in the temperature range 2120 to 2750 K is

$$k_2 = 8.13 \times 10^{14} \exp(- 9540 \pm 800 \text{ K} / \text{T}) \text{ cm}^3 \text{ mol}^{-1} \text{ s}^{-1} \qquad (18)$$

with the uncertainties in the A factor of ± 10%. The rate coefficients determined by the two methods were in essence indistinguishable. Compared to Eq. (8), the k_2 values from Eq. (18) are about 35% high in the overlapping temperature range. Because Eq. (18) has higher activation energy than Eq. (8), the value of Eq. (18) is about 70% higher than that of Eq. (8), extrapolated to 2750 K. As pointed out in the literature [8], the k_2 values at high temperatures should be higher than those obtained by extrapolation of the low temperature expression because of the contribution from the reaction of $O(^3P)+H_2(v \geq 1)$. To find the possible reason(s) of discrepancy, computer simulations were performed under the condition of Figure 1 of Davidson and Hanson [11]. The reaction mechanism of Masten et al. [22] was modified by replacing the k_2 expression by Eq.(18) and adding N/O, N/H, and H/N/O reactions with rate coefficient expressions from Hanson and Salimian [27]. In the simulation, $\sigma(O)$ of 14000 $atm^{-1}cm^{-1}$ and absorbance of NO of 0.158 at 130.5 nm were used as provided [28] to convert the absorption profiles to O-atom concentration profiles.

For the photolysis experiment, Eq. (18) predicts O-atom decay quite well while Eq. (8) generates more O-atoms with a slightly slower decay rate. During the course of simulations it was found that $[O]_{max}$ and t_{max} (time to reach $[O]_{max}$) were dependent upon the reaction rate of N + NO = N_2 + O. When the rate coefficient of Davidson and Hanson [29] for this reaction was used, a much shorter t_{max} with a higher $[O]_{max}$ (about 20%) than the experimental observations resulted. For the pyrolysis experiment, if N_2O was used as an O-atom source, $[O]_{max}$ was too low and t_{max} was too long compared to the

experiment. In order to match the experimental O-atom profile, first, some other O-atom source, e.g., NO_2 instead of N_2O should be used as an O-atom source [28]; second, the initial concentration of NO_2 should be higher than the N_2O concentration appearing in the caption of Figure 1 in Ref. 11. Accordingly, the initial NO_2 concentration was adjusted to give an excellent match to the converted experimental O-atom profile. After this was done Eq.(18) was replaced by Eq.(8). Again, with Eq.(8), high O-atom concentrations with a slightly slower decay rate compared to the experiment could be observed. Since the mixture compositions are not known exactly, it was difficult to conclude that the k_2 expressions obtained from pyrolysis and photolysis methods were indistinguishable. For k_2 evaluation, the most important element is the absorption cross section of O-atom. It has been well known that calibration for the atomic species using the atomic resonance atomic spectroscopy method is extremely difficult. For example, the absorption cross sections of H(D)- and O-atom vary depending upon the construction and run condition of microwave discharge lamps [30, 31, 32, 33]. Therefore, it may be better to use the self-calibration scheme to match the experimental absorption profiles. If $\sigma(O)$ is reduced by about 35% from the value used by Davidson and Hanson, then our k_2 expression (Eq.(8)) would also give an excellent match to the experimental profiles. Furthermore in Davidson and Hanson's experiments, especially at high temperatures, the flow effect could not be ignored because NO was photolyzed at long time after the shock wave passage (ca. 550 μs) and subsequent decay of O-atoms was used for the evaluation of k_2 values. In such cases, a possible change of flow conditions should be properly considered. There is also a possibility of O-atom depletion to the boundary layer which causes a fast O-atom decay because very small O-atom

concentrations were monitored throughout the experiments. Nonetheless, even though considering the enhancement of the rate coefficient at high temperatures by vibrational excitation of H_2, our rate coefficient expression yields considerably smaller values as compared to Eq.(18) at high temperatures.

One of the most thorough theoretical estimates made on reaction rates is for reaction of $O(^3P) + H_2 = OH + H$. Bowman et al. [34] calculated this reaction rate coefficient using the reduced-dimensionality collinear exact quantum with bend (CEQB/G) reaction probability and transmission coefficient based on an effective potential energy surface given by the ab initio MOD POLCI potential energy surface [35] plus ground state adiabatic bending energy. The calculated rate coefficients were fitted to an Arrhenius expression in the temperature of 1400 to 1900 K [12] and were given by

$$k_2 = 2.89 \times 10^{14} \exp(-7240 \text{ K} / T) \text{ cm}^3 \text{ mol}^{-1} \text{ s}^{-1}. \qquad (19)$$

Equation (19) gives about 16% and 26% higher values than Eq.(8) at temperature of 1400 K and 1900 K, respectively (Figure II.8). Previous calculations by Bowman and his coworkers using the collinear exact quantum (CEQ) reaction probability and transmission coefficient based on MOD POLCI surface without incorporating ground state bending energy [35] yielded slightly lower values than the CEQB/G method [34], and hence gave better matches to the experiments. Recently Truhlar and coworkers also calculated the rate coefficients for the $O(^3P) + H_2 = OH + H$ reaction using the ICVT/LAG (Improved Canonical Variational Transition State Theory with Least-Action
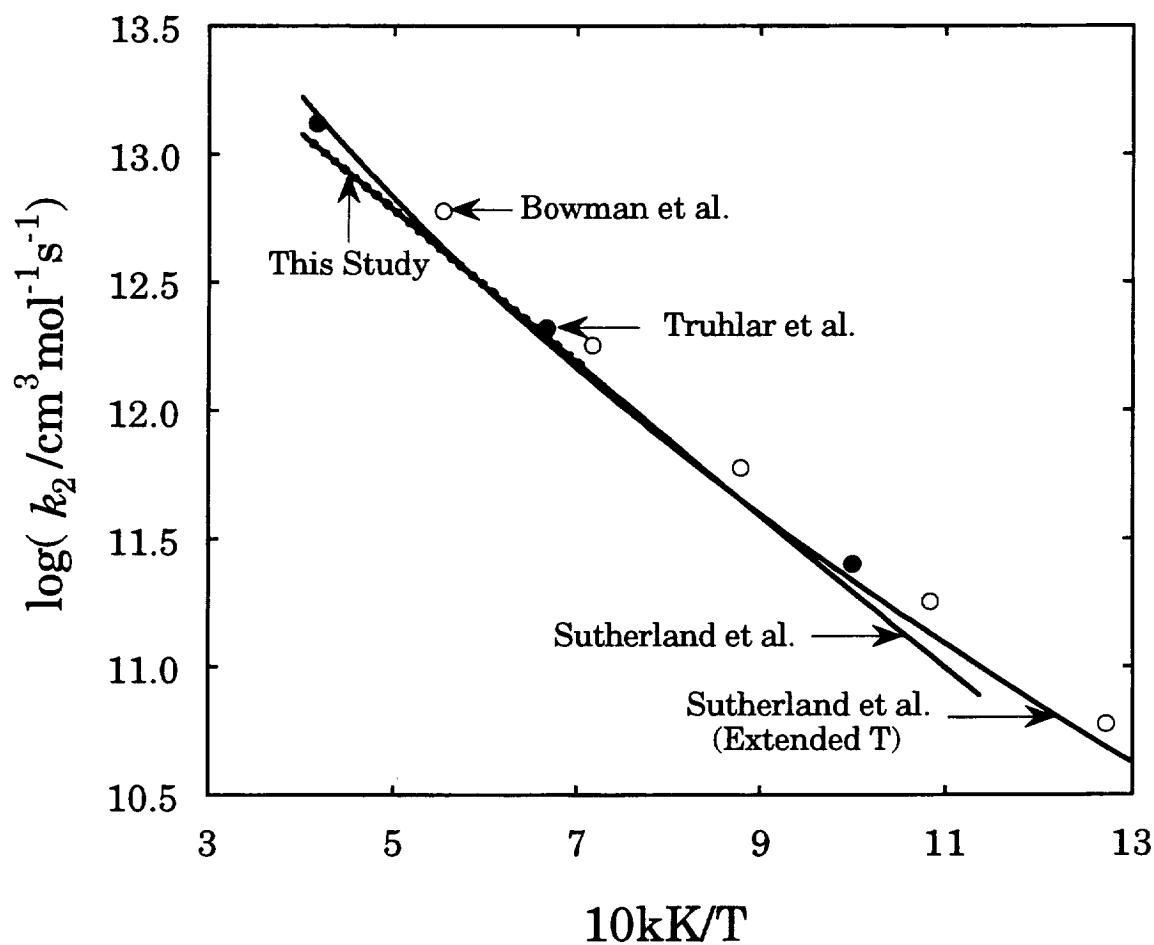
Figure II.8 Comparison of the present results for k_2 with the high temperature and the extended temperature fits of Sutherland et al.[Ref. 8] and the theoretical calculation of Bowman et al.[Ref. 34, 35] and of Truhlar and his coworkers [Ref. 12, 36].

Ground-state transmission coefficient) method [36 and references therein]. The potential energy surface used (J_3 surface) was the modification of RMOS-MOD POLCI surface for collinear O-H-H geometries of Lee et al. [35] augmented by including bend potentials for $^3A''$ and $^3A'$ surfaces. The classical barrier height was recalibrated to 13.0 kcal/mol to match to the experiments. The rate coefficients computed at high temperatures (in units of $cm^3mol^{-1}s^{-1}$) are 2.53×10^{11}, 2.11×10^{12}, and 1.33×10^{13} at 1000 K, 1500 K and 2400 K, respectively (Figure II.8). At low temperatures (T < 500 K), there were excellent matches to the experiment of Presser and Gordon [13] within 7%, the computation being 7% higher at 472 K. Inspection of the results indicates that if a curve is used to fit the data, it is highly curved upward. Compared to the results of the present study, computations give about 8% higher values at 1500 K and 24% higher at 2400 K. The discrepancy between the present results and the calculations is possibly due to the assumption of non-recrossing of trajectories and/or too much reaction flux through the $^3A'$ potential energy surface at high temperatures.

Summary

The measurement of the rate coefficients for $O(^3P)$ + H_2 = OH + H reaction by OH laser absorption spectroscopy coupled to a shock-tube technique has been described and discussed.

In the experiments, actual pressures behind the reflected shock waves

were measured and used together with the adiabatic equation of state to correct the calculated ideal shock properties. The corrected temperatures were about 1.4% higher than the ideal shock temperatures. Hence this temperature correction has the effect of lowering the reaction rate coefficients. Experimental conditions were chosen such that the $O(^3P) + H_2 = OH + H$ reaction gave the highest sensitivity to the experimental observables used in the optimization of the rate coefficient. The OH absorption profiles were successfully reproduced with Table II.3 reaction mechanism containing k_2 expression below.

The present data can be best fitted by an Arrhenius expression in the temperature range 1424 K to 2427 K:

$$k_2 = (1.88 \pm 0.07) \times 10^{14} \exp(- 6897 \pm 53 \text{ K} / T) \text{ cm}^3 \text{ mol}^{-1} \text{ s}^{-1} \qquad (20)$$

with the error limits of ± 12%. The results of this study agree quite well with the high temperature rate coefficient expression of Sutherland et al. [8]. However, Eq.(8) disagrees with the measurement of Natarajan and Roth, Shin et al., Davidson and Hanson, and Yang et al. who used N_2O as an O-atom source [9, 10, 11, 26] and simulated either the O-atom concentration profile converted from the absorption profile with the absorption cross section of O-atom [9, 11] or maximum OH formation rate obtained from the absorption profile with the OH absorption coefficient [10, 26]. The discrepancies can be resolved or lessened if one considers the difficulty in calibrating the O-atom absorption cross section and the uncertainty of the N_2O decomposition rate. It is worthy to note that the extended temperature expression of Sutherland et al.

[8] gives considerable overprediction of k_2 values at high temperatures compared to both our and their own high temperature data. This suggests that the upward curvature of the k_2 expression due to tunneling at low temperatures and contribution from $O(^3P) + H_2(v \geq 1)$ at high temperatures may not be adequately represented by a 3-parameter non-Arrhenius equation.

The theoretical calculations [12, 34, 36] are in good agreement with the extended temperature expression of Sutherland et al., which is the combined results of the low temperature data of Presser and Gordon [13] and middle to high temperature data of Sutherland et al. [8]. Since the extended temperature expression of Sutherland et al. overpredicts the high temperature data, theoretical calculations also overestimate the high temperature reaction rates. Further theoretical developments would be required to resolve the existing discrepancies between the experimental and calculated k_2 values especially at high temperatures.

References

1. Warnatz, J. In *Combustion Chemistry*; Gardiner, W. C., Jr., Ed.; Springer-Verlag: New York, 1984; Chapter 5.

2. Westenberg, A. A.; De Haas, N. *J. Chem. Phys.* **1967**, *46*, 490.

3. Zellner, R. In *Combustion Chemistry*; Gardiner, W. C., Jr., Ed.; Springer-Verlag: New York, 1984; Chapter 3.

4. Baulch, B. L.; Drysdale, D. D.; Horn, D. G.; Lloyd, A. C. *Evaluated Kinetic Data for High Temperature Reactions*; Butterworths: London, 1972; Vol. 1.

5. Cohen, N.; Westberg, K. R. *J. Phys. Chem. Ref. Data* **1983**, *12*, 531.

6. Schott, G. L.; Getzinger, R. W.; Seitz, W. A. *Int. J. Chem. Kinet.* **1974**, *6*, 921.

7. Pamidimukkala, K. M.; Skinner, G. B. *J. Chem. Phys.* **1982**, *76*, 311.

8. Sutherland, J. W.; Michael, J. V.; Pirraglia, A. N.; Nesbitt, F. L.; Klemm, R. B. *Twenty-First Symposium (International) on Combustion*; The combustion Institute: Pittsburgh, 1986; p 929.

9. Natarajan, K.; Roth, P. *Combust.Flame* **1987**, 70,267.

10. Shin, K. S.; Fujii, N.; Gardiner, W. C., Jr. *Chem. Phys. Lett.* **1989**, *161*, 219.

11. Davidson, D. F.; Hanson, R. K. *Combust. Flame* **1990**, *82*, 445.

12. Garrett, B. C.; Truhlar, D. G.; Bowman, J. M.; Wagner, A. F.; Robie, D.; Arepalli, S.; Presser, N.; Gordon, R. J. *J. Am. Chem. Soc.* **1986**, *108*, 3515.

13. Presser, N.; Gordon, R. J. *J. Chem. Phys.* **1985**, 82,1291.

14. Michael, J. V.; Sutherland, J. W. *Int. J. Chem. Kinet.* **1986**, *18*, 409.

15. McBride, B. J.; Gordon, S.; Reno, M. A. "Coefficients for Calculating Thermodynamic and Transport Properties of Individual Species". NASA TM-4513; National Aeronautics and Space Administration: Washington D. C., 1993.

16. Hindmarsh, A. C. "Towards a Systematic Collection of ODE Solvers". Presented at the 10th IMACS World Congress on System Simulation and Scientific Computation, Montreal, August 1982.

17. Gardiner, W. C., Jr.; Walker, B. F.; Wakefield, C. B. In *Shock Waves in Chemistry*; Lifshitz, A., Ed.; Marcel Dekker: New York ,1981; Chapter 7.

18. Gardiner, W. C., Jr. *J. Phys. Chem.* **1977**, *81*, 2367.

19. Oldenborg, R. C.; Loge, G. W.; Harradine, D. M.; Winn, K. R. *J. Phys. Chem.* **1992**, 96, 8426.

20. Michael, J. V. *Prog. Energy Combust. Sci.* **1992**, *18*, 327.

21. Frenklach, M.; Wang, H.; Rabinowitz, M. J. *Prog. Energy Combust. Sci.* **1992**, *18*, 47.

22. Masten, D. A.; Hanson, R. K.; Bowman, C. T. *J. Phys. Chem.* **1990**, *94*, 7119.

23. Dixon-Lewis, G. *Combust. Sci. Technol.* **1983**, *34*, 1.

24. Albers, E. A.; Hoyermann, K.; Wagner, H. Gg.; Wolfrum, J. *Thirteenth Symposium (International) on Combustion*; The Combustion Institute: Pittsburgh, 1971; p 81.

25. Frank, P.; Just, Th. *Ber. Bunsen-Ges. Phys. Chem.* **1985**, *89*, 181.

26. Yang, H. X.; Shin, K. S.; Gardiner, W. C., Jr. *Chem. Phys. Lett.* **1993**, *207*,69.

27. Hanson, R. K.; Salimian, S. In *Combustion Chemistry*; Gardiner, W. C.,Jr., Ed.; Springer-Verlag: New York, 1984; Chapter 6.

28. Davidson, D. F. private communication, 1994.

29. Davidson, D. F.; Hanson, R. K. *Int. J. Chem. Kinet.* **1990**, *22*, 843.

30. Lifshitz, A.; Frenklach, M. *J. Chem. Phys.* **1977**, *67*, 2803.

31. Lifshitz, A.; Skinner, G. B.; Wood, D. R. *J. Chem. Phys.* **1979**, *70*, 5607.

32. Chiang, C. C.; Lifshitz, A.; Skinner, G. B.; Wood, D. R. *J. Chem. Phys.* **1979**, *70*, 5614.

33. Pamidimukkla, K. M.; Lifshitz, A.; Skinner, G. B.; Wood, D. R. *J. Chem. Phys.* **1981**, *75*, 1116.

34. Bowman, J. M.; Wagner, A. F.; Walch, S. P.; Dunning, T. H., Jr. *J. Chem. Phys.* **1984**, *81*, 1739.

35. Lee, K. T.; Bowman, J. M. *J. Chem. Phys.* **1982**, *76*, 3583.

36. Joseph, T.; Truhlar, D. G.; Garrett, B. C. *J. Chem. Phys.* **1988**, *88*, 6982.

REPORT DOCUMENTATION PAGE

1. AGENCY USE ONLY (Leave blank)	2. REPORT DATE	3. REPORT TYPE AND DATES COVERED
	May 1995	Final Contractor Report

4. TITLE AND SUBTITLE

High Temperature Kinetic Study of the Reactions $H + O_2 = OH + O$ and $O + H_2 = OH + H$ in H_2/O_2 System by Shock Tube - Laser Absorption Spectroscopy

5. FUNDING NUMBERS

WU–505–62–52
G–NAG3–1307

6. AUTHOR(S)

Si-Ok Ryu, Soon Muk Hwang, and Kenneth J. DeWitt

7. PERFORMING ORGANIZATION NAME(S) AND ADDRESS(ES)

University of Toledo
Department of Chemical Engineering
Toledo, Ohio 43606

8. PERFORMING ORGANIZATION REPORT NUMBER

E–9670

9. SPONSORING/MONITORING AGENCY NAME(S) AND ADDRESS(ES)

National Aeronautics and Space Administration
Lewis Research Center
Cleveland, Ohio 44135–3191

10. SPONSORING/MONITORING AGENCY REPORT NUMBER

NASA CR–195473

11. SUPPLEMENTARY NOTES

Project Manager, Martin J. Rabinowitz, Internal Fluid Mechanics Division, NASA Lewis Research Center, organization code 2650, (216) 433–5847.

12a. DISTRIBUTION/AVAILABILITY STATEMENT

Unclassified - Unlimited
Subject Category 25

This publication is available from the NASA Center for Aerospace Information, (301) 621–0390.

12b. DISTRIBUTION CODE

13. ABSTRACT (Maximum 200 words)

The reactions (1) $H + O_2 = OH + O$ and (2) $O + H_2 = OH + H$ are the most important elementary reactions in gas phase combustion. They are the main chain-branching reaction in the oxidation of H_2 and hydrocarbon fuels. In this study, rate coefficients of the reactions (1) and (2) have been measured over a wide range of composition, pressure, density and temperature behind the reflected shock waves. The experiments were performed using the shock tube- laser absorption spectroscopic technique to monitor OH radicals formed in the shock-heated $H_2/O_2/Ar$ mixtures. The OH radicals were detected using the $P_1(5)$ line of (0,0) band of the $A^2\Sigma^+ \leftarrow X^2\Pi$ transition of OH at 310.023 nm (air). The data were analyzed with the aid of computer modeling. In the experiments great care was exercised to obtain high time resolution, linearity and signal-to-noise. The results are well represented by the Arrhenius expressions. The rate coefficient expression for reaction (1) obtained in this study is $k_1 = (7.13 \pm 0.31) \times 10^{13} \exp(-6957 \pm 30 \text{ K/T}) \text{ cm}^3\text{mol}^{-1}\text{s}^{-1}$ (1050 K $\leq$ T $\leq$ 2500 K) and a consensus expression for k_1 from a critical review of the most recent evaluations of k_1 (including our own) is $k_1 = 7.82 \times 10^{13} \exp(-7105 \text{ K/T}) \text{ cm}^3\text{mol}^{-1}\text{s}^{-1}$ (960 K $\leq$ T $\leq$ 5300 K). The rate coefficient expression of k_2 is given by $k_2 = (1.88 \pm 0.07) \times 10^{14} \exp(-6897 \pm 53 \text{ K/T}) \text{ cm}^3\text{mol}^{-1}\text{s}^{-1}$ (1424 K $\leq$ T $\leq$ 2427 K). For k_1, the temperature dependent A-factor and the correlation between the values of k_1 and the inverse reactant densities were not found. In the temperature range of this study, non-Arrhenius expression of k_2 which shows the upward curvature was not supported.

14. SUBJECT TERMS

Chain reaction; Chemical kinetics; Combustion of H_2/O_2 system; Rate coefficient; Shock tube; Laser absorption spectroscopy

15. NUMBER OF PAGES

123

16. PRICE CODE

A06

17. SECURITY CLASSIFICATION OF REPORT	18. SECURITY CLASSIFICATION OF THIS PAGE	19. SECURITY CLASSIFICATION OF ABSTRACT	20. LIMITATION OF ABSTRACT
Unclassified	Unclassified	Unclassified	